Fall 1978

COLLISIONLESS EVOLUTION OF THE AURORAL ELECTRON VELOCITY DISTRIBUTION FUNCTION

JAMES DEAN RICKMAN JR.

COLLISIONLESS EVOLUTION OF THE AURORAL ELECTRON VELOCITY DISTRIBUTION FUNCTION

by

James D. Rickman, Jr.
B.S., Case-Western Reserve University, 1970

A DISSERTATION

Submitted to the University of New Hampshire
in Partial Fulfillment of
the Requirements for the Degree of

Doctor of Philosophy
in
Physics

September 1978

This thesis has been examined and approved.

Thesis Director, Richard L. Kaufmann
Professor of Physics

Roger L. Arnoldy
Professor of Physics

John F. Dawson
Associate Professor of Physics

Lennard A. Fisk
Associate Professor of Physics

Barry J. Harrington
Assistant Professor of Physics

Date June 30, 1978

ACKNOWLEDGEMENTS

I wish to thank my thesis advisor, Dr. Richard Kaufmann, for his constant support and guidance during many years of thesis research and study. I gratefully acknowledge my debt to Dr. Roger Arnoldy for the use of his rocket data and many valuable discussions concerning its interpretation. Most important of all, I wish to thank my wife Elena and my children Jimmy and Scott for their patience, love and support during this long effort.

The research presented here was supported by the Atmospheric Research Section of the National Science Foundation under grant NSF-ATM77-01014.

TABLE OF CONTENTS

Page

Appendices

LIST OF TABLES

LIST OF FIGURES

LIST OF FIGURES (continued)

ABSTRACT

COLLISIONLESS EVOLUTION OF THE AURORAL ELECTRON VELOCITY DISTRIBUTION FUNCTION

by

JAMES D. RICKMAN, Jr.

The time evolution of the electron velocity distribution function determined by the collisionless Boltzmann equation is calculated in one dimension (one space and one velocity dimension) and 2 1/2 dimensions (two space and three velocity). The calculations assume a cold stationary background of ions and a spatially varying electron density that gives rise to an electrostatic electric field calculated from Poison's equation. Test cases are presented to show that the one-dimensional computer calculation gives the correct results for Landau damping of a high initial electric field and the two-stream instability. The 2 1/2 dimensional calculation is tested for Landau damping of parallel and 45° plasma waves and shown to give the correct results.

One-dimensional calculations of the interaction between high energy (2 keV) high temperature (640 eV) accelerated Maxwellian electron beams and low temperature

(10 eV) background electrons with beam to background density ratios from .28 to $.28 \times 10^{-5}$ are made to simulate the interaction of high energy auroral electron beams with ionosphere and high altitude backgrounds. They show that the beam electrons give energy to the background electrons through the electric field and are absorbed in the background within about 100 km of travel removing the unstable two peaked structure in the one-dimensional distribution function. The one-dimensional calculation for a beam to background density ratio of $.28 \times 10^{-5}$ shows a growth of low phase velocity plasma waves and a decrease in the slope of the electron distribution function calculated from collisional interactions in the energy range 45 to 320 eV in agreement with experimental measurements.

A 2 1/2 dimensional beam background interaction calculation for a beam to background electron density ratio of 5 also shows an increase in electron population in the energy range between the background and the beam. The two peaked structure in the one-dimensional integrated electron distribution function $F(v_{\parallel})$ is removed within several kilometers of travel for a 2 keV electron beam. The one-dimensional distribution function $F(v_{\parallel})$ evolves to a monotone decreasing function of the velocity parallel to the magnetic field $(v_{\parallel})$. However, the two dimensional distribution function $f(v_{\parallel}, v_{\perp})$ retains a slight peaked or plateau structure along the parallel velocity direction.

The large spatial extent of reported satellite measurements of strongly field aligned high energy beam electron distribution function peaks and the rapid dissipation of unstable two peaked structure in the one-dimensional function implies a continuous parallel acceleration region of at least 1,000 km in extent at an altitude of 7,000 to 8,000 km above the aurora oval. An increase in the electron population in the velocity range between the beam and background required to give agreement with rocket data at 200 km may be obtained by a parallel acceleration region extending to rocket altitudes. Anisotropic beam peaks in the one-dimensional distribution function formed by the rocket altitude acceleration process must be diminished within milliseconds by the growth of parallel plasma waves since anisotropic beam peaks in the one-dimensional distribution function are not usually observed in data taken over a period of seconds. Evidence for continuous acceleration at rocket altitudes is found in the occasional measurement of short duration (less than one second) electron beam "bursts" of strongly field aligned high energy electrons at rocket altitudes.

CHAPTER I

INTRODUCTION

1.1 The Auroral Phenomenon

Syun-Ichi Akasofu has described the auroral phenomenon by the analogy:[1] "The magnetosphere of the earth acts like a gigantic cathode-ray tube that marshals charged particles into beams and focuses them on the earth's polar regions. The aurora is a shifting pattern of images displayed on the flourescent screen provided by the atmosphere." The predominant visual emission during an aurora is the yellowish-green light (5577 Å) emitted by oxygen atoms excited in collisions with low energy (~10 eV) secondary electrons[2]. A weaker atomic oxygen line occurs in the red at 6300 Å, and there is a weak molecular nitrogen ion line at 4278 Å (violet).[2-4]

The auroral glow occurs most strongly at altitudes between 100 and 300 km[3] and encircles the entire earth at between 65 and 75 degrees latitude in both hemispheres[2]. Data from a typical sounding rocket flight[5] into an aurora in the northern hemisphere (Aurora Borealis) is shown in figure 1. The flight was made from Poker Flat, Alaska (latitude 65° N). The rocket attained a maximum altitude of 223 km at 240 seconds after launch. The intensity of the atomic oxygen yellowish-green line as measured by the rocket photometer is shown in the lower curve of figure 1 as a function of time after launch. The photometer acceptance angle was along the magnetic field line beneath the rocket. The photometer data shows a light intensity well above background (dashed line) at 150 and 250 seconds into the flight. The rocket begins to lose altitude beyond 240 seconds so that the volume of emitting atmosphere beneath the rocket (where the photometer is pointed) decreases. The peaks in light intensity are well correlated with the total electron energy flux at the rocket shown in the top curve of figure 1. This is expected, since it is the secondary electrons produced in ionizing collisions between ionospheric constituents and high energy electrons traveling along the magnetic field lines that excite oxygen atoms to emit the 5577 Å green auroral line.[2] A high electron energy flux indicates that high energy electrons are near the rocket giving rise to secondaries and auroral emissions.

Figure 2 shows the differential electron flux measured by rocket electrostatic analyzers[6] as the rocket passes through the first auroral region encountered. The flux is the number of electrons per second per unit energy interval per unit detector aperature area per unit solid angle accepted by the detector. The rocket detectors accept electrons traveling with velocities over a wide range of orientations with respect to the local magnetic field line. However, the data of figure 2 includes only those electrons traveling with a velocity directed within 10° of the magnetic field line direction (downward toward the earth in the northern hemisphere). The sharp peak at 3 KeV (dark circles) is typical of down coming auroral electron energy spectra. This is the beam of high energy electrons traveling along the earth's magnetic field lines that gives rise to low energy secondaries between 10 and 1000 eV (open circles)[7 8]. The secondaries cause the auroral emissions through excitation and recombination reactions with atmospheric constituents.

Figure 2 does not show the ionospheric background flux expected below 1 eV. According to the Jones and Rees model[9] an average energy of .2 eV (kT=.13 eV) is expected for an ionospheric background at 200 km. The model gives a density of 7.6×10^4 cm^{-3} for the auroral region ionosphere background at 200 km. The local density of primary and secondary electrons in figure 2 can be determined from the flux by the method described in Appendix A. The calculation

gives a value of 5.3 cm^{-3} for the primary beam (10^3-10^4 eV) density and 5.2 cm^{-3} for the secondary electron (10 -10^3 eV) density from the flux of figure 2. Therefore, the sum of the primary and secondary electron densities is about four orders of magnitude smaller than the background ionosphere electron density at 200 km.

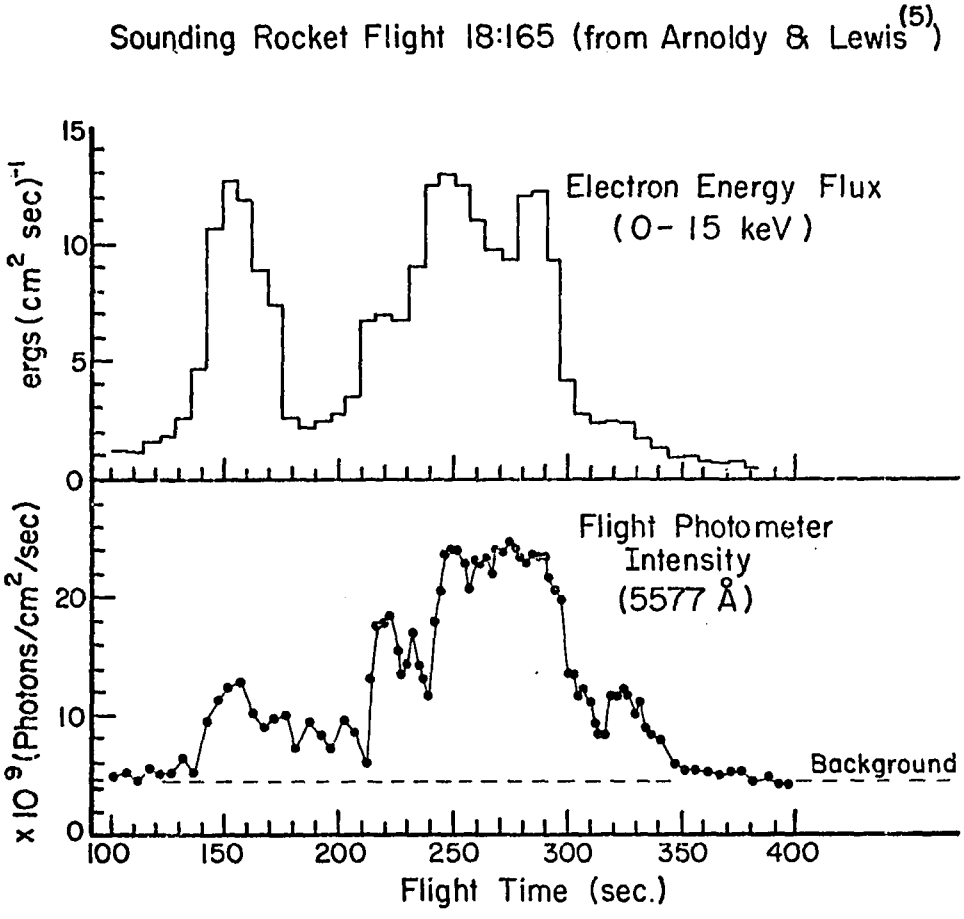
Sounding Rocket Flight 18:165 (from Arnoldy & Lewis[5])
Electron Energy Flux
(0 - 15 keV)
ergs (cm² sec)⁻¹
15
10
5
0
Flight Photometer
Intensity
(5577 Å)
Background
x 10⁹ (Photons/cm²/sec)
20
10
0
100
150
200
250
300
350
400
Flight Time (sec.)

Figure 1

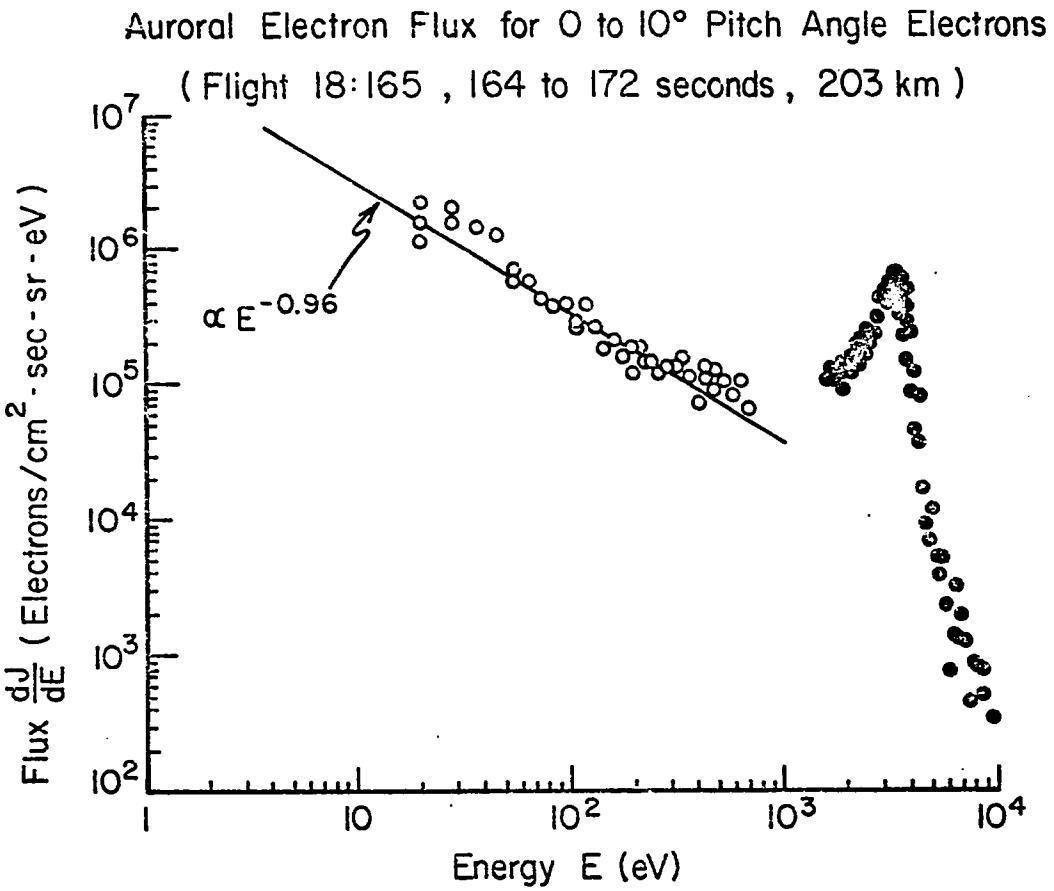
Auroral Electron Flux for 0 to 10° Pitch Angle Electrons
(Flight 18:165 , 164 to 172 seconds , 203 km)
$\propto E^{-0.96}$
Flux $\frac{dJ}{dE}$ (Electrons/cm^2 - sec - sr - eV)
10^7
10^6
10^5
10^4
10^3
10^2
1
10
10^2
10^3
10^4
Energy E (eV)

Figure 2

1.2 Current Atmospheric Scattering Models

Atospheric scattering models using the Fokker-Planck diffusion equation to compute the electron energy spectrum at lower altitudes (100-300 km) from an incident beam entering the atmosphere at high altitudes (~600 km) have been successful in modeling the production of low energy secondary and degraded primary electrons. Figure 3 shows the results of an electron spectra calculation made by Banks et. al.[7] starting with the incident flux shown at 585 km. The incident flux was taken from rocket detector measurements made by Reasoner and Chappell[10]. The calculation assumes an isotropic flux and gives the flux integrated over the entire downward hemisphere. The integrated flux per unit solid angle ($\frac{dJ}{dE}$ (cm^{-2}-sec^{-1}-sr^{-1}- eV^{-1})) is obtained by dividing by the 2π sterradians in the downward hemisphere.

The atmospheric scattering calculations of Banks et. al.[7] and Strickland[8] show an E^{-2} dependence for the low energy electron flux. However, the data of Reasoner and Chappell[10], Feldmann and Doering[11], Sharp and Hayes[12] and that of flight 18:165 in figure 2 show an E^{-1} dependence for the low energy (20-1000 eV) electron flux. Strickland and Papadopoulos[16 13] have suggested that plasma instabilities give rise to the growth of electrostatic waves that derive their energy from the high energy electron beam. An electrostatic wave with a phase velocity near the beam

velocity grows during the evolution of the beam instability and gives rise to a low phase velocity electrostatic wave through parametric coupling. The low phase velocity waves accelerate low energy electrons to higher energy. This may account for a smaller decrease in electron flux with increasing energy for the low energy electrons than that predicted by atmospheric scattering alone. It is one of the purposes of this thesis to investigate the growth of electrostatic waves from velocity space plasma instabilities described by the collisionless Boltzmann equation and to determine whether or not they can account for the discrepancy between measured auroral electron spectra and atmospheric scattering calculations.

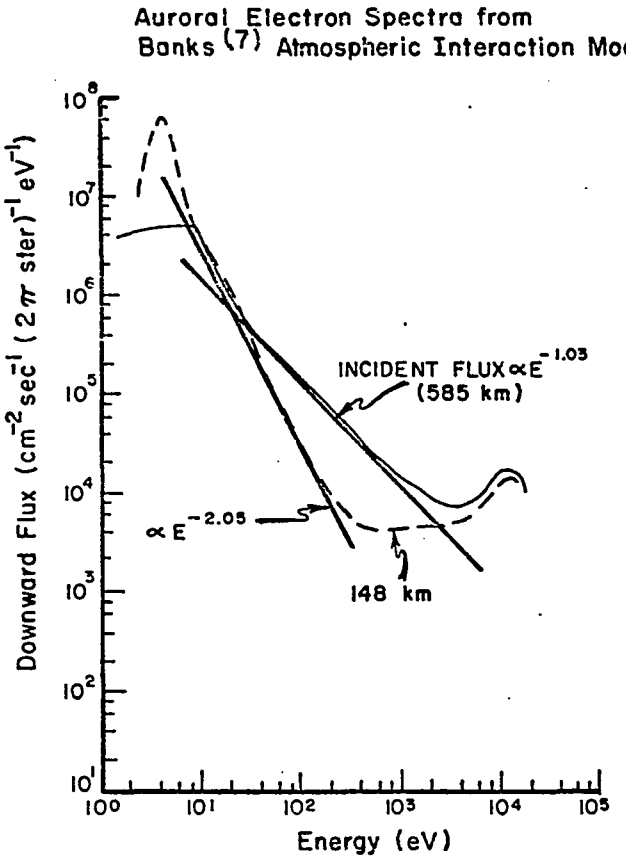
Auroral Electron Spectra from
Banks (7) Atmospheric Interaction Model
Downward Flux (cm⁻² sec⁻¹ (2π ster)⁻¹ eV⁻¹)
Energy (eV)
INCIDENT FLUX ∝ E^-1.03
(585 km)
∝ E^-2.05
148 km

Figure 3

1.3 Where Do They Come From ?

The ultimate source of the electrons that form the high energy auroral electron beam is the flux of particles from the sun known as the solar wind[14]. The solar wind is a neutral plasma consisting of protons and electrons (with some minor constituent positive ions). The electrons have a density of 5 cm^{-3} and a mean energy of 100 eV[14 15]. Through some process not yet understood, these electrons must be accelerated to kilovolt energies to form the auroral electron beam. Various mechanisms involving anomalous plasma resistivity concepts[13 16] and kinetic Alfvén waves[17] have been proposed. Several regions of the earth's magnetosphere contain accelerated solar wind particles of kilovolt energies. Table 1 summarizes electron properties for regions of the magnetosphere shown in figure 4 (taken from Frank[18]). Scanning through the table one finds that the plasma sheet, magnetopause and ring current contain electrons of kilovolt energies and densities on the order of 1 cm^{-3}, and therefore, are likely candidates for the magnetosphere source of high energy auroral electrons.

Figure 5 shows a model of particle flow in the plasma sheet proposed by Rostoker and Böstrom[30] to account for Birkland current flow along the magnetic field lines into the aurora oval measured by Zmuda and Armstrong[31] and Cloutier et. al.[32]. The driving force for the Birkland currents is the convective motion of the plasma sheet

particles[33 34] outward toward the edges of the plasma sheet (direction indicated by $\vec{V}$ in figure 5) and the magnetosheath boundary (figure 4). This convective motion produces a Lorentz force ($q/m\ \vec{V}x\vec{B}$) on the drifting electrons and protons. A current ($\vec{J}$) is produced perpendicular to the outward convective flow (arrows connecting constant potential sheets) . In the equilibrium condition, where the particles drift at constant velocity, the Lorentz force must be balanced by an oppositely directed force due to an electric field. Thus, the electric field is opposite the direction of current flow and normal to equipotential surfaces formed along magnetic field lines connecting the plasma sheet to the auroral arc region. The electric field is created by charge separation due to oppositely directed Lorentz forces on the drifting plasma sheet protons and electrons. The current loop is closed in the auroral oval and gives rise to diffuse auroral emissions from interaction of the high energy (~1 KeV) current carrying plasma sheet electrons with the ionosphere.

The ionospheric electric field is the result of charge separation in the plasma sheet and the formation of equipotential surfaces along magnetic field lines extending into the aurora oval. In a collisionless plasma ions and electrons both drift with the same velocity $\vec{E}x\vec{B}/B^2$ in response to an electric field, so that no net current is produced. However, when the electron or ion to neutral collision frequency is a significant fraction of the

electron or ion cyclotron frequency, current flow along a transverse electric field (Pederson currents) and in the direction $\vec{B}x\vec{E}$ (Hall current) is observed.[74] Collisions with background neutrals cause the electrons and ions to drift with different velocities and directions depending on their relative neutral collision frequencies and cyclotron frequencies and gives rise to net current flow.

Pederson currents close the current loop in the auroral ionosphere. These currents are formed by the flow of ions above 100 km and electrons below 100 km[73] perpendicular to the magnetic field in response to a transverse electric field. The maximum Pederson current flow between the equipotential surfaces formed along the magnetic field lines must occur at an altitude of about 120 km where the Pederson conductivity reaches a maximum.[74] The Hall conductivity is about the same order of magnitude at this altitude[76] and may give rise to auroral currents in the $\vec{E}x\vec{B}$ direction to form the polar electrojet.

The Earth's Magnetosphere from Frank (18)

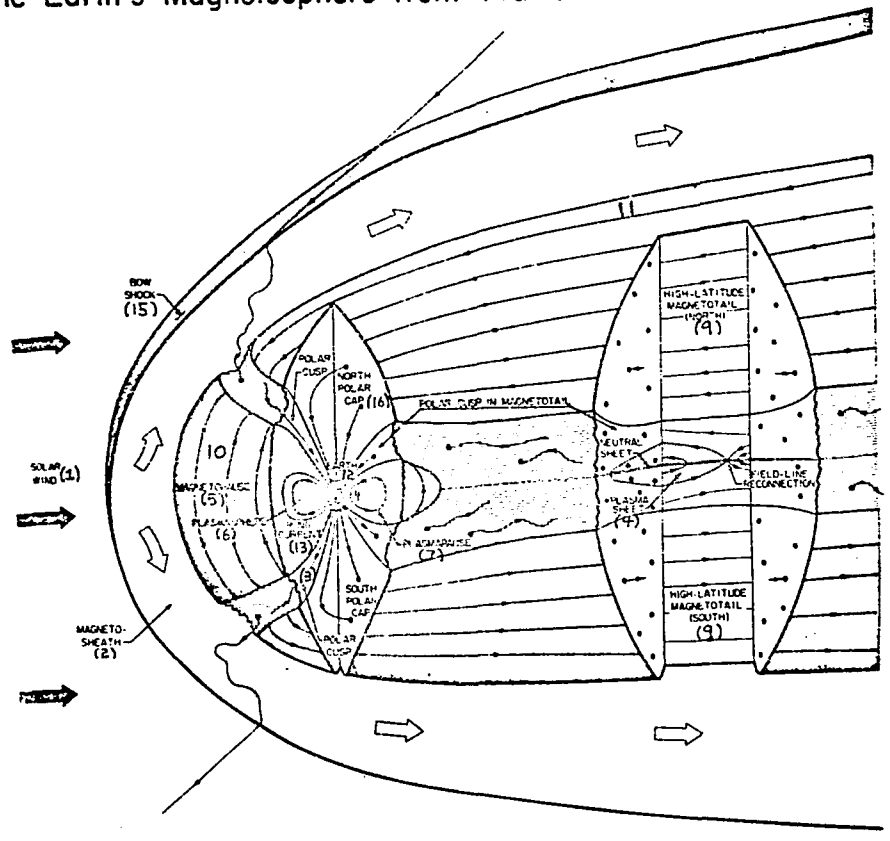

Figure 4

TABLE 1

TYPICAL MAGNETOSPHERE ELECTRON PARAMETERS

Figure Key	Region	Electron Density	Electron Energy	Reference
1	Solar Wind	5 cm^{-3}	100 ev	15,19,14
2	Magnetosheath	10	200	20
3	Polar Cusp	10	200	20,22
4	Plasma Sheet	.3	1,000	20,24,15,21
5	Magnetopause	10	1,000	15
6	Plasmasphere	100	1	15,25
7	Plasmapause			
8	Ionosphere	10^5	.1	24,15
9	High Lat. Tail	10^{-3}	10	25,21
10	Outer Radiation Zone	.1	2,000	20
11	Mantle	1	200	22
12	Auroral Zone	$5/10^5$	2,000/.13	23,27,29
13	Ring Current	1	5×10^3	15
14	Van Allen Belts	10^{-4}	10^6	15
15	Bow Shock	5	13	14
16	Polar Cap	10^{-3}	10^3	26,22

Birkland Current Flow according to Rostoker & Boström Model[30]

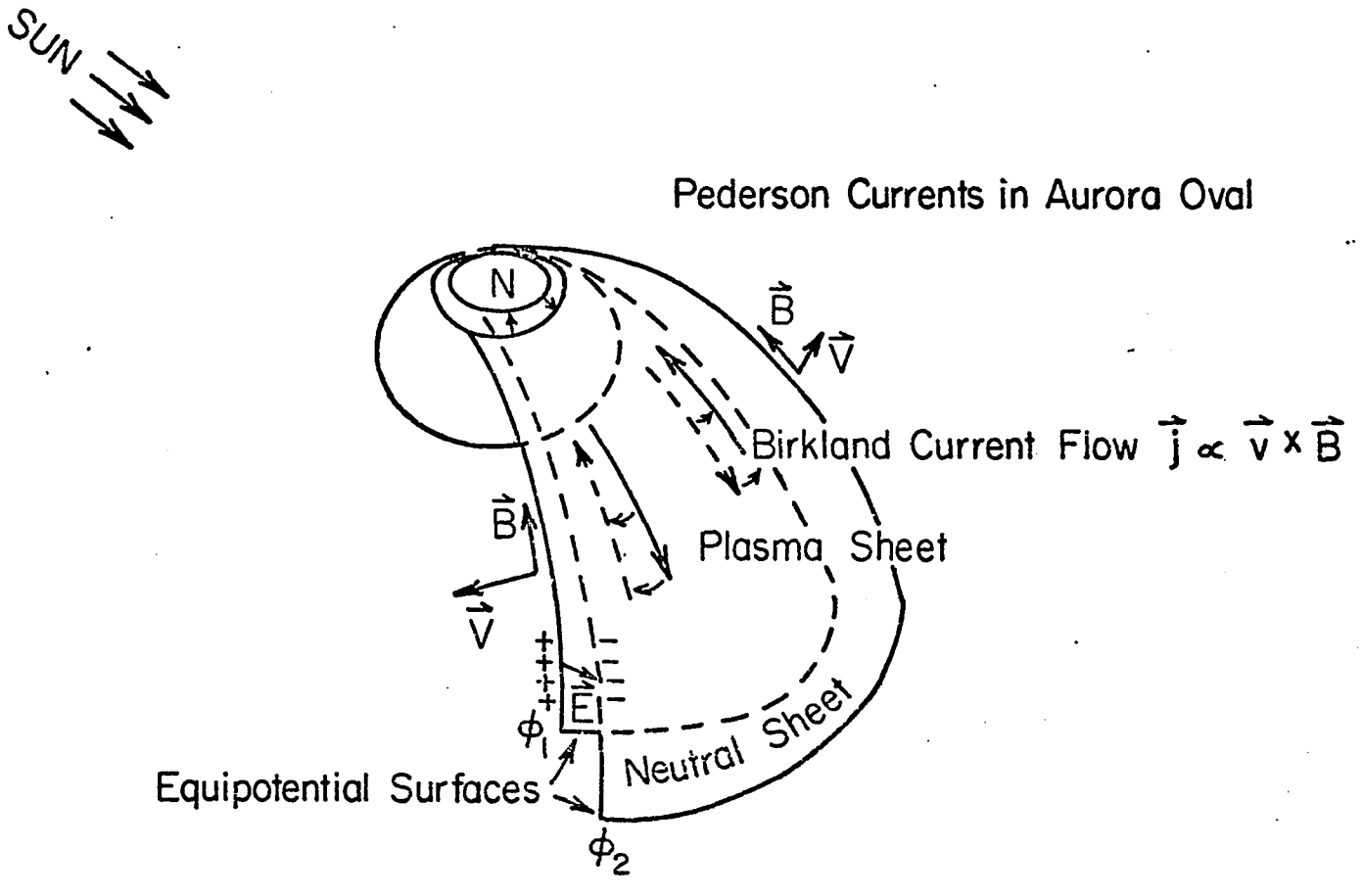

Figure 5

A graph of a near plasma sheet 19Re (earth radii) electron spectra measured by electrostatic analyzers on Vela 3B is shown in figure 6 as taken from Hones et. al.[35] The electron density is ~1 cm^{-3} and the mean energy is 1000 eV. The dotted line is a fit of a Maxwellian energy distribution with a temperature corresponding to kT=695 eV to the satellite data. The spectra shows that the plasma sheet can be a source of high energy auroral electrons convected to the auroral oval by a mechanism such as the Rostoker and Böstrom[30] model described above. The subsequent interaction of the high energy plasma sheet electrons with the ionosphere background and the production of secondaries and degraded primaries might give a spectrum similar to that measured by rocket analyzers such as that shown in figure 2.

Although electrons with plasma sheet distributions have been found in relatively diffuse auroral glows[3 25], electron distributions with peak energies several kilovolts higher than the typical plasma sheet distribution (see figure 2) are measured in bright discrete auroral arcs. Several acceleration mechanisms[13 16 17] have been proposed to increase the energy of plasma sheet particles from typical peak values of .5 to 1 keV found in the plasma sheet to the 2 - 20 keV values measured in discrete auroral arcs (figure 2). An accelerated Maxwellian model proposed by Kaufmann, Walker and Arnoldy[64] is used to model the high energy electron beam that gives rise to the discrete auroral

arcs that we are concerned with here. In this model a Maxwellian distribution of plasma sheet electrons with zero drift velocity is accelerated through an electrostatic potential difference with a resulting gain in energy and the establishment of a high drift velocity. The mechanism for the creation of the electric field is not specified, but the acceleration region is believed to be just above the auroral ionosphere at about 7,000 km.[77 78]

This thesis will analyze a simulation of the interaction of high energy plasma sheet electrons with the ionosphere in and above the auroral oval in terms of the collisionless evolution of the electron velocity distribution function according to the collisionless Boltzmann equation. At this time the models that have been developed have been collisional models based on atmospheric scattering and diffusion equations[7 8 36]. They have not included the electric fields produced by the electrons themselves or the effect of the earth's magnetic field on individual particle motion. This thesis will analyze the effect of self-generated electric fields and the earth's magnetic field on the electron velocity distribution function, but neglect the collisional effects considered in other models. This can be done because the collisionless effects alter the electron distribution function several orders of magnitude faster than the effects of ionospheric collisions above 300 km in the region of interest (see table 3).

Plasma Sheet Electron Spectra From Hones, et al.(35)

VELA 3B, October 8, 1965 at 19 Re
in Plasma Sheet .9 Re above Neutral Sheet

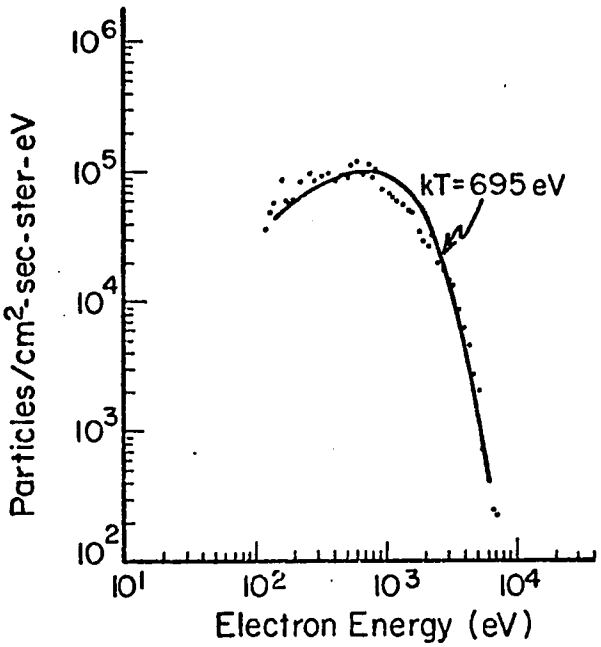

Figure 6

CHAPTER II

TIME EVOLUTION OF THE ELECTRON DISTRIBUTION FUNCTION

2.1 Electron Distribution Function

The electron distribution function $f(\vec{x},\vec{v},t)$ is related to the probability density function for electrons in the six dimensional space spanned by $\vec{x}$ and $\vec{v}$ by a constant equal to the average number of electrons per unit volume[38]. The number of electrons in the velocity and space volume elements $d^3\vec{v}$ and $d^3\vec{x}$ about $\vec{v}$ and $\vec{x}$ at time t is[37]

$$N(\vec{x},\vec{v},t) = f(\vec{x},\vec{v},t)\, d^3\vec{x}\, d^3\vec{v} \qquad (2.1)$$

In the absence of collisions, the distribution function at a later time $t+\delta t$ can be related to the distribution function at time t according to[37]

$$f(\vec{x} + \vec{v}\delta t,\ \vec{v} + \frac{\vec{F}}{M}\delta t,\ t + \delta t) = f(\vec{x},\vec{v},t)\ , \qquad (2.2)$$

where $\vec{F}$ is an external force. However, if collisions are taken into account, forces between electrons not included in $\vec{F}$ act to accelerate the particles during the collision process. Collisional accelerations are taken into account by rewriting equation 2.2 as

$$f(\vec{x} + \vec{v}\delta t,\ \vec{v} + \frac{\vec{F}}{M}\delta t,\ t + \delta t) = f(\vec{x},\vec{v},t) + \frac{\partial f}{\partial t})_{coll}\ \delta t \quad , \qquad (2.3)$$

or using the Taylor's series expansion of $f(t+\delta t)$ as $\delta t \to 0$

$$(\frac{\partial}{\partial t} + \vec{v}\cdot\vec{\nabla} + \frac{\vec{F}}{M}\cdot\vec{\nabla}_v)\ f(\vec{x},\vec{v},t) = \frac{\partial f}{\partial t})_{coll} \qquad (2.4)$$

Equation 2.4 is called the Boltzmann equation and it gives a general description of the time evolution of the electron distribution function.

The collisionless changes in the distribution function investigated here will be those that occur on a time scale much shorter than the time between electron collisions for altitudes above 300 km (see table 3), so that the collisional term of equation 2.4 $(\frac{\partial f}{\partial t})_{COLL}$ is small by comparison with the collisionless terms and can be

neglected. The resulting collisionless Boltzmann equation or Vlasov equation[40] describes the evolution of the electron distribution function for external electric and magnetic fields together with the average fields produced by the electrons on a time scale short by comparison with the collision time. Table 2 shows the electron-molecular nitrogen (N_2) collision frequency ν as a function of electron energy. The collision frequencies were calculated from the experimentally determined values of the "probability of collision" Pc found in Brown[41] for electrons in air. It can be seen from the table that the collision frequency is on the order of

$$\nu(\text{sec}^{-1}) \simeq 2 \times 10^{-7} N(\text{CM}^{-3}) \qquad (2.5)$$

over the energy range 10 to 10,000 eV, where n is the nitrogen density.

The collisionless plasma instabilities studied in chapters 3 and 4 take at most 2,000 plasma oscillation periods (ω_p^{-1}) to evolve the distribution function to its near final form for ionospheric electron densities (see table 5), where[42]

$$\omega_p(\text{rad/sec}) = 2\pi \cdot 9000 \sqrt{N_e(\text{CM}^{-3})} \qquad (2.6)$$

and ne is the electron density.

Table 2

Electron-Molecular Nitrogen Collision Frequency Calculated From the Experimental Results in Brown[41]

Electron Energy E (eV)	Collision Frequency to Nitrogen Density Ratio ν/n $(sec^{-1}\text{-}cm^{-3}) \times 10^{7}$
10	1.71
100	3.36
500	3.63
1,000	1.85
5,000	1.19
10,000	1.68

Therefore, the ratio of collisionless instability development time $\tau(\sim 2{,}000\ \omega_p^{-1})$ to mean electron-neutral collision time $(\tau_c = \nu^{-1})$ is

$$\tau/\tau_c = \frac{2\times10^{-7}\ N(CM^{-3})}{9000\ \sqrt{N_e(CM^{-3})}} \times 2{,}000 \qquad (2.7)$$

$$= 4.4 \times 10^{-8}\ N/\sqrt{N_e} \quad .$$

Table 3 shows the electron and nitrogen density as a function of altitude as given in the Jones and Rees[9] auroral ionosphere model. According to table 3, the collisionless velocity instabilities grow about ten times fastster than the mean collision time (τ_c) at 320 km. The collision and instability times become equal at 200 km and collisions are the dominant mechanism below 200 km. The evolution of the electron distribution function due to collisionless plasma instabilities described by the Vlasov equation occur at least an order of magnitude faster than changes in the distribution function due to collisional processes above 300 km. Therefore, the collision term of equation 2.4 is neglected and the collisionless Vlasov equation is used to describe the evolution of the electron distribution function in the high altitude auroral ionosphere.

Electrons in the magnetosphere and in the high energy beam that gives rise to the aurora are accompanied by an equal density of protons that maintain charge neutrality. Therefore, one should write a Vlasov equation for protons as well as for electrons. The equations are coupled through the calculation of the electric field from Poisson's equation relating the electric field to total charge density. However, this treament neglects the acceleration of positive ions and protons compared with that of the electrons because of their much larger masses (Mp=1837Me). This will exclude low frequency, slow growth instability modes such as the ion acoustic and ion cyclotron modes from the mechanisms that produce changes in the electron distribution function.

The computationally useful distribution function is related to the measurable electron flux in Appendix A. For an isotropic flux and a distribution function written in spherical velocity coordinates (equation A11 in Appendix A)

$$f(v) = \frac{M}{2E}\frac{dJ}{dE} \quad . \qquad (2.9)$$

Figure 7 shows the isotropic electron distribution function calculated from the sounding rocket data of Figure 2 using equation 2.9. It can be shown that all isotropic

distributions are stable to Vlasov velocity space instabilities[43]. Therefore, if an evolution of the electron distribution function is to be observed, the distribution function and flux must be determined for anisotropic distributions as a function of electron velocity direction as well as magnitude.

A typical two dimensional distribution function calculated from rocket flux data at 225 km is shown in figure 8 taken from Kaufmann et. al.[44] The rocket flux data used in the calculation of the distribution function of figure 8 was analyzed as a function of pitch angle α (angle between electron velocity and magnetic field line), so that the distribution function as a function of velocity parallel to ($v_{//}$) and perpendicular to ($v_{\perp}$) the magnetic field is calculated from (equation A13, in Appendix A)

$$f(v_{//}, v_{\perp})\, dv_{//}\, dv_{\perp} = \frac{M}{E \sin \alpha}\, dJ(E,\alpha) \quad , \tag{2.10}$$

where it has been assumed that the flux is isotropic about the magnetic field, and $dv_{//}$ and $dv_{\perp}$ can be calculated from

$$\begin{aligned} v_{//} &= v \cos \alpha \\ v_{\perp} &= v \sin \alpha \end{aligned} \tag{2.11}$$

and the pitch angle and energy range of the data samples. The perspective drawing in figure 8 shows a slight anisotropic peaking in f for electrons with their velocities along the field line. However Kaufmann et. al.[44] have concluded that the distribution function is stable to parallel and perpendicular electrostatic waves.

In chapter 3 of this thesis the evolution of strongly anisotropic beams streaming into a background plasma will be determined from the one-dimensional Vlasov equation. This will be an attempt to simulate the initial interaction of streaming plasma sheet electron beams in the Birkland currents with the background electrons in and above the auroral ionosphere. Chapter 4 will solve the 2 1/2 dimensional (two space and three velocity dimensions) Vlasov equation for anisotropic, high altitude beam-background interactions.

Table 3

Density vs Altitude from Jones and Rees[9]

Altitude	Electron Den.	Nitrogen Den.	Oxygen Den.	Time Ratio
(KM)	$ne(cm^{-3})$	$n_{n2}(cm^{-3})$	$n_o(cm^{-3})$	τ/τ_c
100	1.15×10^{3}	8.55×10^{12}	2.19×10^{11}	1.11×10^{4}
200	7.6×10^{4}	4.92×10^{9}	4.01×10^{9}	.78
320	3.38×10^{4}	1.91×10^{8}	5.99×10^{8}	.14
600	4.95×10^{3}	2.31×10^{5}	1.29×10^{7}	8.0×10^{-3}
1000	1.09×10^{3}	3.86×10	8.99×10^{4}	1.2×10^{-3}

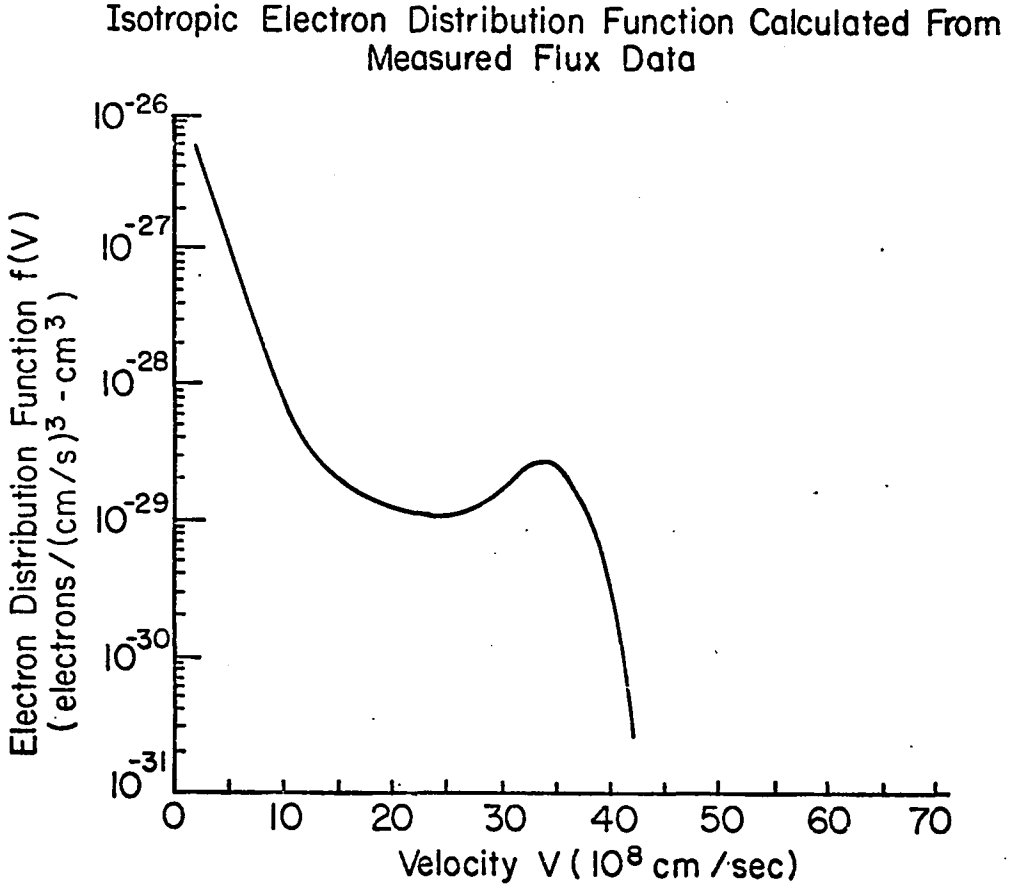
Isotropic Electron Distribution Function Calculated From Measured Flux Data
Electron Distribution Function f(V) (electrons/(cm/s)^3 - cm^3)
10^{-26}
10^{-27}
10^{-28}
10^{-29}
10^{-30}
10^{-31}
0
10
20
30
40
50
60
70
Velocity V (10^8 cm /sec)

Figure 7

Two-Dimensional Aurora Oval Electron
Distribution Function from Kaufmann *et al.*[44]

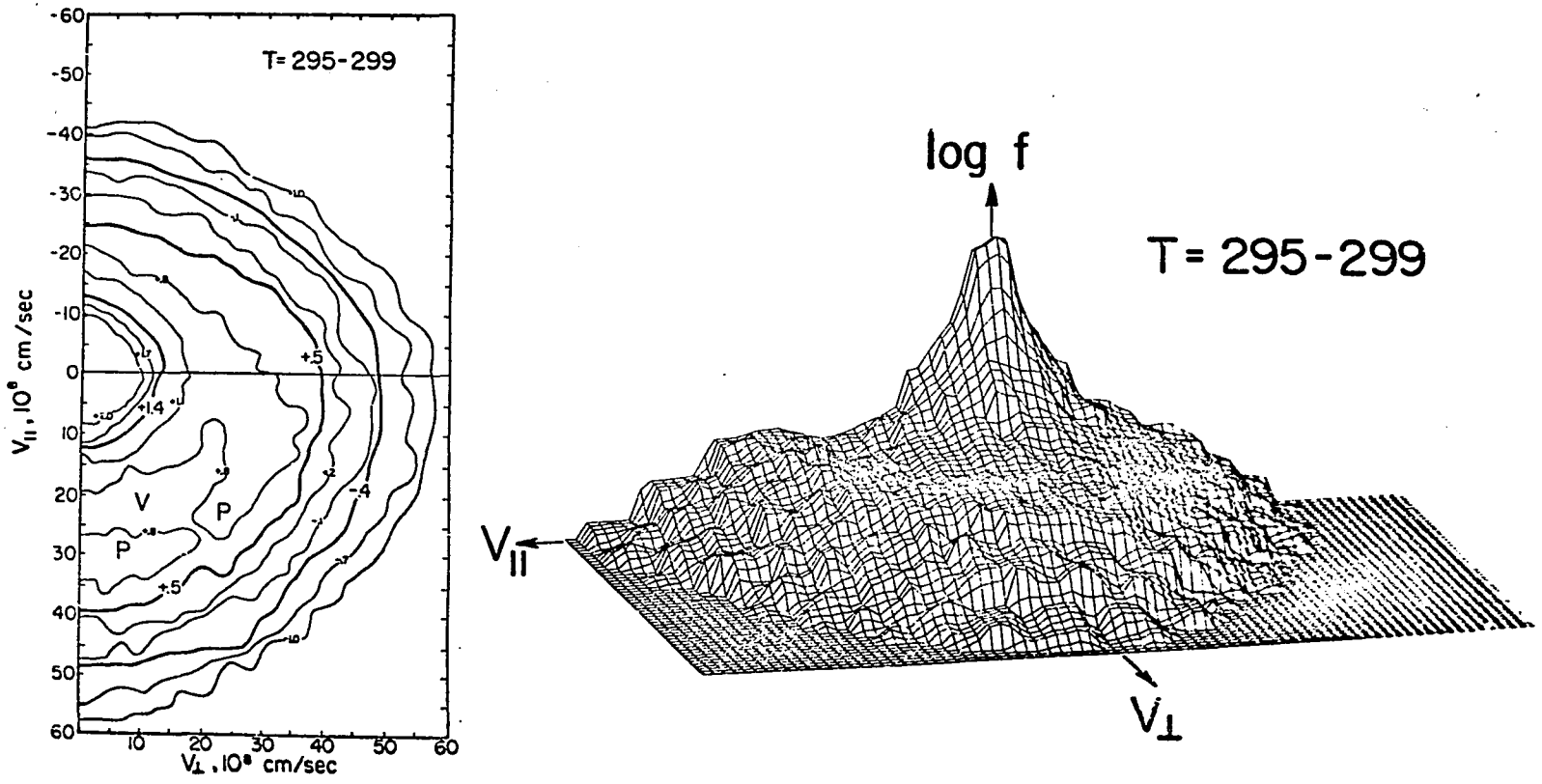

Figure 8

2.2 Coordinate System and Final Equations

The coordinate system used for the solution of the Vlasov equation is shown in figure 9. It has been chosen so that the notation agrees with that found in Cheng[45] whose numerical methods are used in chapters 3 and 4. Notice that $v_\perp$ is in the x, $y_\perp$-plane at an angle ϕ with the x-axis. The velocity coordinate system consists of the B-axis for $v_{||}$ and the x and $y_\perp$ axes which define $v_\perp$ and ϕ. The coordinate space axes are taken along the x, y and z axes. The magnetic field $\vec{B}$ makes an angle θ with the z-axis and is perpendicular to the x, $y_\perp$-plane. This thesis will show the integration of the Vlasov equation for $\theta = \pi/2$ only. In this case the magnetic field is along the y-axis so that $v_{||}$ is along y and the $y_\perp$-axis is in the negative z direction.

The Vlasov and Poisson equations to be solved are

$$\frac{\partial f}{\partial t} + \vec{v}\cdot\vec{\nabla} f - \frac{e}{M}\left(\vec{E} + \frac{\vec{v}\times\vec{B}}{C}\right)\cdot\vec{\nabla}_v f = 0$$

$$\vec{\nabla}\cdot\vec{E} = 4\pi Ne\left(1 - \int_{\substack{\text{all}\\ \text{velocity}}} f(\vec{x},\vec{v},t)\, d^3\vec{v}\right) , \qquad (2.12)$$

Coordinate System

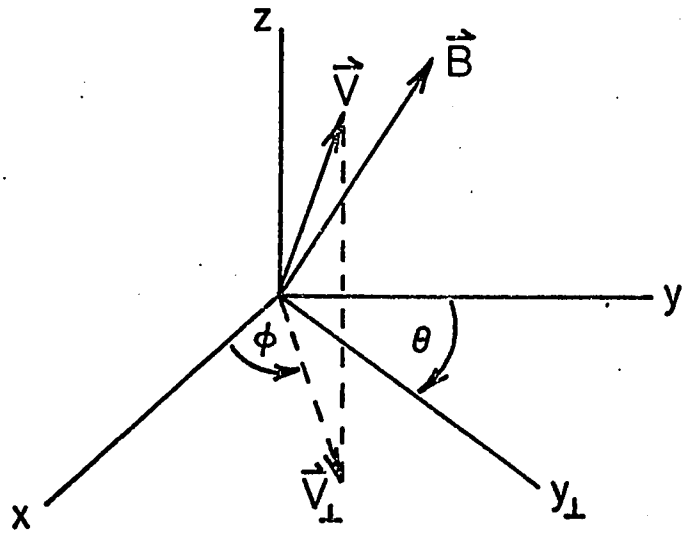

Figure 9

where n is the average electron density and the normalization

$$\int_{\substack{\text{volume}\\ V}} \int_{\substack{\text{all}\\ \text{velocity}}} f(\vec{x},\vec{v},t)\, d^3\vec{x}\, d^3\vec{v} = V \text{ (total system volume)}, \quad (2.13)$$

has been used. The positive term in the charge density in Poisson's equation is the proton or positive ion density, which is always equal to the average positive charge density for the stationary ion assumption made, and the negative term including the integral over f is the electron charge density. The growth of electrostatic instabilities in the plasma will manifest itself by ordered electron charge density variations in space of increasing amplitude giving rise to electrostatic electric fields through Poisson's equation. These electric fields accelerate the electrons to increase the amplitude of the charge density spatial variation still further.

The equations to be used are written in dimensionless form wherein the lengths are measured in Debye lengths (λ_D) and time in plasma periods (ω_p^{-1}) (see Appendix B). In these units the Vlasov and Poisson

equations are

$$\frac{\partial f}{\partial t} + \vec{v}\cdot\vec{\nabla} f - (\vec{E} + \vec{v} \times \vec{\omega}_c)\cdot\vec{\nabla}_v f = 0$$

$$\frac{\partial E_x}{\partial x} + \frac{\partial E_y}{\partial y} = 1 - \int_{\substack{\text{all} \\ \text{velocity}}} f(\vec{x},\vec{v},t)\, d^3\vec{v} \quad , \tag{2.14}$$

where the Poisson equation has been written in the two space variables to be used (x and y), and the electron cyclotron frequency ω_c and dimensionless electric field E are given by

$$\vec{\omega}_c = \frac{e\vec{B}}{MC}\ \omega_p^{-1}$$

$$\vec{E} = \frac{e}{M\lambda_D\ \omega_p^{\,2}}\ \vec{E}(\text{cgs units}) \tag{2.15}$$

The plasma frequency ω_p and Debye length (λ_D) are

$$\omega_p^{\,2} = 4\pi Ne^2/m$$

$$\lambda_D = KT/4\pi Ne^2 \quad , \tag{2.16}$$

from which it can be inferred that the thermal velocity $\sqrt{kT/m}$ is equal to $\lambda_D \omega_p$.

The final dimensionless form of the Vlasov equation referred to the coordinate system shown in figure 9 is (see Appendix B)

$$\frac{\partial f}{\partial t} + (v_\perp \cos\phi \ \frac{\partial f}{\partial x} + v_{||} \ \frac{\partial f}{\partial y}) + \tag{2.17}$$

$$- \frac{\partial f}{\partial v_\perp} \ E_x \cos\phi \ - E_y \frac{\partial f}{\partial v_{||}} \ + \ \frac{\partial f}{\partial \phi} \left(\frac{E_x \sin \phi}{v_\perp} \ + \omega_c\right) = 0 \ ,$$

where the electric field components are to be determined from the solution to the Poisson equation (equation 2.14). Chapter 3 will describe the solution to the one dimensional system of equations which allow a parallel velocity ($v_{||}$) and space (y) dependence only. Chapter 4 gives the numerical solution to the full three velocity and two space

dimensional system described by equation 2.17, but at the cost of using a coarse mesh of fewer grid points upon which the solution is available.

CHAPTER III

ONE DIMENSIONAL BEAM-BACKGROUND INTERACTION

Typical auroral electron spectra observed at rocket altitudes (100-1000 Km) show an approximately isotropic distribution function in velocity space[44 5 10] (see figure 8). The one dimensional projection of the electron distribution function onto the $f(v_{\parallel}, v_{\perp}), v$ plane may show a peaked structure and give instability growth according to the one-dimensional Vlasov theory, but it is well known[43] that isotropic distributions are stable in the three dimensional Vlasov equation description. The one dimensional analogy to the three dimensional problem must be constructed by integrating the distribution function over all nonparallel velocity coordinates. This leads to a stable monotone decreasing one-dimensional distribution function for isotropic distributions, even though an isotropic peak may be present in the three-dimensional

representation.

The one dimensional Vlasov theory can be used to model anisotropic "bursts" occasionally observed[52 53 16] at rocket altitudes. These "bursts" are fluxes of high energy electrons that are strongly field aligned. The flux of electrons streaming along the field is ten times greater[52] than the flux in other directions. The one dimensional model may also be used to model streaming, field aligned plasma sheet electrons as the make their way to the aurora oval (see figure 5) and undergo interactions with background plasmas in space or above the aurora oval.

3.1 Numerical Methods

The one dimensional Vlasov equation (see Appendix B)

$$\frac{\partial f}{\partial t} + v \frac{\partial f}{\partial y} - E_y \frac{\partial f}{\partial v} = 0 \qquad (3.1)$$

is solved using the splitting scheme of Cheng and Knorr[46]. In this method the electrons are assumed to travel at constant velocity for one half a time step. The electric field is then calculated from the distribution function. Next, new electron velocities are calculated by constant acceleration from the electric field over a full time step. Finally, another space shift at the newly calculated velocity is made over one half a time step. The entire sequence of shifting results in a new distribution function f^{N+1} related to the old one f^N by[46]

$$f^{n+1}(x,v) = f^n(x-\Delta t(v+E\Delta t/2),v+E\Delta t) \ , \qquad (3.2)$$

where $t_{N+1} = t_N + \Delta t$ defines n and the electric field is evaluated at $t_N + \Delta t/2$ so that

$$E = E(x_{N+1} - \frac{v\Delta t}{2} , t + \frac{\Delta t}{2}) \ . \qquad (3.3)$$

The path that an electron moving from x_N, v_N to x_{N+1}, v_{N+1} would take during a complete time step is shown in figure 10a, together with the corresponding changes in the distribution function. A Maxwellian velocity dependence and an x space dependence has been sketched in 10b-10d. In 10b the distribution function f^N changes to a new form f* due to an assumed shifting in space of electrons initially at x to the new position $\bar{x}$ (see 10a) while at constant velocity. Figure 10c shows the change in the distribution function f * to f** that results from electrons being instantaneously accelerated to a new velocity $v_{N+1} = v_N + E\,\Delta t$ (see 10a) while at a constant spacial position. The final space shift is shown in figure 10d, and the net result of these shifts is calculated in the sequence of equations to the right. Cheng and Knorr[46] show that the result of these shifts (equation 3.2) is equivalent to an integration of the characteristic equations

$$\frac{\partial x}{\partial t} = v$$

$$\frac{\partial v}{\partial t} = -E(x,t) \qquad (3.4)$$

correct to second order in Δt, and that a solution to the characteristic equations is equivalent to a solution of the

Vlasov equation.

The distribution function is numerically computed on the discrete mesh of grid points shown in figure 11. An expression for the number of grid points is shown under each sketch. The new, shifted distribution functions f* , f** and f^{N+1} (see figure 10) are calculated by interpolating the old distribution function existing prior to the shift to obtain its value for coordinate values specified by the shifting equations:

$$f^{*}(y_i,v_j) = f^{N}(y_i - v_j \frac{\Delta t}{2} , v_j)$$

$$f^{**}(y_i,v_j) = f^{*}(y_i, v_j + E_i \Delta t) \qquad (3.7)$$

$$f^{N+1}(y_i,v_j) = f^{**}(y_i - \frac{v_j \Delta t}{2} , v_j)$$

It can be seen from equations 3.7 that the coordinate values for which f^{N}, f* and f** on the right hand sides of equations 3.7 are to be evaluated lie in between grid points and must be obtained by interpolation.

Interpolation in the y-direction is done by Fourier interpolation using the expansion[47]

$$f(y) = \frac{1}{2} A_0 + \sum_{j=1}^{\frac{N}{2}-1} \left(A_j \cos\left(\frac{2\pi}{L} jy\right) + B_j \sin\left(\frac{2\pi}{L} jy\right)\right) + \frac{1}{2} A_{\frac{N}{2}} \cos\left(\frac{2\pi}{L} N \frac{y}{2}\right) \tag{3.8}$$

where

$$A_j = \frac{2}{N} \sum_{k=0}^{N-1} f(y_k = k\Delta y) \cos\left(\frac{2\pi}{L} jy_k\right) \qquad j = 0, \ldots, \frac{N}{2}$$

$$B_j = \frac{2}{N} \sum_{k=0}^{N-1} f(y_k) \sin\left(\frac{2\pi}{L} jy_k\right) \qquad j = 1, \ldots, \frac{N}{2} - 1 \quad . \tag{3.9}$$

The velocity shifts are done by interpolating f* to find its value at $f^*(y_i, v_j + E_i \Delta t)$ using the natural cubic spline[48] interpolation

$$f(v) = a_i(v-v_i)^3 + b_i(v-v_i)^2 + C_i(v-v_i) + d_i \tag{3.10}$$

where $v_i < v < v_{i+1}$. The coefficients a_i, b_i, c_i and d_i are

determined by fitting the interval between adjacent data points (v_i, v_{i+1}) with a cubic equation of the form shown in 3.10 and matching first and second derivatives with the cubic equations used to fit adjacent intervals. The second derivatives of the cubic equations fitting the first and last interval are assumed to be zero at the first and last point in the natural cubic spline interpolation used here.[49]

The electric field is calculated from Poisson's equation after one half a time step. The equation to be solved is

$$\frac{\partial E}{\partial y} = 1 - \int_{-\infty}^{\infty} f(v,y)dv \qquad (3.11)$$

The velocity integration of the distribution function is done by first fitting the distribution with a cubic spline curve in the velocity coordinate and then integrating the fitted curve. Subroutines from the IMSL[50] program library are used to perform the spline fit and subsequent integration. After integrating the distribution function over velocity , Poisson's equation has the form

$$\frac{\partial E}{\partial y} = 1 - F(y) \quad . \qquad (3.12)$$

This equation is solved by Fourier transform methods[54 55]

by making the substitutions

$$E_\ell(y_\ell = \ell\Delta y,\ t) = \frac{1}{L}\sum_{n=-N/2}^{N/2-1} E_n(t)e^{ik_n y_\ell}$$

$$F_\ell(y_\ell,\ t) = \frac{1}{L}\sum_{n} F_n(t)e^{ik_n y_\ell} \quad , \tag{3.13}$$

where the finite Fourier transform components are given by

$$E_n(t) = \Delta y \sum_{\ell=0}^{N-1} \underline{F}_\ell(y_\ell,t)\ e^{-ik_n y_\ell}$$

$$F_n(t) = \Delta y \sum_{\ell} F_\ell(y_\ell,t)\ e^{-ik_n y_\ell} \quad , \tag{3.14}$$

with $k_N = 2\pi\ n/L$ and an even number of grid points N. These relations assume that the electric field is periodic in a length L, so that the maximum wavelength included in the finite Fourier series fit to the electric field is L. The length of the repetition interval L is equal to $N\Delta y$, where Δy is the spacing between adjacent grid points (see figure 11) and N is the total number of grid points.

The substitution of the finite Fourier series equations 3.13 into Poisson's equation 3.12 leads to

$$\frac{1}{L} \sum_n ik_n E_n e^{ik_n y_\ell} = 1 - \frac{1}{L} \sum_n F_n e^{ik_n y_\ell} \quad . \tag{3.15}$$

The zeroth finite Fourier transform amplitude of $F(v,t)$ is given by

$$F_0(t) = \frac{1}{L} \sum_{\ell=0}^{N-1} F_\ell(y_\ell,t)\, \Delta y$$

$$\xrightarrow[\Delta y \to 0]{} \frac{1}{L} \int_{-\Delta y/2}^{L-\Delta y/2} F(y,t)dy \tag{3.16}$$

$$\longrightarrow \frac{1}{L} \int_0^L \int_{-\infty}^{\infty} f(y,v,t)dvdy$$

$$\longrightarrow 1 \quad ,$$

where the last equation expresses the normalization of the distribution function. The F_0 term of the sum in equation 3.15 is cancelled by the unity positive charge term so that the equation can be solved for the electric field finite Fourier transform coefficients to give

$$E_N = i \frac{F_N}{K_N} \quad , \quad N \neq 0 \tag{3.17}$$

The zeroth electric field Fourier transform coefficient (E_0) is taken to be zero for a periodic potential (V) since

$$E_0 = \sum_{\ell=0}^{N-1} E(y_\ell)\,\Delta y$$

$$\xrightarrow[\Delta y \to 0]{} \int_0^L E(y)\,dy$$

$$\longrightarrow \int_0^L \left(-\frac{dv}{dy}\right) dy \qquad (3.18)$$

$$\longrightarrow v(0) - v(L)$$

$$\longrightarrow 0$$

The final form of the electric field equation is obtained by rewriting the summation in equation 3.13 as

$$E_\ell(y_\ell,t) = \frac{2}{L}\,\text{Real}\left\{\sum_{n=1}^{N/2} E_n\, e^{iK_n y_\ell}\right\} - \frac{E_{N/2}}{L}\, e^{iK_{N/2}\, y_\ell} \qquad (3.19)$$

where $E_{N=0}(t)=0$ has been used. The electric field transform components from equation 3.17 are substituted into 3.19 to give the final form

$$E_\ell(y_\ell,t) = \frac{2}{L}\ \text{Real}\ \left\{ \sum_{n=1}^{N/2} \frac{i\,F_n}{K_n}\ e^{iK_n y_\ell} \right\} -$$

$$\frac{i\,F_{N/2}}{L\,K_{N/2}}\ e^{i\,K_{N/2}\,y_\ell} \qquad (3.20)$$

where $k_N = 2\pi\ n/L$.

The computer program used to carry out the time evolution of the one dimensional distribution function is called VLAS1D, and is listed in Appendix C together with programs to calculate the initial distribution function and electric field.

Splitting Scheme

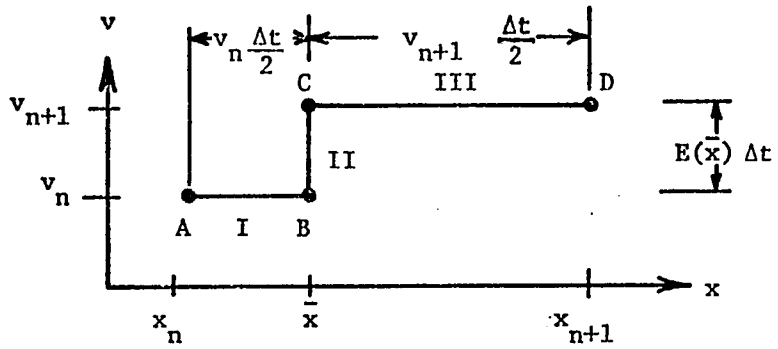

a) Path in Phase Space

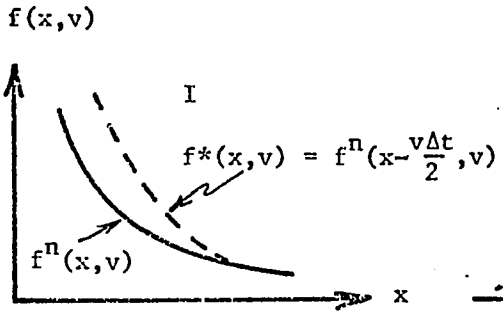

b) Space shift corresponding to I in 10a

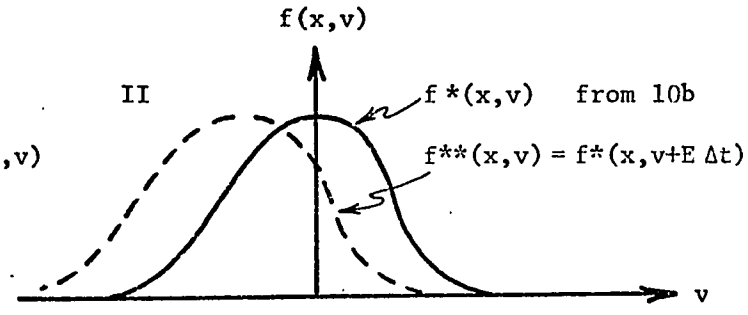

c) Velocity shift corresponding to II in 10a

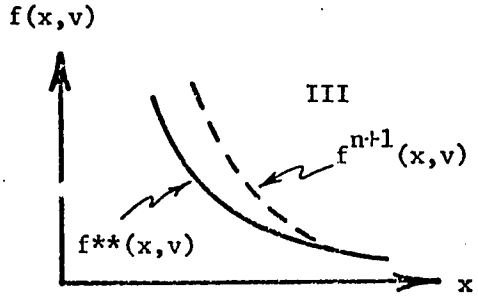

d) Space shift corresponding to III in 10a

e) Equations

$$f^{n+1}(x,v) = f^{**}(x-\frac{v\Delta t}{2},v)$$

$$= f^*(x-\frac{v\Delta t}{2},v+E\ \Delta t)$$

$$= f^n(x-\frac{v\Delta t}{2}-(v+E\Delta t)\frac{\Delta t}{2},\ v+E\ \Delta t)$$

$$f^{n+1}(x,v) = f^n(x-(v+E\ \Delta t/2)\Delta t,\ v+E\ \Delta t)$$

Figure 10

Discrete Grid Points for Numerical Calculation of the Distribution Function

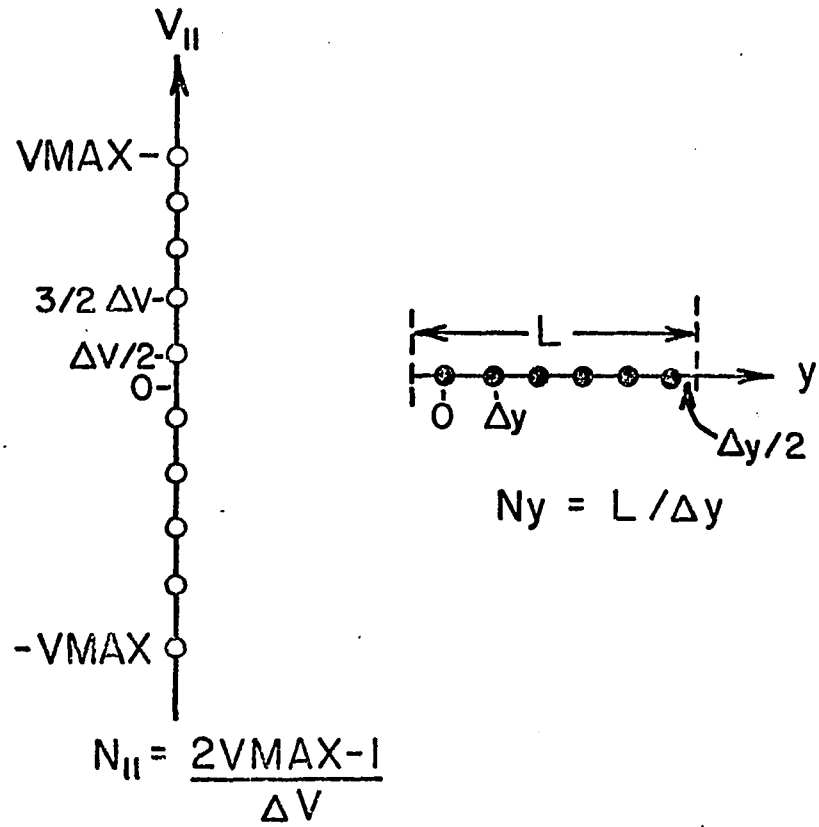

Figure 11

3.2 Test Cases

The time evolution of the distribution function calculated by VLAS1D is compared with the numerical results found in Cheng and Knorr[46] for Landau damping in a Maxwellian plasma and electric field growth in the two stream instability. The parameters used in all of the VLAS1D computer runs are listed in section C.2 in Appendix C. Rows B and C of figures 12 and 13 correspond to cases T2 and T4 in tables C-2 in Appendix C. Row B in figure 14 corresponds to case TS1 in Appendix C.

The initial distribution function

$$f(y,v,0) = \frac{1}{\sqrt{2\pi}} e^{-v^2/2} (1 + A \cos ky) \qquad (3.21)$$

is used as the initial condition for a one dimensional Vlasov equation calculation. The distribution has a Maxwellian velocity dependence with a spacial variation that gives rise to an initial electric field. This can be seen by substituting the initial distribution function into Poisson's equation 3.11. After integrating the distribution function over velocity, Poisson's equation becomes

$$\frac{\partial E_y}{\partial y} = - A \cos ky \qquad (3.22)$$

and the solution is

$$E_y(t=0) = \frac{-A}{K} \sin Ky \qquad (3.23)$$

for $E(y=0,t=0) = 0$.

The time development of the initial distribution function given by equation 3.21 is shown in figure 12 for A=k=.5. The top row of figures is from Cheng and Knorr[46] and the remaining two rows were calculated by VLAS1D (cases T2 and T4). The times are in units of plasma periods (ω_p^{-1}) and the velocity is in units of thermal velocity ($\sqrt{kT/m}$). The spacial dependence has been removed by integrating the distribution function f(y,v,t) over the interval 0 to L to obtain F(v,t). Notice the plateau structure at t=10 in all three runs. This feature is the well known[56 57] result of the Landau damping of an initial electric field by energy exchange with the particles. The electric field accelerates electrons with velocities just below the field phase velocity (shown by the arrow on the lowest velocity axis in the t=0 curve of figure 12) to higher velocities forming a plateau structure.

The filamentation starting at t=30 plasma periods cannot be determined analytically from the analytic quasilinear theory that is used to predict the plateau structure at t=10. It is due to a nonlinear coupling

between the free streaming shifts (figure 10b) and the first mode in the electric field acceleration (equation 3.13 and figure 10c).[46] Nonlinear analytic theory[46] gives a wavelength of $2\pi/kt$ for the filamentation, so that after a long time period the filamentation wavelength becomes too small to be observed (compare t=30 and t=60 curves in figure 12).

The electric field Fourier transform components (see equation 3.13) are shown in figure 13 for the distribution function calculations of figure 12. The first Fourier component E is the amplitude of the time varying term in the sum shown in equation 3.13 divided by the repetition length L with a wavenumber

$$K_1 = \frac{2\pi}{L} \tag{3.24}$$

The value of L, The repetition length, is chosen to make the wave number of the first Fourier component k equal to the initial distribution function spatial term wavenumber k, so that the maximum Fourier wavelength L is equal to the initial distribution function spacial variation wavelength $2\pi/k$. The first Fourier component is the only nonzero component at t=0, since the wavenumber of the corresponding term in the Fourier equation 3.13 is exactly equal to that of the initial electric field k (as shown in 3.23) and no additional Fourier series terms are needed to fit the

initial electric field. Therefore, the initial electric field is (from equations 3.23 and 3.13 with $E_{N\neq \pm 1}=0$)

$$\begin{aligned} E_\ell(y_\ell,0) &= -\frac{A}{K}\sin K y_\ell \\ &= \frac{1}{L}\left(E_1 e^{iK_1 y_\ell} + E_{-1} e^{iK_1 y_\ell}\right) \\ &= \frac{2}{L}\,\text{Real}\,\left(E_1(t=0)e^{iK_1 y_\ell}\right) \end{aligned} \tag{3.25}$$

which implies that

$$\frac{E_1(t=0)}{L} = \frac{A}{2K}\,i \tag{3.26}$$

Figure 13 shows the magnitude of E_1/L at $t=0$ for $A=k=.5$. It can be seen from the graph that the value of E_1/L at $t=0$ is .5 in agreement with that expected from equation 3.26. The frequency of the rapidly oscillating electric field Fourier amplitudes shown in figure 13 can be determined from warm Maxwellian dispersion relation ($\omega = \omega_p$ (1+ 3/2 k^2)).[56]

The distribution function calculations made by VLAS1D are done for two time step sizes and compared in figure 12. The center row of figures is made with $\Delta t=.2$ plasma periods and the lower sequence for $\Delta t=1$. It can be seen that the distribution function sequences are in close

agreement (within 5%) and the VLAS1D calculations compare favorably with the results of Cheng and Knorr[46] shown in row "a" of figure 12 for a time step of t=0.125. However, the electric field calculations shown in figure 13 show that the larger time step for the VLAS1D calculation in row "c" results in a field that gives only fair agreement within an order of magnitude with the more accurate results for smaller time step sizes shown in rows "a" and "b". The VLAS1D calculation of the electric field using the smaller time step size of $\Delta t=.2$ is shown in figure 13b. It shows excellent agreement with the field calculated by Cheng and Knorr[46] shown in row "a". The sum of the electron kinetic energy and electric field energy was calculated by numerical integration for each time frame and found to be conserved to within 1% in the VlAS1D calculation of figure 12b and to within 6% for the calculation of figure 12c. The total number of particles in the system is conserved to within .1% for all calculations.

The computation time required to plot row "b" in figures 12 and 13 by VLAS1D is 22 minutes of CPU time (case T2 in Appendix C) compared with a computation time of 2.5 minutes for row "c" (case T4 in Appendix C). The loss of accuracy in calculating the electric field with the large time step size $\Delta t=1$ used in figures 12c and 13c is acceptable in view of the accurate distribution function calculation still available at this time step size (compare 12b and 12c). Adopting the larger time step size reduces

the required CPU time by a factor of 10 which is an important pratical consideration. Therefore, a time step size of $\Delta t=1$ plasma periods is used for the remaining one dimensional calculations.

The evolution of the electron distribution function from an initially symmetric two-stream distribution is shown in figure 14. The initial distribution function has the form

$$f(x,v,0) = \frac{1}{\sqrt{2\pi}} v^2 e^{-\frac{v^2}{2}} (1 + A \cos Kx) \quad , \qquad (3.27)$$

The calculations for figure 14 were made with A=.05 and k=.5 (case TS1 in Appendix C). The initial value of the electric field Fourier amplitude is expected to be A/2k = .05 from equation 3.26, and this value agrees with the t=0 value for the electric field amplitude shown in figure 14c as calculated by VLAS1D. All of the electric field Fourier components increase in magnitude over the time period t=0 to t=10. This indicates that the initial two-stream distribution is unstable to Vlasov velocity space instabilities and particle kinetic energy is transformed into the energy of the electric field. The increase in particle energy density near zero velocity shown in figure 14a and 14b at t=10 compared with that at t=0 shows that electrons of higher velocity have lost energy to increase the distribution function, and therefore particle density,

at lower velocities. The kinetic energy lost by the particles goes to increase the electric field energy as shown by the increasing electric field amplitudes in figure 14c over the t=0 to t=10 time period. The distribution function magnitudes calculated by Cheng and Knorr[46] shown in figure 14a agree to within 5% with those calculated by VLAS1D with a time step size of $\Delta t=1.0$ shown in figure 14b. The electric field calculation by VLAS1D is a rough order of magnitude reproduction of the corresponding Cheng and Knorr[46] curve (not shown).

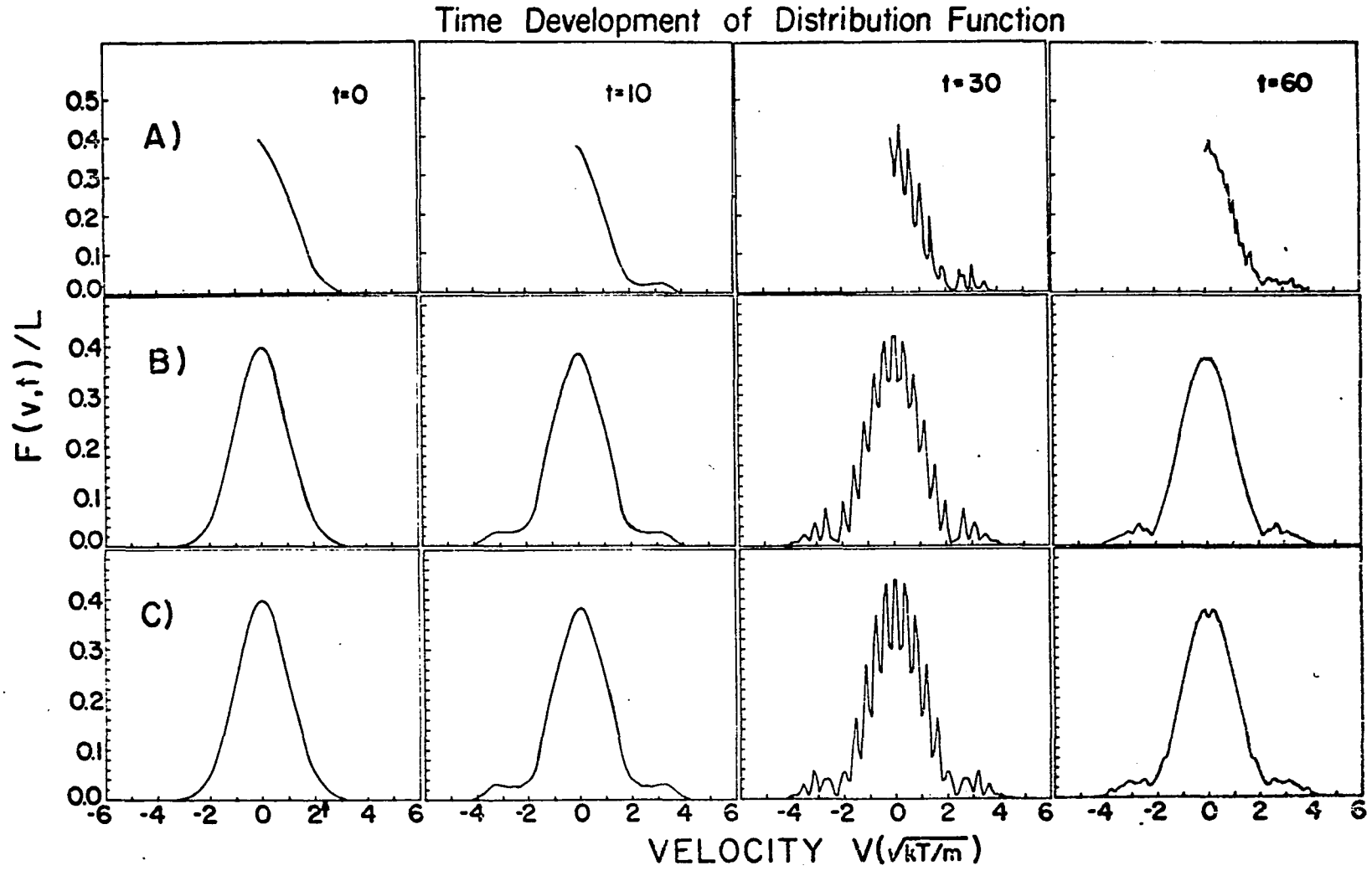
Time Development of Distribution Function
t=0
t=10
t=30
t=60
A)
B)
C)
F(v,t)/L
0.5
0.4
0.3
0.2
0.1
0.0
-6
-4
-2
0
2
4
6
VELOCITY V(√kT/m)

Figure 12

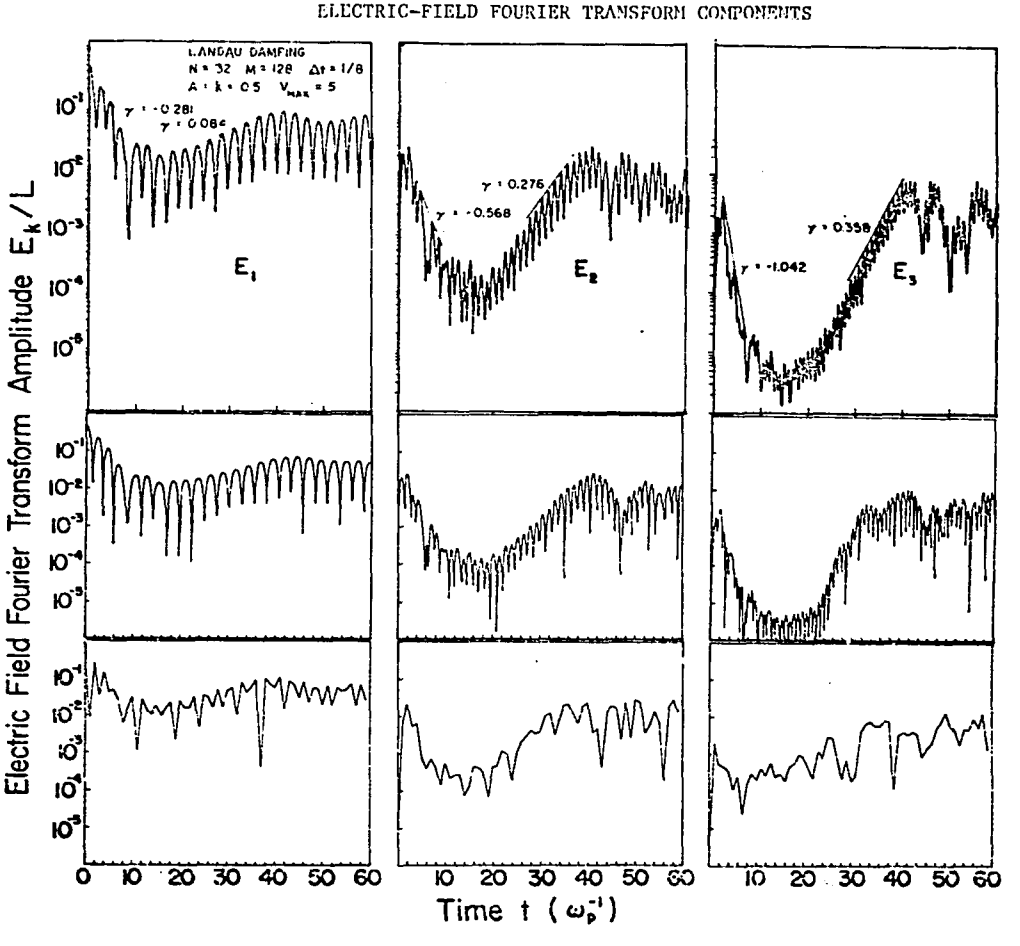
ELECTRIC-FIELD FOURIER TRANSFORM COMPONENTS
LANDAU DAMPING
N = 32 M = 128 Δt = 1/8
A = k = .5 V_MAX = 5
γ = -0.281
γ = 0.084
γ = 0.276
γ = -0.568
γ = 0.358
γ = -1.042
E1
E2
E3
Electric Field Fourier Transform Amplitude E_k/L
Time t (ω_p^-1)

Figure 13

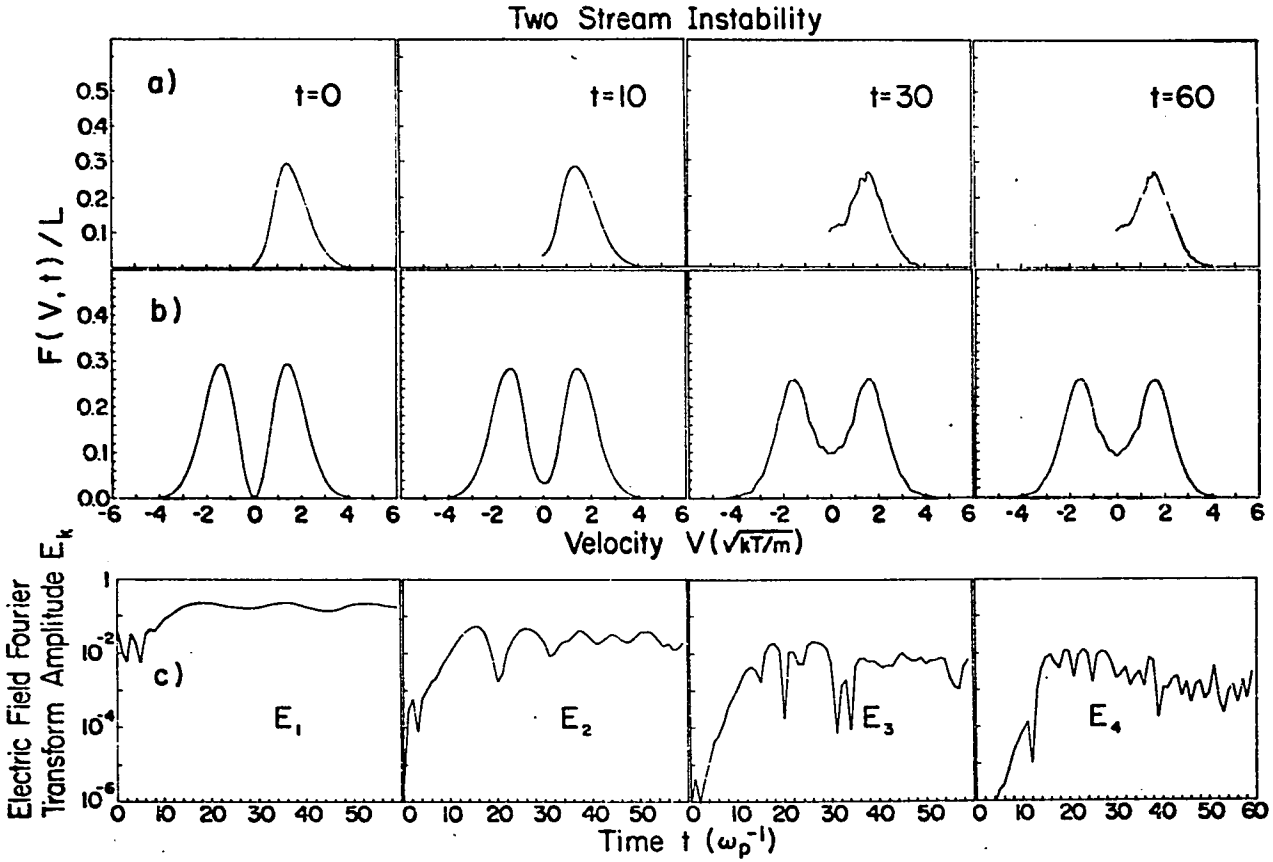
Two Stream Instability
a)
t=0
t=10
t=30
t=60
b)
F(V,t)/L
Velocity V(√kT/m)
c)
E1
E2
E3
E4
Electric Field Fourier Transform Amplitude Ek
Time t (ωp⁻¹)

Figure 14

3.3 Beam Background Interaction

The high energy auroral electrons are modeled by an accelerated Maxwellian distribution such as the beam shown in figure 15. The one dimensional Maxwellian velocity distribution function

$$F(v) = \sqrt{\beta/\pi}\ e^{-\beta v^2} \quad , \tag{3.28}$$

has an average drift velocity of zero and a temperature of $kT = \beta^{-1}$. The integral of the distribution function over velocity is normalized to one by the factor $\sqrt{\beta/\pi}$. The mechanism for the acceleration of solar wind or plasma sheet particles to the kilovolt energies measured in auroral electron distributions and ocassionally plasma sheet distributions (see figures 2 and 6) is not yet understood. However, for the purpose of forming a beam-background interaction model an accelerated Maxwellian distribution is used for the beam.[64] In this beam model it is assumed that electrons traveling in the direction of the acceleration region (electrons with velocity v greater than 0) are accelerated through a potential difference that increases their kinetic energy to

$$\frac{1}{2} Mv'^2 = \frac{1}{2} Mv^2 + \frac{1}{2} Mv_0^2 \quad , \quad v > 0 \tag{3.29}$$

where $1/2mv_0^2$ is the gain in kinetic energy. It can be seen from 3.29, that the minimum value of the electron velocity v' after acceleration is v_0. The distribution function describing the accelerated electrons Fa is related to the distribution function prior to acceleration, F in equation 3.28, according to

$$F_a(v')dv' = F(v = \sqrt{v'^2 - v_0^2}) \quad dv \quad , \tag{3.30}$$

where equation 3.30 expresses conservation of particles. The substitution of the expression for F(v) from equation 3.28 into equation 3.30 leads to

$$F_a(v')dv' = \sqrt{\beta/\pi} \quad e^{-\beta(v'^2-v_0^2)} \left(\frac{v'}{\sqrt{v'^2-v_0^2}} \quad dv'\right) \quad , \tag{3.31}$$

where the term in parentheses is equal to dv. In order to simplify the beam model, the distribution function expansion for electron velocities greater than v_0 is used. In this case the v' in the numerator and denominator cancel to first order in $(v_0/v')^2$, and the distribution function becomes

$$F_a(v')dv' = A\, e^{-\beta(v'^2-v_0^2)} \, dv' \quad , \quad v' > v_0 \quad , \tag{3.32}$$

where A is the new normalization constant required to insure

that the integral of the distribution function over all velocity is equal to one.

The time evolution of the electron distribution function for an electron beam with a density of .2825 that of the background electron density is shown in figure 15a. The beam temperature was chosen to correspond to the 640 eV beam width calculated by Kaufmann et. al.[58] from sounding rocket measurements in an auroral plasma. A background temperature of 10 eV is used in the calculation of the background distribution function from equation 3.28. The complete set of parameters used for the calculations made in figures 15 and 16 are shown in Appendix C (Rows a, b, c and d correspond to cases AM2, AM3, AM20 and AM4 in Appendix C.) Calculations for beam to Maxwellian background ratios (n_b/n_m) of .02825, .002825 and 0.2825×10^{-5} are shown in rows b, c and d of figure 15.

The electric field Fourier transform coefficients defined in equation 3.13 corresponding to the distribution function calculations of figure 15 are shown in figure 16. The electric field grows from a value of 10^{-2} to about .5 for the Fourier components shown in rows a and b. The energy required for the growth in the electric field comes from the kinetic energy in the high energy electron beam electrons. For example, the total kinetic energy of the electrons as determined by integration of the distribution function decreases by a factor of two over the time interval

from t=20 to t=30 in the sequence shown in figure 15a, while the corresponding electric field amplitudes shown in figure 16a grow by from 1 to 3 orders of magnitude. The kinetic energy in the time interval t=30 to t=60 in the row b sequence of figure 15 decreases by one third as the corresponding electric field amplitudes grow by several orders of magnitude over the same time interval.

The growth rate of the electric field can be estimated from the linear Vlasov theory[59 60] or the cold plasma, hydrodynamic theory[61]. The choice of the appropriate theory for estimation of the growth rate depends on the ratio of the beam-background density n_b/n_m and the beam velocity v_0. Mikhailovskii[62] gives the criteria

$$(N_b/N_e)^{1/3} \; v_0 \gg 1 \qquad (3.33)$$

for the growth of the hydrodynamic two stream instability in a low beam density plasma ($n_b/n_e \ll 1$), where n_e is the total beam plus background electron density. If 3.33 is not satisfied, then the growth rate is determined from the kinetic theory for a warm plasma. Table 4 shows the appropriate analytical expression for the resonant growth rate for each of the distributions shown in figure 15.

The analytical growth rates γ are shown in table 4. The electric field growth rates for a beam density to background density ratio of .2825 range from .14 to .533 in the electric field calculations made by VLAS1D shown in figure 16a. This is in good agreement with the analytical order of magnitude estimate shown in row one of table 4 of .5 for equal densities in the beam and background. The analytical growth rate of .2 for a density ratio of .02825 shows fair agreement with the .06 to .16 growth rates calculated by VLAS1D and shown in figure 16b. However, the hydrodynamic analytical theory predicts a growth rate of .1 for a density ratio of .002825 and no growth is seen in the electric field calculation for this ratio shown in figure 16c over a time period of 60 plasma periods . This is probably due to the increasing time lag between the initial perturbation and the onset of growth with decreasing beam to background density ratio. Both the linear kinetic and the hydrodynamic theories require initial plasma waves of finite amplitude to exist throughout the plasma. The plasmas described by the distribution functions shown in figure 15 are perturbed with an initial electric field corresponding to the first Fourier components shown in figure 16. However, it may take some time for plasma waves at other wave numbers to develop throughout the plasma by a coupling between the beam kinetic energy and electric field energy. In order for the instability to grow, there must be time for the electric field to cause velocity perturbations in the

beam electrons which in turn must cause particle acceleration leading to charge bunching to further enhance the electric field.

It can be seen from figure 16 that the time required for the creation of density periodicity and the associated electric fields of sufficient amplitude to give growth according to the linear Vlasov or hydrodynamic theory is about 20 plasma periods for a density ratio of .2825 and 30 plasma periods for a density ratio of .02825 (compare 16a with 16b). This is probably because the higher density of background electrons relative to beam electrons, the less effective the beam electrons are in creating the ordered periodic motion in background particles required for the creation of an electrostatic electric field throughout the plasma. The absence of growth in the electric field shown in figure 16c for a beam to background density ratio of .002825 may be due to the increased time required for the beam electrons to order the motion of the background and attain a coupling between their velocity perturbations and the electric field required to give growth according to the linear Vlasov or hydrodynamic theory.

The low growth rate of 5.7×10^{-4} calculated from the linear Vlasov theory for a density ratio of $.2825 \times 10^{-5}$ indicates that no growth should be expected before about 1.77×10^{3} plasma periods. The numerical results of Papadopoulos[63] show that a time of 5,000 plasma periods is

required for electric field energy growth to maximum value for a beam-background density ratio of $3x10^{-2}$. Table 5 shows the characteristic growth time τ equal to the time required for the electric field to grow to its maximum value for each of the sequences shown in figure 15. The time in seconds is obtained by dividing the times shown in figure 16 by the plasma angular frequency (ω_p). The electron density n used in the calculation of the plasma frequency ω_p is determined from the beam-background density ratio n_b/n_m and a typical auroral beam density of 1 cm^{-3} [58]. The distances (y_c) that the 2 keV ($5.37x10^4$km/sec) beams in figure 15 travel during the characteristic instability growth times are also shown in table 5. The characteristic growth times for density ratios of .002825 and $.2825x10^{-5}$(rows c and d of figure 15 and 16 and table 5) were estimated from the numerical results presented by Papadopoulos [63]and the analytical calculations shown in table 4.

The distance travelled by 2 keV accelerated Maxwellian electrons passing through a Maxwellian background before dissipation of the one-dimensional beam peak by assimilation into the background is less than 100 km or about .01 earth radii (Re) according to table 5. The distance that plasma sheet particles travel in making their way to the aurora oval in the Rostoker and Boström[30] model is from 5 to 15 earth radii. Therefore, it can be concluded that streaming anisotropic plasma sheet electrons must not

pass through a background plasma of zero drift velocity if they are to reach the aurora oval with an anisotropic field aligned distribution function. If background plasmas of greater than 100 km in extent are encountered, the anisotropic electron beam will lose energy to an electrostatic electric field in the growth of longitudinal Langmuir waves according to the one dimensional model presented here. The beam electrons will eventually be assimilated into the background and the electric field will begin to decay by Landau damping (see figure 13) raising the plasma temperature.

Streaming plasma sheet electrons encounter background plasmas of sufficient density (~1 cm^{-3}) to extinguish the one-dimensional, anisotropic beam peak through energy loss in Langmuir oscillations. However, quasi-isotropic high energy electrons are measured by rocket detectors at ionospheric altitudes of 200 km (see figures 7 and 8). In view of the fact that isotropic distributions are stable to Vlasov instabilities[43], that isotropic high energy electrons are measured at low altitudes and that a high energy anisotropic beam streaming into the ionosphere would dissipate within one hundred kilometers of travel, it is suggested that the high energy beam is pitch angle scattered by three dimensional velocity instabilities within a hundred kilometers of their first encounter with background electrons from the aurora oval. If the anisotropic beam does not scatter to become quasi-isotropic

such as the electrons represented by the distribution shown in figure 8, they will lose energy to the background and be assimilated within a few hundred kilometers of travel. Occasionally an anisotropic strongly field aligned electron beam "burst" is measured[52 53 16]. These "bursts" are short lived lasting at most a few seconds[52]. They may be due to acceleration by a local electric field in the ionosphere within a hundred kilometers of the observation point (otherwise they would decay or be pitch angle scattered by the time they reach the rocket), or the "burst" electrons may have penetrated into the ionosphere through a region of exceptionally low elecron density. This low density region would be a short lived hole in the region above the ionosphere where the electrons are usually pitch angle scattered.

A beam of "burst" electrons in the ionosphere of the auroral oval encounters an isotropic power law distribution of secondary electrons produced by ionization of ionospheric constituents. According to Banks et. al.[7] and Strickland et. al.[8] the differential electron flux (dJ/dE) should be proportional to the inverse square of the energy (E^{-2}) in the energy range from 10 to 200 eV. Measured secondary distributions show an E^{-1} dependence[13 16 63] over this energy range (see figure 2). According to Papadopoulos, the difference may be attributed to the growth of an electric field with a phase velocity equal to the beam velocity and parametric coupling to lower phase velocity waves at the

velocities equal to the low energy secondary electron velocities. The low phase velocity waves would accelerate electrons to higher energies reducing the flux dependence on energy from E^{-2} to E^{-1} through a process similar to the Landau damping of a high initial electric field shown in figure 12 that leads to the formation of a plateau structure. The growth of an electric field through the beam instability described above depends on the existence of an anisotropic electron beam "burst" streaming along the magnetic field lines. The more typical quasi-isotropic high energy distributions measured are stable to parallel Langmuir waves[44 43] and will not lead to electric field growth. Electrons in the beam travel a few kilometers through the background before the instability can develop (see table 5) so that uniform plasma regions of at least several kilometers extent must exist in the auroral ionosphere in order to make the infinite extent one dimensional plasma model used here applicable.

The one dimensional distribution function used to model the three dimensional differential electron flux is determined from the relation between number density (dn) and the electron distribution function $f(v_x, v_y, v_z)$ (see eq. A-7, in Appendix A)

$$dN\ dv = (f(v_x, v_g, v_z) dv_x\ dv_y\ dv_z)\ x$$

$$\left(\frac{dA \cos\theta}{4\pi r^2}\right)\ (r^2\ d\Omega\ dt) \qquad (3.33)$$

and the definition of differential electron flux dJ/dE (see equation A-1, Appendix A)

$$\frac{dJ}{dE} = \frac{dN\ dv}{(dA\ \cos\ \theta)\ dt\ dE\ d\Omega} \ , \tag{3.34}$$

where dV is the volume element of the electron source, dA cos(θ) is the surface area normal to the flux through which dn dv particles pass in a time dt and $d\Omega$ is the solid angle subtended by the source volume (dV) at the normal area (dA cos(θ)). The expression for the equations 3.33, 3.34 and $dJ/dE=A\ E^{-2}$ is

$$f(v_x,v_y,v_z) = \frac{4\ \pi\ A}{n}\ v_y^{-4}\ \delta(v_x)\ \delta(v_z) \ , \tag{3.35}$$

where the x and y velocities are taken to be zero in the one dimensional model used here. The constant is determined from the normalization

$$\int_{v_{min}}^{\infty} f(v_y)\ dv_y = N_b/N_e \tag{3.36}$$

which sets the secondary background electron density equal to the high energy beam density (n_b). The minimum secondary background velocity v_{min} was chosen to be equal to the velocity of 10 eV electrons, and the final expression

for the one dimensional velocity distribution function for secondary background electrons is

$$F(v_y) = (N_b/N_e) \frac{3\, v_{min}^3}{v_y^4} \quad . \tag{3.37}$$

Figures 17, 18 and 19 show the interaction between a high energy electron beam and background consisting of a 10 eV Maxwellian and the power law secondaries represented by the distribution shown in equation 3.37. The Maxwellian background was chosen to have a density 10^5 times that of the secondaries and beam electrons (see table C-1 in Appendix C) roughly corresponding to the relative density observed in the auroral ionosphere[9]. Auroral ionosphere models[9] show a ~0.2 eV Maxwellian background mean energy. However, a value of 10 eV was used to give more velocity grid points in the Maxwellian background. The ratio of the background temperature to the beam temperature (corresponding to 640 eV) remains low with a value of 0.016. The full velocity distribution function used to initiate the VLASID calculations shown in figures 17, 18 and 19 is

$$F(v_y) = \frac{N_n}{N_e} \sqrt{\frac{\alpha_1}{\pi}}\; e^{-\alpha_1 v_y^2} + \frac{N_b}{N_e} \sqrt{\frac{\alpha_2}{\pi}}\; e^{-\alpha_z v_y^2} +$$

$$\begin{cases} 3\, N_2/N_e \quad \dfrac{v_{min}^2}{v_y^4} & , \quad |v_y| > v_{min} \\ 0 & , \quad \text{otherwise} \end{cases} \tag{3.38}$$

where the value of v_{min} is chosen to correspond to an electron energy of 10 eV.

The distribution function shows almost no change over the time period t=0 to t=120 plasma periods shown in figure 17. According to the numerical results of Papadopoulos[63] and analytic calculations from linear theory (table 4) several thousand plasma periods are required for a beam instability to give electric field growth with a phase velocity equal to the beam velocity. The magnitude of the first two Fourier component electric field amplitudes are shown in the lower right of figure 17. They show no time averaged growth over the time period from t=0 to t=60 plasma periods. Little change in the distribution function is observed over the initial 120 plasma periods of interaction. However, some change has occurred over the interval t=0 to t=10 plasma periods. Electrons with a velocity of about 18 (in units of thermal velocity $\sqrt{kT/m}$) indicated by the arrow have been accelerated to higher velocities (cross hatch) by the electric field.

The distribution function sequence shown in figure 18 was started with a high initial electric field with a phase velocity equal to the velocity of the beam peak (v=20 in figure 18). The initial electric field amplitude is taken as E =0.5 (see table C-1 in Appendix C) and an upcoming beam of electrons reflected or mirrored by a strong

magnetic field at lower altitudes is also included in the model (beam on left hand side of figure 18). After ten plasma periods, electrons from the sharp peak of the beam lose energy to the electric field and appear in the lower velocity range indicated by the cross hatch in the t=10 graph in figure 18. Electrons with velocities just below the beam peak and phase velocity of the initial electric field are accelerated into the cross hatch region leaving a deficiency of electrons.

The t=60 curve shows an acceleration of electrons formerly in regions 1 and 2 to higher velocities. The dotted line shows the outline of the t=0 distribution function. The peaked structure between -15 and -18 velocity units occurs at velocities corresponding to the phase velocities of the electric field Fourier components used in the Fourier series representation of the electric field. Computation time limitations prevented the use of more Fourier series terms (15 were used) in the electric field calculation. Additional electric field Fourier components may have resulted in a continuum structure over the region where peaking occurs. The peaked structure on the right hand side of the t=60 curve of figure 19 has been replaced with a smooth curve through the peaks (open circles). The net result of the particle accelerations leading to the distribution depicted in the t=60 curve of figure 18 is a transfer of electrons with velocity magnitudes less than 5 (which corresponds to an energy of 125 eV according to the

energy axis shown below the t=150 curve in figure 18) to velocities in the range 5 to 16 velocity units (corresponding to an energy range from 125 to 1,280 eV). It can be seen from the t=10 curve that the loss of energy by particles in regions 4 and 5 of the t=60 curve increases the population density in region 3 of the t=60 curve and the hatched area of the t=10 graph.

The t=150 curve of figure 18 shows a further evolution for the distribution function. More electrons of low energy from region 2 have been accelerated to higher energies. This acceleration is caused by growing low phase velocity electric fields that are coupled to the initial electric field with a phase velocity equal to the velocity of electrons in the beam peaks[13 16 63]. The electric field Fourier component amplitudes over the range of phase velocities indicated by the solid bar on the velocity axis of the t=150 curve of figure 18 are shown in figure 19. The electric field components have phase velocities between 2 and 4 velocity units (corresponding to an electron energy range of 20 to 80 eV). It can be seen from figure 19 that all of the electric field amplitudes shown have grown by an order of magnitude over the t=120 to t=180 time period. These low phase velocity components show an essentially constant magnitude over the time period t=0 to t=60 plasma periods (not shown) so that it can be concluded that it takes about 60 plasma periods for the parametric coupling between the initial high phase velocity electric field and

the lower phase velocity electric field modes to begin to develop.

A smooth curve connecting the distribution function peaks (open circles) in the velocity range 4 to 18 has been drawn in the t=150 curve of figure 18. Comparison of this smooth curve with the initial distribution function (shown as a dotted line) emphasizes the transfer of electrons from the low velocity region between 3 and 6 velocity units (corresponding to an electron energy range of 45 to 80 eV) to higher velocities and energies. This increase in electron density at higher energy at the expense of the low energy electron density and the growth of low phase velocity electric field components shown in figure 19 agrees with the general result expected from the parametric coupling model proposed by Papadopoulos[13 16 63].

The slope of the evolved secondary distribution in the energy range 45 to 180 eV (3 to 6 velocity units) is lower in magnitude than the initial distribution (dotted line) in agreement with particle simulation results obtained by Papadopoulos and Rowland[65] over the energy range 11 to 110 eV. They report a "break" in the slope of the distribution function to higher magnitudes below 5 eV for an initial electric field amplitude of 0.5 (in the dimensionless units described in Appendix B equation B-4). The initial electric field used to start the sequence shown in figure 18 was 0.5 (see table C-1, Appendix C, run AM27).

It can be seen from the t=150 curve of figure 18 that a sharp "break" is present at the 45 eV (3 velocity units) intersection of the smooth curve through the peaks structure and Maxwellian background. A sharp "break" in the distribution function to higher slope magnitudes below 20 eV was also measured by Feldman and Doering[11] in sounding rocket data taken at 155 km.

The alternately dashed and dotted line in the t=150 curve of figure 18 is the electron distribution function measured in sounding rocket flight 18:165 and displayed in figure 7. The scale for this distribution is located on the right of the figure. The slope of the measured distribution is lower in magnitude than the smooth curve drawn through the peaks of the evolved distribution over the energy range of 45 to 320 eV (3 to 8 velocity units). The initial distribution in this energy range (dotted line) is equal to the sum of a 10 eV Maxwellian background and power law secondaries with a slope corresponding to a flux differential flux given by

$$\frac{dJ}{dE} \alpha E^{-2} , \qquad (3.39)$$

which is determined from ionospheric scattering calculations.[78] However, a flux dependence of

$$\frac{dJ}{dE} \propto E^{-1} \tag{3.40}$$

is found in sounding rocket data over the energy range 50 to 500 eV (see figure 2). The initial distribution (dotted line) with ionospheric scattering secondaries and an E^{-2} flux dependence is evolved by means of the collisionless Vlasov equation (solid line) to closer agreement with a distribution function corresponding to the E^{-1} measured (see figure 2) energy dependence of the flux over the energy range 45 to 320 eV represented by the alternately dashed and dotted distribution function curve. Therefore, it can be concluded that collisionless Vlasov instabilities can be responsible for the discrepancy between ionospheric scattering calculations[7 8] of the secondary electron distribution function and that obtained from sounding rocket data (figure 2). However, in order for the collisionless model to account for the measured energy dependence of the secondary electron flux, a high phase velocity electric field[63 16 65] must be created by the beam instability resulting from an anisotropic streaming beam of high energy electrons in the auroral ionosphere. Because anisotropic high energy electron "bursts"[52 53 16] are measured infrequently and the typical electron distribution measured (figure 8)[44 5 10] is isotropic and stable to Vlasov

instabilities[43], it must be shown that high phase velocity electrostatic waves are a regular feature of the typical auroral ionosphere and that anisotropic beams occur with sufficient frequency and spacial extent to account for the measured differential electron flux by means of the collisionless plasma wave instability model.

Table 4

Analytical Electric Field Growth Rates from Mikhailovskii[62]

n_b/n_m	v_o	$(n_b/n_e)^{1/3}v_o$	Growth Rate γ	Equation in Reference 62
.2825 (row a of figs. 15 and 16)	3.51	Does not apply	.05	1.45
.02825 (row b)	7.66	2.33	$\frac{3}{2^{4/3}}(n_b/n_e)^{1/3} = .2$	3.6
.002825 (row c)	15.694	2.22	" $= .1$	3.6
$.2825\times10^{-5}$ (row d)	20.0	.283	$1/2(n_b/n_e)v_o^2 = 5.7\times10^{-4}$	3.12

Table 5

Characteristic Growth Times (for a beam density of $1cm^{-3}$)

Density Ratio (n_b/n_m)	Background Density $n_m(cm^{-3})$	Growth Time $\tau(\omega_p^{-1})$	Plasma Frequency ω_p(rad/sec)	Growth Time τ(sec)$=\tau/\omega_p$	Distance y_c(KM)
.2825 (row a)	3.54	30	$1.1x10^5$	$2.7x10^{-4}$	15
.02825 (row b)	3.54x10	44	$3.4x10^5$	$1.3x10^{-4}$	7
.002825 (row c)	$3.54x10^2$	$2x10^3$	$1.1x10^6$	$1.8x10^{-3}$	97
$.2825x10^{-5}$ (row d)	$3.54x10^5$	$2x10^3$	$3.4x10^7$	$5.9x10^{-5}$	3.2

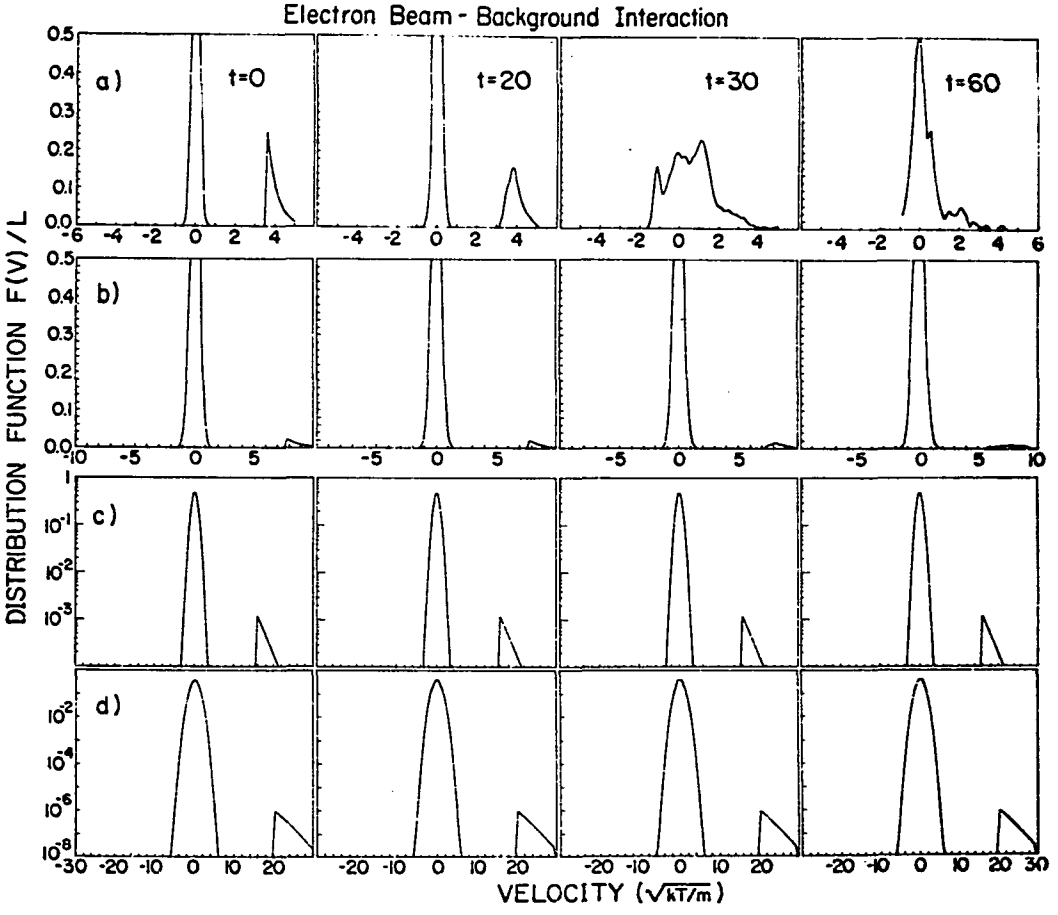
Electron Beam - Background Interaction
a)
t=0
t=20
t=30
t=60
b)
c)
d)
DISTRIBUTION FUNCTION F(V)/L
VELOCITY (√kT/m)

Figure 15

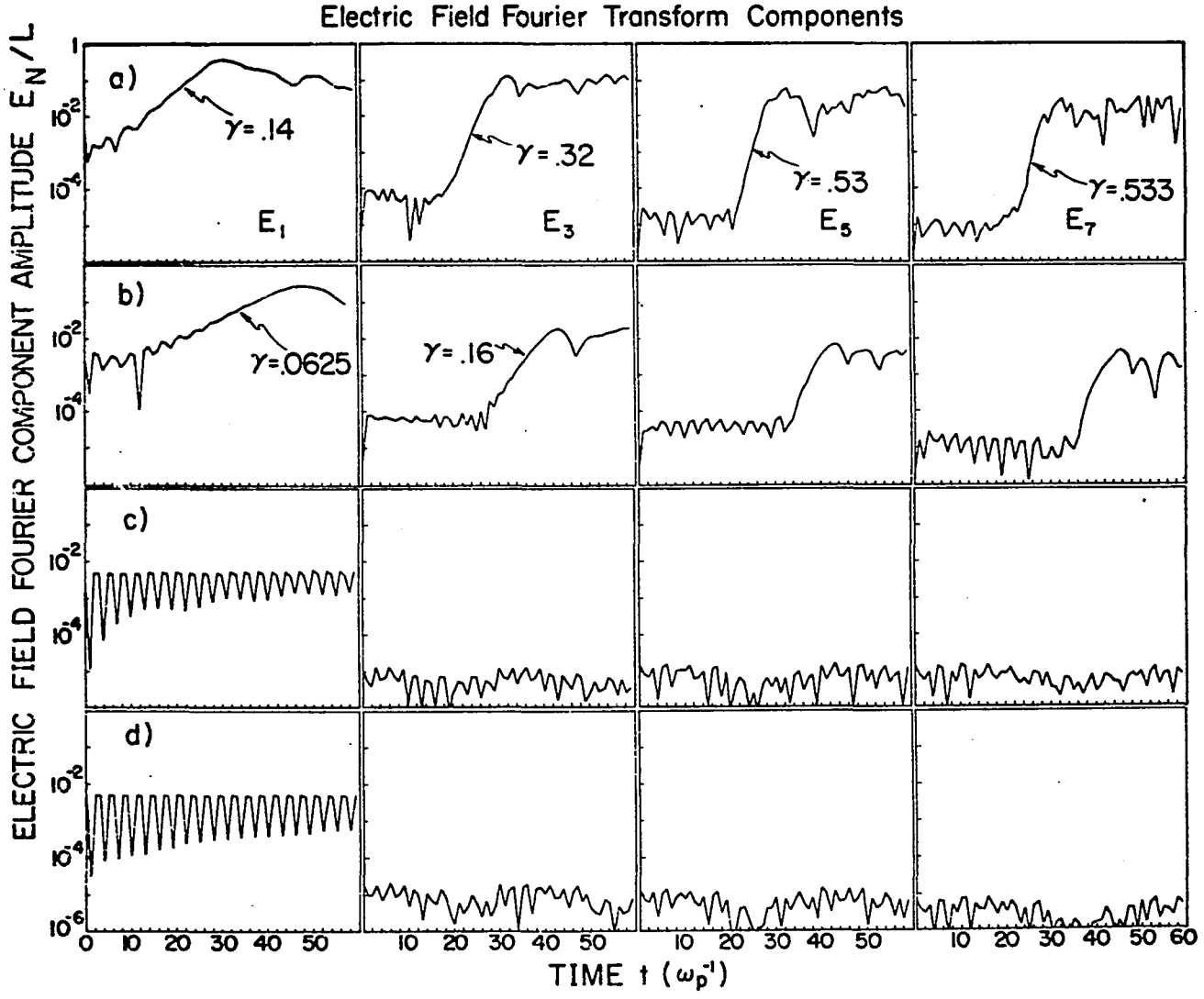
Electric Field Fourier Transform Components
ELECTRIC FIELD FOURIER COMPONENT AMPLITUDE E_N/L
a)
b)
c)
d)
$\gamma = .14$
$\gamma = .32$
$\gamma = .53$
$\gamma = .533$
$\gamma = .0625$
$\gamma = .16$
E_1
E_3
E_5
E_7
TIME t (ω_p^{-1})

Figure 16

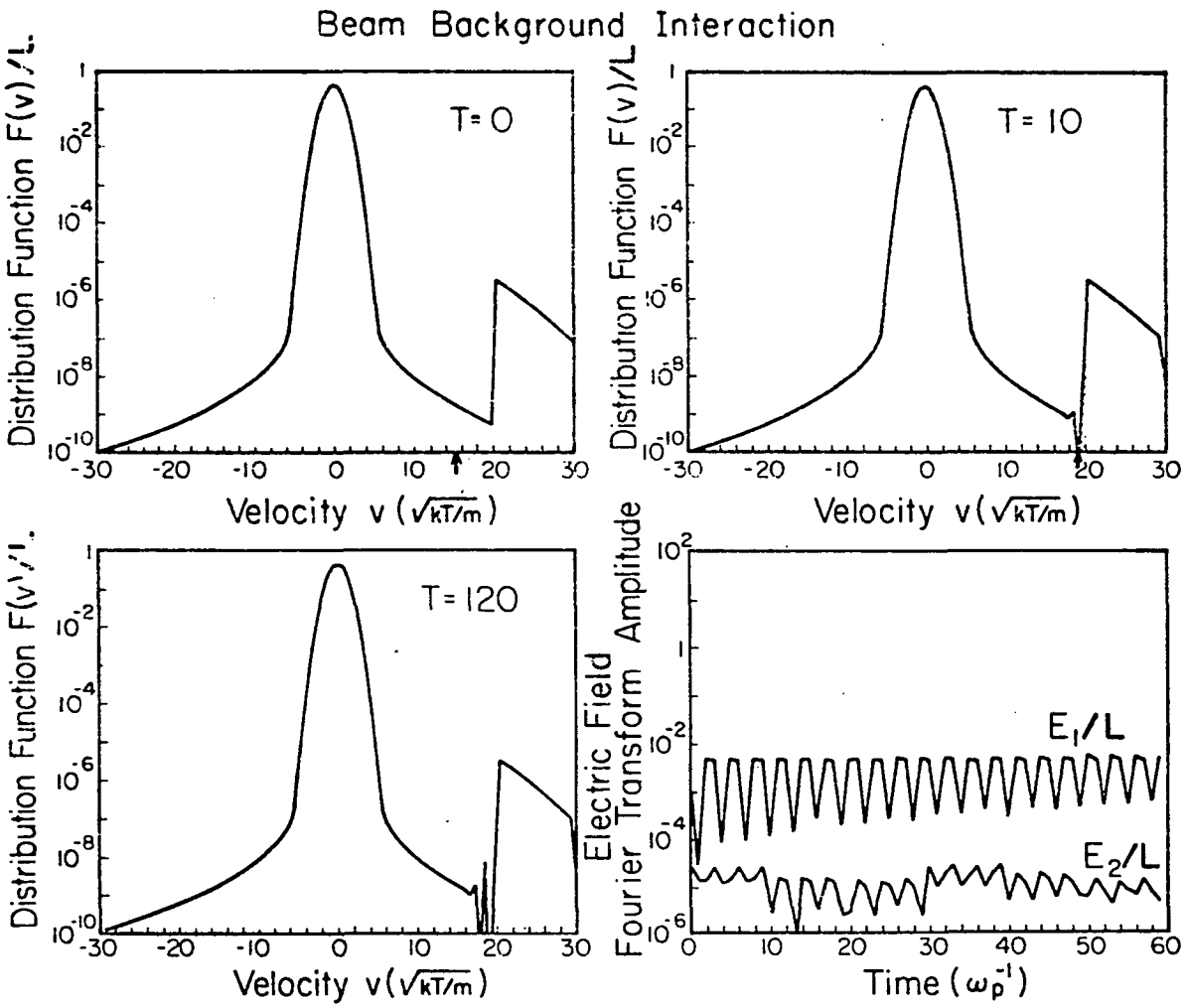
Beam Background Interaction
Distribution Function F(v)/L
T= 0
T= 10
T= 120
Velocity v (√kT/m)
Electric Field Fourier Transform Amplitude
E1/L
E2/L
Time (ωp⁻¹)

Figure 17

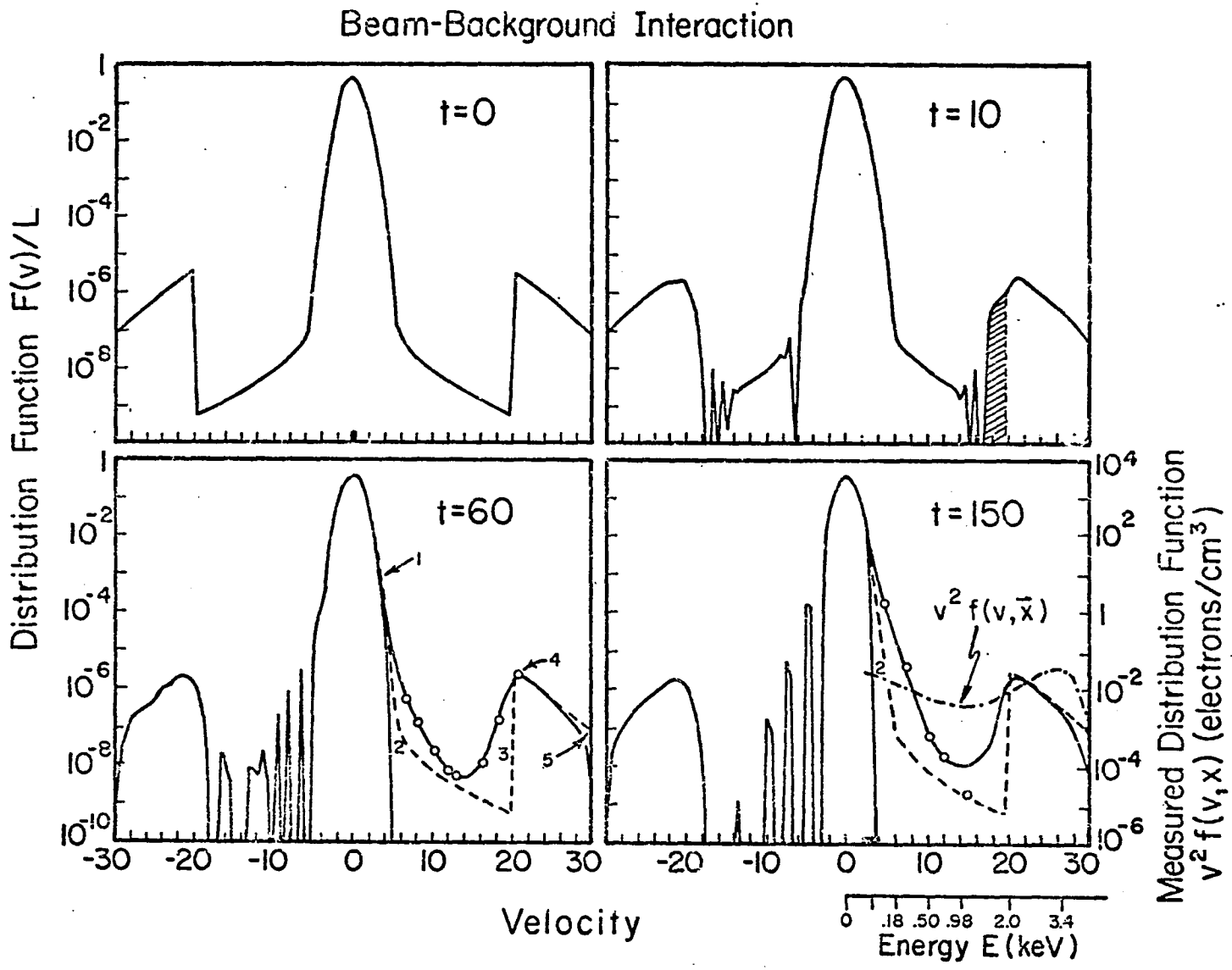
Beam-Background Interaction
t=0
t=10
t=60
t=150
Distribution Function F(v)/L
Velocity
Energy E(keV)
0 .18 .50 .98 2.0 3.4
$v^2 f(v,\vec{x})$
Measured Distribution Function
$v^2 f(v,x)$ (electrons/cm^3)

Figure 18

ELECTRIC FIELD FOURIER COMPONENTS vs TIME (ω_p^{-1})

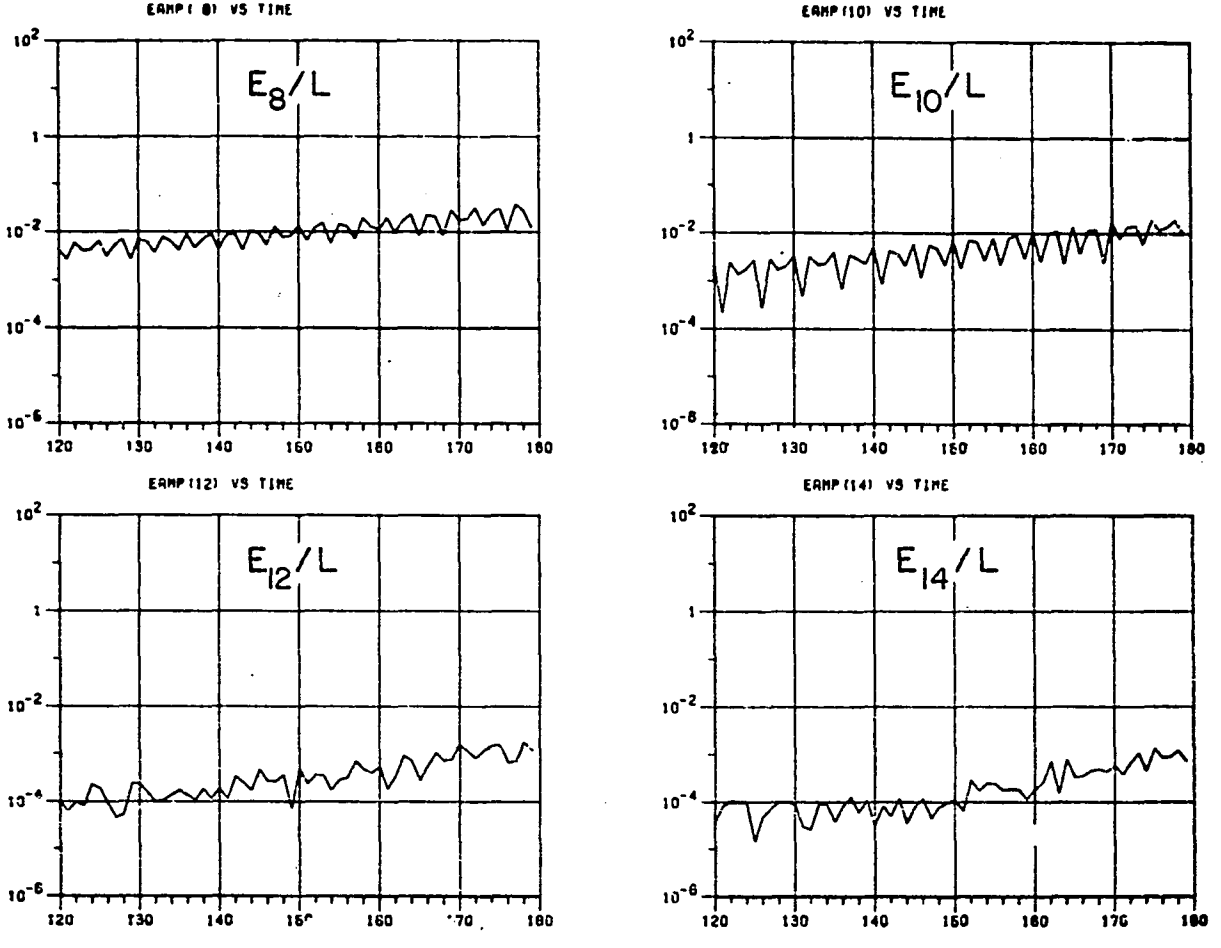

Figure 19

CHAPTER IV

THREE DIMENSIONAL BEAM BACKGRROUND INTERACTION

The results of the one dimensional beam-background calculations presented in chapter 3 show that a streaming anisotropic beam of high energy electrons from the plasma sheet or an acceleration region above the auroral ionosphere is largely dissipated within 100 km of travel unless it is pitch angle scattered to form an isotropic beam stable to Vlasov instabilities removing the unstable two peak structure in the one-dimensional distribution function. A 2-1/2 dimensional Vlasov equation theory, two space and three velocity dimensions, is used to model the interaction between an anisotropic high energy electron beam and a low energy background in this chapter.

4.1 Numerical Methods

The three velocity dimension, two space dimension Vlasov equation is derived in Appendix B for the co-ordinate system shown in figure 9 of chapter 2 or figure B-1 in Appendix B. The computations are made for cases in which the magnetic field lies along the y-axis ($\theta = \pi/2$) and the distribution function is independent of the spacial coordinate z-axis. The Vlasov and Poisson equations for this configuration are (equations B-20 and B-8 in Appendix B)

$$\frac{\partial f}{\partial t} + [v_{\perp} \cos\phi \frac{\partial f}{\partial x} + v_{\parallel} \frac{\partial f}{\partial y}] +$$

$$- \frac{\partial f}{\partial v_{\perp}} E_x \cos\phi - E_y \frac{\partial f}{\partial v_{\parallel}} + \frac{\partial f}{\partial \phi} [\frac{E_x \sin\phi}{v_{\perp}} + \omega_c] = 0$$

$$\frac{\partial E_x}{\partial x} + \frac{\partial E_y}{\partial y} = 1 - \int_{\substack{\text{all} \\ \text{velocity}}} f(\vec{x},\vec{v},t)\, d^3\vec{v} \quad . \tag{4.1}$$

This set of equations is solved by a splitting scheme similar to that used by Cheng[45]. First the free streaming equation

$$\frac{\partial f}{\partial t} + v_{\perp} \cos \phi \frac{\partial f}{\partial x} + v_{\parallel} \frac{\partial f}{\partial y} = 0 \qquad (4.2)$$

is integrated for half a time step. (Note that $v_x = v_{\perp} \cos(\phi)$ and $v_y = v_{\parallel}$) Next the electric field is calculated from Poison's equation, and the acceleration equation

$$\frac{\partial f}{\partial t} - \frac{\partial f}{\partial v_{\perp}} E_x \cos \phi + \frac{\partial f}{\partial \phi} \left[\frac{E_x \sin \phi}{v_{\perp}} + \omega_c\right] = 0 \qquad (4.3)$$

is integrated for a full time step. Finally, the parallel acceleration equation

$$\frac{\partial f}{\partial t} - E_y \frac{\partial f}{\partial v_{\parallel}} = 0 \qquad (4.4)$$

is integrated for a full time step and another integration over half a time step is made using the free streaming equation (equation 4.2). The result of this sequence of time integrations is the determination of a new distribution function f^{N+1} at $t_{N+1} = (N+1)\,\Delta t$ that is related to the initial distribution function at time t_N by[45]

$$f^{N+1}(\vec{x},\vec{v},t_{N+1}) = f^{N}(\vec{x}',\vec{v}',t_N) \quad , \tag{4.5}$$

where

$$\vec{x}' = \vec{x} - \Delta t/2\ (\vec{v} + \vec{v}')$$

$$\vec{v}' = \vec{v} * (\vec{x} - \vec{v}\ \Delta t/2) \quad , \tag{4.6}$$

and $\vec{v}*$ is the solution to the characteristic equations

$$\frac{dv*}{dt} = -[\vec{E} + \vec{v}* \times \vec{\omega}_c]$$

$$\vec{v}* = \frac{d\vec{x}}{dt} \quad . \tag{4.7}$$

Cheng[45] has shown that the sequence of integrations described above is equivalent to the propagation of electrons along their characteristic orbits described by the solution to equations 4.7 correct to second order in the time step Δt.

The free streaming equation 4.2 is solved by Fourier interpolation to give a new distribution function f* related to the inital distribution (f^N) half a time step earlier by

$$f^*(\vec{x},\vec{v},t_n + \Delta t/2) = f^n(\vec{x}-\vec{v}\ \Delta t/2,\vec{v},t_n) \quad . \tag{4.8}$$

Two subsequent Fourier interpolations are made for the two space variables in the model. The two one dimensional space shifts

$$1) \quad f'(x,y,\vec{v},t_n + \Delta t/2) = f^n(x-v_x\ \Delta t/2,y,\vec{v},t_n)$$

$$2) \quad f^*(x,y,\vec{v},t_n + \Delta t/2) = f'(x,y-v_y\ \Delta t/w,\vec{v},t_n + \Delta t/2) \tag{4.9}$$

that result in the final distribution function f* given by equation 4.8 are made by subsequent one dimensional Fourier interpolations using the Fourier series fit to the spatial grid points described by equations 3.8 and 3.9. The computation time for the Fourier interpolation is reduced by using the fact that the shift $\Delta_k = v_k\ \Delta t/2$ is the same for all time steps at a given velocity grid point v_k. That is, the velocity grid points and time step size are predetermined and remain fixed throughout the time

integration.

A more convenient expression for the Fourier interpolation is obtained by first substituting equation 3.9 for the Fourier series amplitudes into Fourier series equation 3.9 to get

$$f(y_i + \Delta_k) = \sum_{j=0}^{N/2} \left\{ \left(\frac{1}{N} \sum_{\ell=0}^{N-1} f(y_\ell) \cos(k_j y_\ell)\right) \right. \tag{4.10}$$

$$\left. \cos k_j(y_i + \Delta_k) + \left(\frac{1}{N} \sum_{\ell=0}^{\frac{N}{2}-1} f(y_\ell) \sin(k_j y_\ell)\right) \sin k_i(y_i + \Delta_k) \right\}$$

where $k_j = j\, 2\pi / L_y$. Next, the y_ℓ terms that appear in the summations in equation 4.10 are written as the sum of the i-th point y_i and a multiple of the step size in the y-direction Δy. This leads to

$$f(y_i + \Delta_k) = \frac{1}{N} \sum_{n=0}^{N-1} f(y_i + m\Delta x) \sum_{j=0}^{N/2} \left\{ \cos k_j(y_i + m\Delta y) \right.$$

$$\left. \cos k_j(y_i + \Delta_k) + \sin k_j(y_i + m\Delta y) \sin k_j(y_i + \Delta_k) \right\} , \tag{4.11}$$

where the summation over m replaces the sum over ℓ with $y_\ell = y_i + m\,\Delta x$ for the appropriate value of m. If the term in

brackets in equation 4.11 is denoted as $g_m(\Delta_k)$, then the equation has the form

$$f(y_i + \Delta_k) = \sum_m f(y_i + m\Delta x)\, g_m(\Delta_k) \quad , \tag{4.12}$$

where the summation over j is included in g_m. A simplified expression for g_m is obtained by the following sequence of equations:

$$\begin{aligned} g_n(\Delta_k) &= \frac{1}{N} \sum_{j=0}^{N/2} \Big\{ \cos k_j(y_i + m\Delta y) \cos k_j(y_i + \Delta_k) + \\ &\qquad \sin k_j(y_i + m\Delta y) \sin k_j(y_i + \Delta k) \Big\} \\ &= \frac{1}{N} \sum_j \cos k_j(y_i + m\Delta y - y_i - \Delta_k) \\ &= \frac{1}{N} \frac{\sin[\pi(m\Delta y - \Delta_k)] \cos[\pi(m\Delta y - \Delta_k)/L_y]}{\sin[\pi(m\Delta y - \Delta_k)/L_y]} \end{aligned} \tag{4.13}$$

where the last equality is taken from Cheng and Knorr[46] and the matrix of values of $\Delta_k = v_k \Delta t/2$ is fixed for a given time step size and velocity matrix. The values of $g_{m,k}$ for all grid point values of velocity v_k and position y_m are calculated once at the beginning of each computer run in subroutine SPACE of program VLAS3D (see Appendix D). A

separate calculation must be made for the matrix of g values corresponding to the x spacial coordinate and the v and ϕ velocity components (required because $v_x = v \cos(\phi)$). The x and y one-dimensional spatial interpolations are made twice during each time step using the modified Fourier interpolation equation 4.12.

The electric field is calculated from Poisson's equation (4.1) by a double Fourier transform technique[66 67]. In this method the electrostatic potential $\Phi_{\ell,k}$ is written in terms of its two dimensional finite Fourier transform

$$\Phi_{\ell,k}(x_\ell = \ell\Delta x, y_k = k\Delta y) = \frac{1}{L_y L_x} \sum_{1-\frac{Nx}{2}}^{\frac{Nx}{2}-1} \sum_{N=-\frac{Ny}{2}}^{\frac{Ny}{2}-1} \left\{ \phi_{m,n}(\nu_x = \frac{m}{L_x}, \nu_y = \frac{n}{L_y}) \, e^{i(k_{y,n}\, y_k + k_{x,n}\, x_\ell)} \right\}, \; N_x, N_y \equiv \text{even} \tag{4.14}$$

where $k_{y,n} = n\, 2\pi / L_y$, $k_{x,m} = n\, 2\pi / L_x$ and the Fourier transform component $\phi_{m,n}$ is equal to

$$\phi_{m,n} = \Delta y \Delta x \sum_{\ell=0}^{Nx-1} \sum_{k=0}^{Ny-1} \Phi(x_\ell, y_k)\, e^{-i(k_{y,m}\, y_k + k_{x,m}\, x_\ell)} \tag{4.15}$$

The electron charge density $\rho_e(x,y)$ is also written in terms of its Fourier transform components as

$$\rho_e(x,y) = \int_{\substack{\text{all} \\ \text{velocity}}} f(\vec{v},\vec{x})\, d^3\vec{v}$$

$$= \frac{1}{L_x L_y} \sum_{n,m} \rho_{m,n}\, e^{i(k_{y,n}y_k + k_{x,m}x_\ell)} \qquad (4.16)$$

The term in the sum in equation 4.16 with m=n=0 is equal to unity for a distribution function normalization

$$\int_{\substack{\text{all} \\ \text{velocity}}} f(\vec{x},\vec{v})\, d^3\vec{v} = Lx\ Ly \quad . \qquad (4.17)$$

The substitution of equations 4.16 and 4.14 for Φ and ρ_e into Poisson's equation (equation 4.1) leads to

$$\phi_{m,n} = \frac{-1}{4\pi^2} \frac{\rho_{m,n}}{(\frac{N}{Ly})^2 + (\frac{m}{Lx})^2} \quad , \quad m + n \neq 0 \quad , \qquad (4.18)$$

where the relations

$$E_x = -\frac{\partial \Phi}{\partial x}$$

$$E_y = -\frac{\partial \Phi}{\partial y} \qquad (4.19)$$

have been used. The arbitrary reference potential corresponding to $\phi_{m,n} = \phi_{0,0}$ is taken as zero.

The electric field components calculated from equations 4.19, 4.18 and 4.14 are

$$E_x(x_\ell, y_k) = \frac{i\Delta x \Delta y}{2\pi L_x^2 L_y} \sum_{\substack{n,m \\ n+m\neq 0}} \frac{n}{(\frac{n}{Ly})^2 + (\frac{n}{Lx})^2} \left\{ \sum_{\ell',k'} \rho_{\ell,k}(x_{\ell'}, y_{k'}) \right.$$

$$\left. e^{-i(k_{y,n}\, y_{k'} + k_{x,n}\, x_{\ell'})} \right\} e^{i(k_{y,n}\, y_k + k_{z,n}\, x_\ell)}$$

$$E_y(x_\ell, y_\ell) = \frac{i\Delta x \Delta y}{2\pi L_y^2 L_x} \sum_{\substack{n,m \\ n+m\neq 0}} \frac{n}{(\frac{n}{Ly})^2 + (\frac{m}{Lx})^2} \left\{ " \right\} e^{i(n)} \quad , \qquad (4.20)$$

where the summations ranges are

$$n = -\frac{Ny}{2}, \ldots, \frac{Ny}{2} - 1$$

$$m = -\frac{Nx}{2}, \ldots, \frac{Nx}{2} - 1$$

$$\ell = 0, \ldots, Nx - 1$$

$$k = 0, \ldots, Ny - 1 \qquad (4.21)$$

for N_x and N_y even. The electric field calculation is done in subroutine EFOUR of program VLAS3D (see Appendix D).

The acceleration equation (equation 4.3) is integrated by Gazdag's accurate space derivative (ASD) method.[68 69] The distribution function is advanced in time according to third order Taylor's series expansion

$$f(t + \Delta t) = f(0) + \frac{\partial f}{\partial t})_t \Delta t + \frac{1}{2}\frac{\partial^2 f}{\partial t^2})_t \Delta t^2 + \frac{1}{6}\frac{\partial^3 f}{\partial t^3}\Delta t^3 + \theta(\Delta t^4) \qquad (4.22)$$

The first time derivative of f is determined from the acceleration equation to be

$$\frac{\partial f}{\partial t} = \left\{ E_x \left[\cos\phi \frac{\partial}{\partial v_\perp} - \frac{\sin\phi}{v_\perp} \frac{\partial}{\partial \phi} \right] - \omega_c \frac{\partial}{\partial \phi} \right\} = 0 \quad , \qquad (4.23)$$

where the electric field is determined from Poisson's equation as described above at half a time step ($\Delta t/2$). The partial derivative of f in ϕ is determined by writing the Fourier expansions for f in ϕ as

$$f(v_\parallel, v_\perp, \phi_\ell = \ell\Delta\phi, x, y) = \frac{1}{2\pi} \sum_{N=-N_\phi/2}^{\frac{N\phi}{2}-1} F_N(v_\parallel, v_\perp, \nu_\phi = \frac{n}{2\pi}, x, y) e^{in\phi_\ell} \quad , \qquad (4.24)$$

where

$$F_n(\nu_\phi) = \Delta\phi \sum_{\ell=0}^{n_\phi - 1} f(\phi_\ell)\, e^{-in\phi_\ell} \quad , \qquad (4.25)$$

and taking the partial derivative of equation 4.24

$$\left.\frac{\partial f}{\partial \phi}\right)_{\phi_\ell} = \frac{1}{2\pi} \sum_n in\, F_n(v_\phi)\, e^{in\phi_\ell} \qquad (4.26)$$

The Fourier transform of f in ϕ (equation 4.25) and the partial derivative (equation 4.26) must be evaluated for every grid point value of x, y, $v_{//}$, $v_\perp$ and ϕ in order to completely determine the function $\frac{\partial}{\partial \phi} f(v_{//}, v_\perp, \phi, x, y)$. The values of the distribution function used to determine the Fourier transform amplitude in equation 4.25 are those for time t, since the partial derivative terms in the Taylor's series expansion (equation 4.22) are to be evaluated at time t.

The partial derivative of f with respect to $v_\perp$ is determined by making a Fourier expansion of f in $v_\perp$ and differentiating as in equation 4.26 for the partial derivative with respect to ϕ. However, values of the distribution function for negative values of the perpendicular velocity $v_\perp$ are created in order to maintain continuity through the origin in the finite Fourier series fit to the distribution function. Figure 20 shows the method of assigning functional values for negative perpendicular velocities. The value of the distribution function at negative perpendicular velocity is set equal to the distribution function value with ϕ incremented by π.

The negative perpendicular velocity points are added only or the Fourier series representation in the determination of $\frac{\partial f}{\partial v_\perp}$. The perpendicular velocity falls in the range 0 to $v_{\perp\,max}$ in all other cases. The values of $\Delta v_\perp$, $\Delta v_{//}$ and $\Delta\phi$ are also shown in figure 20 in terms of the maximum velocities and number of grid points. The number of grid points in the perpendicular velocity coordinate $N_\perp$ is equal to the number of points for $v_\perp > 0$ while the number of parallel velocity grid points $N_{//}$ includes those for $v_{//} < 0$.

The expression for the partial derivative of f with respect to v is

$$\left(\frac{\partial f}{\partial v_\perp}\right)_{v_{\perp k}} = \frac{-1}{L} \sum_{n=-N+1}^{N-1} \frac{2\pi i}{L}\, m\, F_m\, e^{2\pi i \frac{m}{L} v_{\perp k}} , \quad (4.27)$$

where $L_\perp = 2v_{\perp max}$ and

$$F_m(v_{\parallel},\nu = \frac{m}{L}, \phi, x, y) = \Delta v_\perp \sum_{k=0}^{2N-2} f(v_{\perp k}) e^{\frac{-2\pi i m}{L} v_{\perp k}} \quad . \quad (4.28)$$

The partial derivatives in equations 4.26 and 4.27 are evaluated by subroutine OPERAT in program VLAS3D (see Appendix D) for all grid point values of the five coordinates $v_{\parallel}$, $v_\perp$, ϕ, x and y.

The second and third time derivatives of the distribution function required for the Taylor's series expansion (equation 4.22) are calculated from the time derivatives of the first time derivatives of the acceleration equation (equation 4.23). They are

$$\frac{\partial^2 f}{\partial t^2} = \left\{ E_x \left[\cos\phi \frac{\partial}{\partial v_\perp} - \frac{\sin\phi}{v_\perp} \frac{\partial}{\partial \phi} \right] - \omega_c \frac{\partial}{\partial \phi} \right\} \frac{\partial f}{\partial t} +$$

$$\frac{\partial E_x}{\partial t} \left[\cos\phi \frac{\partial}{\partial v_\perp} - \frac{\sin\phi}{v_\perp} \frac{\partial}{\partial \phi} \right] f \qquad (4.29)$$

$$\frac{\partial^3 f}{\partial t^3} = \left\{ E_x \left[\cos\phi \frac{\partial}{\partial v_\perp} - \frac{\sin\phi}{v_\perp} \frac{\partial}{\partial \phi} \right] - \omega_c \frac{\partial}{\partial \phi} \right\} \frac{\partial^2 f}{\partial t^2} +$$

$$\frac{\partial^2 E_x}{\partial t^2} \left[\cos\phi \frac{\partial}{\partial v_\perp} - \frac{\sin\phi}{v_\perp} \frac{\partial}{\partial \phi} \right] f +$$

$$2 \frac{\partial E_x}{\partial t} \left[\cos\phi \frac{\partial}{\partial v_\perp} - \frac{\sin\phi}{v_\perp} \frac{\partial}{\partial \phi} \right] \frac{\partial f}{\partial t} \quad . \qquad (4.30)$$

The value of $\partial f/\partial t$ in equations 4.29 and 4.39 is determined from the previous calculation in equation 4.23, and the value of $\frac{\partial^2 f}{\partial t^2}$ in equation 4.30 is available from the solution to equation 4.29. The partial derivatives in ϕ and $v_\perp$ of the higher order time derivatives of the distribution function are determined by first taking the Fourier transform and the differentiating as in equations 4.26 and 4.27 for the first time derivative of f. The subroutine used to determine the partial derivatives of f, called OPERAT, is also used to determine the partial derivatives of $\frac{\partial f}{\partial t}$ and $\frac{\partial^2 f}{\partial t^2}$ by simply changing the argument of the

subroutine call statement, replacing the array of values for f with the array for $\frac{\partial f}{\partial t}$ or $\frac{\partial^2 f}{\partial t^2}$.

The first and second time derivatives of the electric field are determined from the time derivative of Poisson's equation

$$\frac{\partial}{\partial x}\left(\frac{\partial^{\ell}}{\partial t^{\ell}} E_x\right) + \frac{\partial}{\partial y}\left(\frac{\partial^{\ell}}{\partial t^{\ell}} E_y\right) = 1 - \int \left(\frac{\partial^{\ell}}{\partial t^{\ell}} f(\vec{x},\vec{v},t)\right) d^3\vec{v} \ ,$$

$$\ell = 0,1,2 \ . \qquad (4.31)$$

This is accomplished by changing the argument of subroutine EFOUR from f to $\frac{\partial f}{\partial t}$ or $\frac{\partial^2 f}{\partial t^2}$ to solve equation 4.31 by the method outlined in equations 4.14 through 4.12 for the electrostatic potential solution to Poisson's equation.

The parallel acceleration equation (equation 4.4) is solved by Fourier interpolation. The new evolved time integrated distribution function f^{new} is related to the intial distribution by

$$f^{new}(v_{\parallel}, v_{\perp}, \phi, x, y) = f^{old}(v_{\parallel} - a_{\parallel}\Delta t, v_{\perp}, \phi, x, y)$$

$$= f^{old}(v_{\parallel} + Ey\Delta t, v_{\perp}, \phi, x, y) \quad . \qquad (4.32)$$

The integrated distribution function is calculated by evaluating the initial distribution at $v_{\parallel} + E_y \Delta t$ for all grid point values of $v_{\parallel}$, $v_{\perp}$, ϕ, x and y. The evaluation at the intermediate (in between parallel velocity grid points) parallel velocity $v_{\parallel} + E_y \Delta t$ is done by a Fourier interpolation in $v_{\parallel}$. The initial distribution function is written in terms of its finite Fourier series representation

$$f^{old}(v_{\parallel k} = k\Delta v_{\parallel} - v_{\parallel max}) = \Delta v_{\parallel} \sum_{n=-\frac{N_{\parallel}}{2}+1}^{\frac{N_{\parallel}}{2}-1} f_n(v_{\parallel} = \frac{n}{N_{\parallel}} \Delta v_{\parallel}) \, e^{\frac{2\pi i n}{L_{\parallel}} v_{\parallel k}} \qquad (4.33)$$

where $L_{\parallel} = 2v_{max}$ and

$$f_n = \frac{1}{L_{\parallel}} \sum_{k=0}^{N_{\parallel}-2} f^{old}(v_{\parallel k}) \, e^{\frac{-2\pi i n}{L_{\parallel}} v_{\parallel k}} \quad . \qquad (4.34)$$

The integrated distribution function f^{new} is determined by evaluating the initial distribution f^{old} at $v_{\parallel} = v_{\parallel k} + E_y \Delta t$ in equation 4.33 so that

$$f^{new}(v_{\parallel k}) = f^{old}(v_{\parallel k} + E_y \, \Delta t)$$

$$= \Delta v_{\parallel} \sum_{n=-\frac{N_{\parallel}}{2}+1}^{\frac{N_{\parallel}}{2}-1} f_n \, e^{\frac{2\pi i n}{L_{\parallel}} (v_{\parallel k} + E_y \, \Delta t)} \quad . \qquad (4.35)$$

Equation 4.35 must be evaluated for all grid point values of $v_{\parallel}$, $v_{\perp}$, ϕ, x and y in order to completely specify the time integrated distribution function f^{new}. The parallel acceleration integration is performed by subroutine ACCEL in program VLAS3D (see Appendix D).

In conclusion, the integration steps required for the complete evolution of the distribution over one time step are:

1. Integrate the free streaming equation (equation 4.2) over half a time step ($\Delta t/2$) using the Fourier series interpolation scheme outlined in equations 4.10 through 4.13. (performed by subroutine SPACE)

2. Solve Poisson's equation (4.1) for the electric field by the two dimensional Fourier transform method outlined in equations 4.14 through 4.21. (performed by subroutine EFOUR)

3. Perform the Taylor's series expansion (4.22) of the distribution function in time to integrate the acceleration equation 4.23 over a full time step. This method requires the evaluation of the first and second time derivatives of the electric field from Poisson's equation as described in number 2 above. (subroutines ACCELL, OPERAT and EFOUR)

4. Integrate the parallel acceleration equation 4.4 over a full time step by the Fourier interpolation method outlined in equations 4.32 through 4.35. (subroutine ACCELL)

5. Integrate the free streaming equation 4.2 another half a time step as described in number 1 above.

The computer program VLAS3D used to integrate the 2 1/2 dimensional Vlasov equation is listed in Appendix D together with supporting programs required to plot the distribution function and electric field and create the initial distribution function matrix. Tables D-1 and D-2 in Appendix D list parameters used for the results of VLAS3D computer runs that appear in this thesis.

4.2 Test Cases

The Landau damping of a high initial electric field is calculated for two cases. The first case is that of an electrostatic wave propagating parallel to the magnetic field while undergoing collisionless Landau damping. In the second case the damping of an electric field propagiating at an angle of 45 degrees to the magnetic field axis is observed. In both test cases a Maxwellian plasma with a temperature corresponding to 10 ev is used for the initial electron distribution function. The initial distribution function has the form

$$f(v_{\parallel},v_{\perp},\phi,x,y) = Ae^{-\alpha(v_{\perp}^2+v_{\parallel}^2)} [1 + c(\cos k_x x + \cos k_y y)] , \quad (4.36)$$

where the space dependent term gives the electron density perturbation required for the initial electrostatic electric field. The parameters used for the results shown in the figures of this chapter are shown in tables D-1 and D-2 of Appendix D.

Figure 21 shows the time evolution of a Maxwellian plasma for a high initial electric field (0.8 in the dimensionless system of units described in Appendix B) in two space and three velocity dimensions. The top row of figure 21 shows the initial distribution function at T=0. The first graph in the top row shows the electron

distribution function value as a function of parallel and perpendicular velocity. The x and y spacial dependence has been removed by integrating the distribution function over the intervals 0 to x_{max} and 0 to y_{max}. The velocity dependence is removed by integrating the distribution function in over the interval 0 to 2π. The distribution function values are denoted by the numbers 0 through 9. The numbers indicate the fraction of the maximum function value that the distribution function takes on at the point in velocity space where the number appears. For example, a "9" indicates that the distribution function is in the range from 0.9 to 1.0 of its maximum value and "0" indicates the value is from 0.0 to 0.1 of its maximum value. The integration and plotting of the distribution function is performed by program PLTF3D listed in Appendix.

The remaining figures in row one of figure 21 show the distribution function as a function of a single velocity variable the others having been integrated out. It can be seen that the one dimensional velocity profiles of the distribution function have an isotropic Maxwellian shape. The open circles indicate the matrix grid points where the function is evaluated and adjacent points are connected by straight lines. All integrations required to produce the graphs in figure 21 are performed by the integration of a natural cubic spline fit to the distribution function grid points using the IMSL[50] mathematical subroutines described in Appendix C and chapter 3.

Row two of figure 21 shows the distribution function after 4 plasma periods of time have elapsed. Comparison of the first figure with the corresponding figure of the row above shows that a plateau structure has developed in the parallel velocity direction. The plateau structure is more clearly shown in the second figure of row two. Energy from the initial electric field has been transformed into electron kinetic energy to form the plateau structure. The phase velocity of the initial plasma wave is 2 parallel velocity units (see parameters in table D-2 of Appendix D). It can be seen that the plateau structure has been formed by electrons in the resonant region about the electric field phase velocity as expected from the linear theory of Landau damping[56] (see figure 12 of chapter 3).

The total number of electrons in the system for an electron density of one electron per unit volume (a cube of side λ_D) is shown at the top of the contour plots in column one of figure 21. In this case the total number of electrons in a cube of volume $\lambda_D L_x L_y$ is 1.5 for the system shown in figure 21. It can be seen by comparison of the initial t=0 and t=4 number calculations that the total number of particles is conserved to within 2%.

Figure 22 shows the electric field energy for one electron per unit volume ($\lambda_D{}^3$) as a function of time. The field energy is in units of the thermal energy (kT). The field energy shown in figure 22 is calculated by integrating

the sum of the squares of the Fourier series amplitudes (see equation 4.20) over the spacial intervals 0 to x_{max} and 0 to y_{max}. The total field energy in this system of units (see Appendix B) is equal to .3 at t=0 and .03 at t=4 according to figure 22. The total electron kinetic energy for an electron density of one electron per unit volume (a cube of side λ_D) is calculated by integrating the product of the distribution function and one half the square of the velocity over all spatial and velocity coordinates. The values are shown at the top of the contour plots in figure 21 to be about 2 thermal energy units (kT). The values of the total electron kinetic plus field energy at times t=0 and t=4 are

$$E_{total}(t=0) = 2.18 + .3 = 2.48$$

$$E_{total}(t=4) = 2.57 + .03 = 2.60 \qquad (4.37)$$

in units of thermal energy kT. Therefore, it can be concluded that the total energy of the system is conserved to within 5%. The period of oscillation of the total field energy is $\Delta t = 2\,\omega_p^{-1}$ from the upper curve in figure 22 which can be compared with the period of $2.6\,\omega_p^{-1}$ for the electric

field amplitude oscillation period for the one dimensional calculation shown in figure 13a of chapter 3.

A three dimensional perspective view of the initial and final electron distribution function as a function of parallel and perpendicular velocity is shown in the last row of figure 21. The first sketch shows the initial distribution function at t=0. The perpendicular velocity coordinate axis is into the paper and the parallel velocity axis is in the plane of the paper with the positive parallel velocities to the right of the origin. The distribution function shown to the right of the t=0 sketch is the evolved distribution function at t=4. Notice the plateau structure along the parallel velocity axis indicated by the left hand arrow. Electrons in the parallel velocity region indicated by the right hand arrow have gained energy from the electric field and have been accelerated to the higher energy velocity magnitude range shown by the arrow to the left. The net result is the well known[56] plateau structure associated with Landau damping of a high initial electric field.

Figure 23 shows the damping of an initial electric field propagating at an angle of 45 degrees to the magnetic field axis. In this case the x and y field components are equal (see table D-2 Appendix D). It can be seen that a plateau structure forms in both the perpendicular and parallel velocity directions. This can be seen in the

perspective view shown at the bottom of figure 23. Here, the arrows in the t=4 sketch indicate plateaus in the perpendicular and parallel velocity directions. Comparison of the t=0 and t=4 contour plots (first column of first two rows of figure 23) shows that the electron number density is conserved to within 3%. Total energy conservation is calculated from the contour plots of figure 23 and the 45 degree electric field energy graph in figure 22 to be conserved to within 7.5%.

4.3 Three Dimensional Beam-Background Interaction

The VLAS3D computer code (see Appendix D) is used to model the interaction between a 10 eV electron background plasma with a streaming Maxwellian of 640 eV thermal energy. An initial electric field energy of .01 kT (3.25 eV) is implemented by a suitable choice of the spacial variation parameters C, k_x and k_y in equation 4.36 (see table D-2 in Appendix D for parameter choice). The electric field energy grows to a value of .05 kT at t=42 ω_p^{-1} and decreases thereafter. The initial values of k_x and k_y are chosen to give plasma waves with phase velocities at the beam peak velocity $3.51\sqrt{kT/m}$ in figure 25, and the repetition length values x_{max} and y_{max} are determined from the initial values of k_x and k_y ($k_x = 2\pi / x_{max}$). The magnetic field strength is chosen such that the cyclotron frequency ω_c is equal to one tenth of the plasma frequency ω_p. This choice of magnetic field gives a cyclotron radius ($r_c = v_\perp / \omega_c$) equal to or less than the repetition lengths (x_{max} and y_{max}) for perpendicular velocities less than or equal to $2\sqrt{kT/m}$. The value of $\omega_c = .1\omega_p$ is typical of the plasma sheet where $n_e \sim 1$ cm^{-3} and B~5x10^{-4} Gauss.[15]

The results of the interaction over a time period of 36 ω_p^{-1} are shown in figure 24. Some important features of the electron distribution function are pointed out by the arrows in the t=0 curve at the top of figure 24. The background indicated by arrow "1" is significantly reduced

over the 36 plasma periods of evolution shown. Most of the electrons lost from the background peak region are accelerated to higher parallel velocity to fill in the "valley" indicated by arrow "2". At t=24 the "valley" has been filled in to form a plateau and at t=36 the plateau region has been populated with additional electrons from the background and beam peak "3". The beam peak is somewhat diminished and "flattened" over the 36 plasma period sequence shown. The distribution function remains essentially unchanged from t=36 to t=60 (not shown) so that it can be inferred that the distribution function is stable to Vlasov instabilities at t=36 within the accuracy provided by this model.

The increase in electron population in the gap between the background and beam (arrow 2) is in agreement with the results obtained in chapter 3 for the beam-background interaction shown in figure 18. The beam dissipation expected from the results of the one-dimensional calculation (see figure 15a) is seen as an evolution of the two peak structure in the one-dimensional distribution function $F(v_{//})$ in the center column of graphs in figure 25 to a stable single peak distribution function. The stable form of the two-dimensional distribution function $f(v_{//}, v_{\perp})$ shown at the bottom of figure 24 retains a plateau or slight peak like structure in the beam and background peaks in the parallel velocity direction even though the one-dimensional form $F(v_{//})$ in figure 25 shows no background peak.

Comparison of the central graphs of $F(v_{||})$ vs $v_{||}$ for all rows in figure 25 shows the evolution of the gentle background electron bump present initially at t=0 to the plateau structure at t=24 predicted by the one-dimensional linear theory[70] and the two-dimensional quasi-plateau at t=36 in figure 24 suggested by the two-dimensional linear theory[72].

The curve of $F(v_{||})$ vs $v_{||}$ in the top row of figure 25 shows the initial distribution function with all space and two velocity components integrated out. The integral under the remaining curve is the electron number density (except that a division by the product $x_{max}\ y_{max}$ =400 must be made because of the distribution function normalization- see equation 4.17). Therefore, it can be seen from the area under the curve, that the number of electrons in the beam is about five times greater than the background number density. This occurs because the parallel velocity grid points are too widely spaced to model the sharp peak that must appear near v =0 in order to make the beam and background densities equal.

The three-dimensional beam distribution function is taken to be a streaming Maxwellian (equation 4.36) rather than the accelerated Maxwellian used in the one dimensional case (equation 3.32). The streaming Maxwellian has a smaller initial (t=0) slope magnitude in the gap region between the background and beam and it extends further into

the background velocity range than the accelerated Maxwellian distribution. This choice is made because of the difficulty in modeling the sharp slope in an accelerated Maxwellian distribution (see figure 17).

Comparison of the central graphs of $F(v_{||})$ vs $v_{||}$ for all rows shows the evolution of the gentle bump present initially at t=0 to the plateau structure at t=24 predicted one dimensionally by linear theory and the quasi plateau at t=36 suggested by two dimensional linear theory[72].

The curves of $F(v_{\perp})$ vs $v_{\perp}$ show little change indicating no net acceleration of electrons to higher perpendicular velocity. This indicates that the instability induces primarily parallel Langmuir wave growth and little pitch angle scattering takes place over the 36 plasma periods shown. The contour plot at t=0 shows a beam peak at $v_{||}=3.5$ and $v_{\perp}=0.5$. However, the stable distribution function at t=36 shows all zeros in the $v_{\perp}=3.5$ column of the contour plot. The anisotropic beam peak initially at $v_{||}=3.5$ and zero degrees pitch angle has not spread to other pitch angles to form a more isotropic beam over a time period of 60 plasma periods (t=60 curves not shown). This is an important point in the interpretation of the one-dimensional results of chapter 3. Those results indicated that an accelerated Maxwellian beam is dissipated by absorption in the background plasma unless they are pitch angle scattered to a more stable isotropic velocity distribution within 30

plasma periods (see figure 15) for an equal density beam background interaction. The fact that the parallel streaming three-dimensional beam-background interaction shown in figures 24 and 25 does not pitch angle scatter to a more isotropic form indicates that anisotropic accelerated Maxwellian beams are quickly dissipated in their one-dimensional representation $F(v_{//})$ by energy exchange with the electrostatic field rather than pitch angle scattered to a more stable form. However, the two-dimensional distribution function $f(v_{//}, v_{\perp})$ may retain a two peaked or peak and plateau structure after evolution (see figure 25) provided that one of the peaks loses enough electrons to the "valley" region to give a monotone decreasing one-dimensional distribution function $F(v_{//})$ from the remaining peak after integration over the perpendicular velocity (see figure 25).

The results presented in chapters 3 and 4 of this thesis are consistent with an auroral model that includes streaming or accelerated Maxwellian plasma sheet particles that interact with the auroral ionosphere to give rise to parallel Langmuir waves and an increase in the population of electrons in the energy range between the background and beam electron energies (see figures 24 and 18). Local acceleration of the streaming plasma sheet particles may occur as evidenced by the measurement of electron "bursts" of strongly field aligned electrons. The locally accelerated electron one dimensional distribution function

peaks are probably dissipated leaving a plateau or slight peak structure in the two-dimensional distribution function within a few hundred kilometers of travel.

Three Dimensional Grid Points

a)

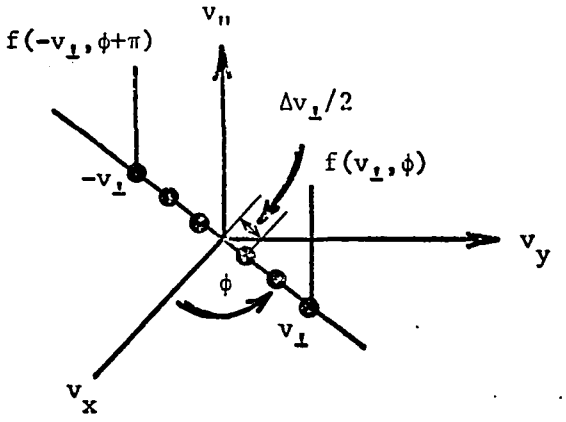

$$f(-v_{\perp},\phi+\pi) = f(v_{\perp},\phi)$$

$$\Delta v_{\perp} = \frac{2\ v_{\perp max}}{2\ N_{\perp} - 1}$$

$$\Delta v_{\parallel} = \frac{2\ v_{\parallel max}}{N_{\parallel} - 1}$$

b)

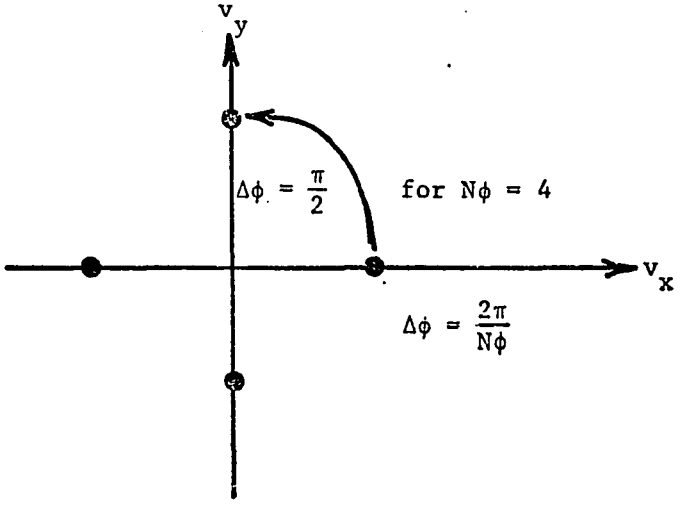

Figure 20

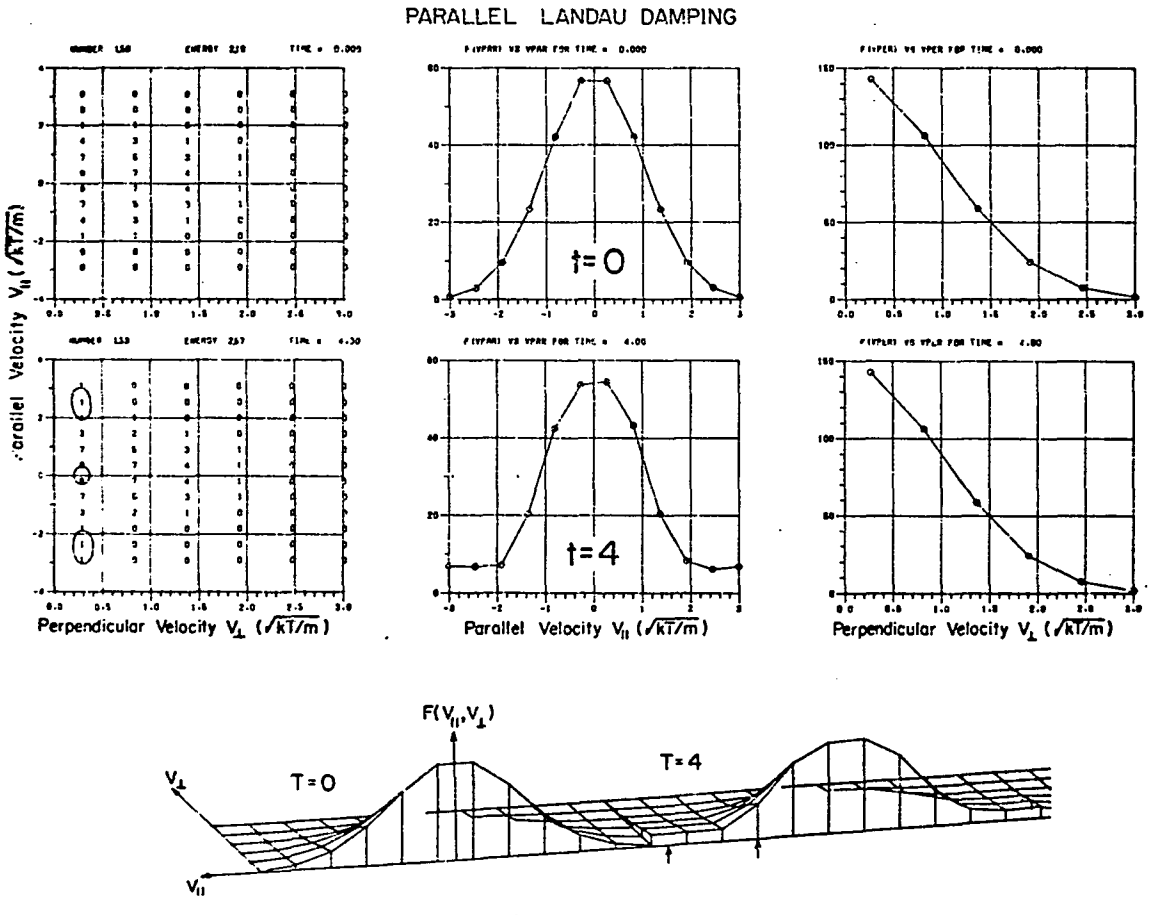
PARALLEL LANDAU DAMPING
t=0
t=4
Parallel Velocity $V_{||}$ ($\sqrt{kT/m}$)
Perpendicular Velocity $V_{\perp}$ ($\sqrt{kT/m}$)
$F(V_{||},V_{\perp})$
T=0
T=4
$V_{\perp}$
$V_{||}$

Figure 21

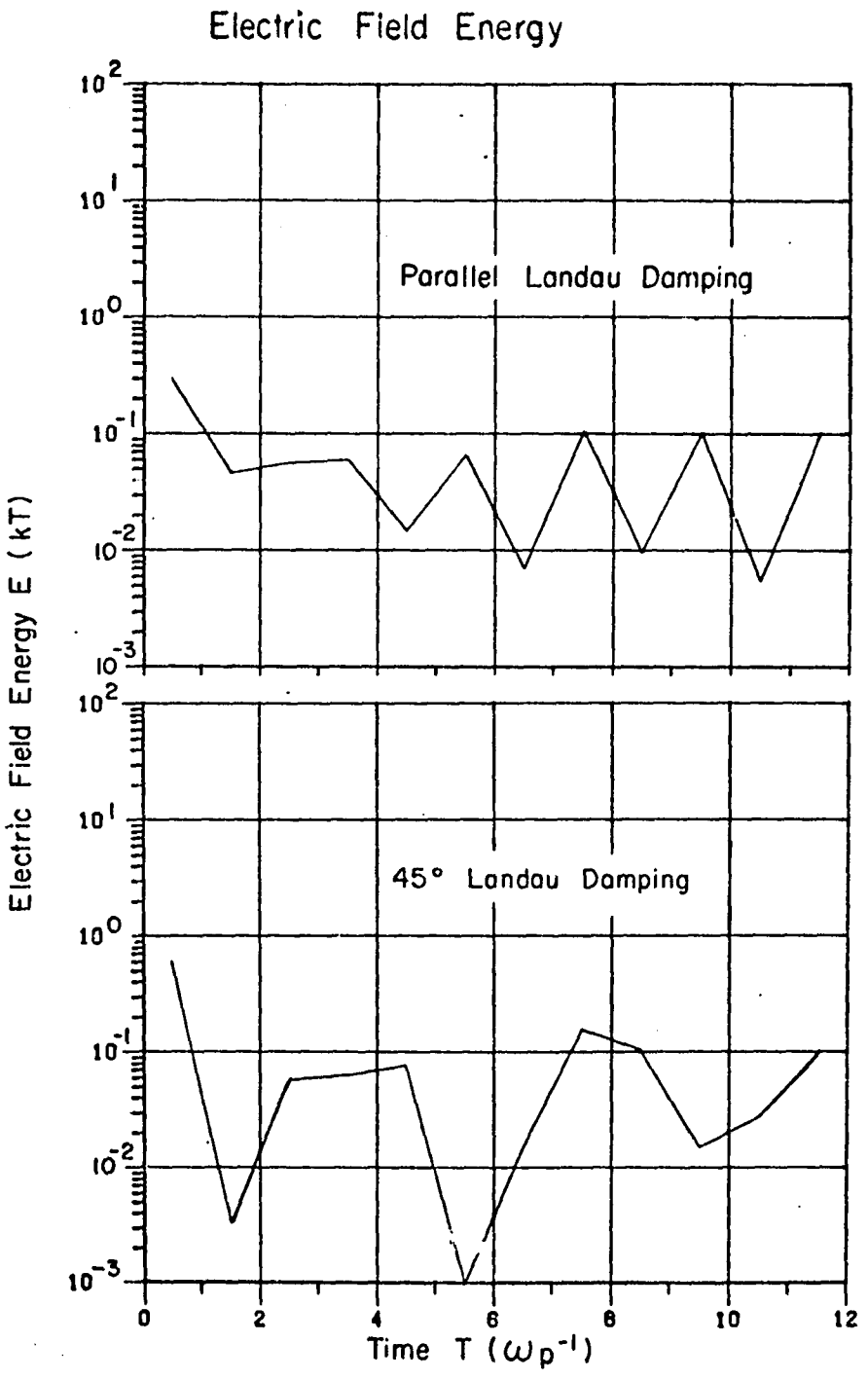
Electric Field Energy
Parallel Landau Damping
45° Landau Damping
Electric Field Energy E (kT)
Time T (ω_p^{-1})
10^2
10^1
10^0
10^{-1}
10^{-2}
10^{-3}
0
2
4
6
8
10
12

Figure 22

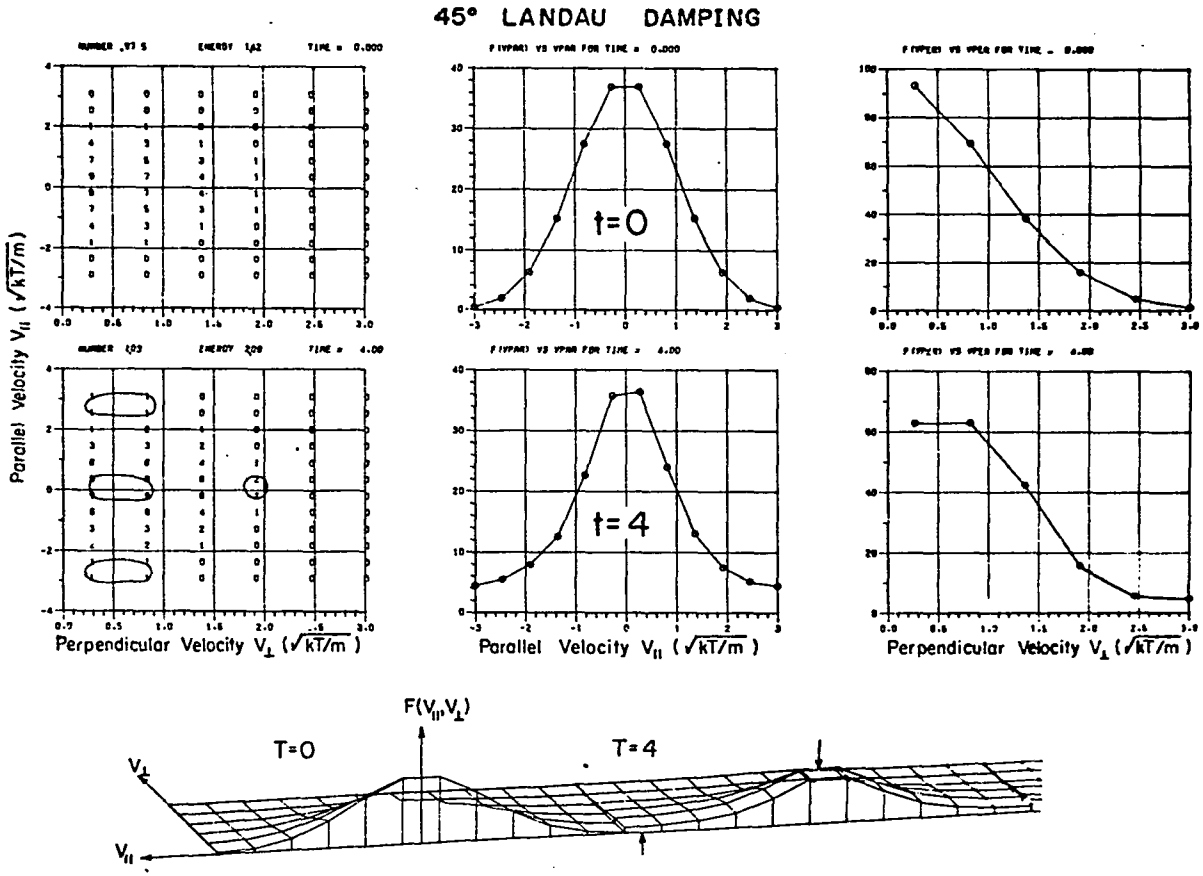
45° LANDAU DAMPING
t=0
t=4
Parallel Velocity $V_{||}$ ($\sqrt{kT/m}$)
Perpendicular Velocity $V_\perp$ ($\sqrt{kT/m}$)
Parallel Velocity $V_{||}$ ($\sqrt{kT/m}$)
Perpendicular Velocity $V_\perp$ ($\sqrt{kT/m}$)
$F(V_{||},V_\perp)$
T=0
T=4
$V_\perp$
$V_{||}$

Figure 23

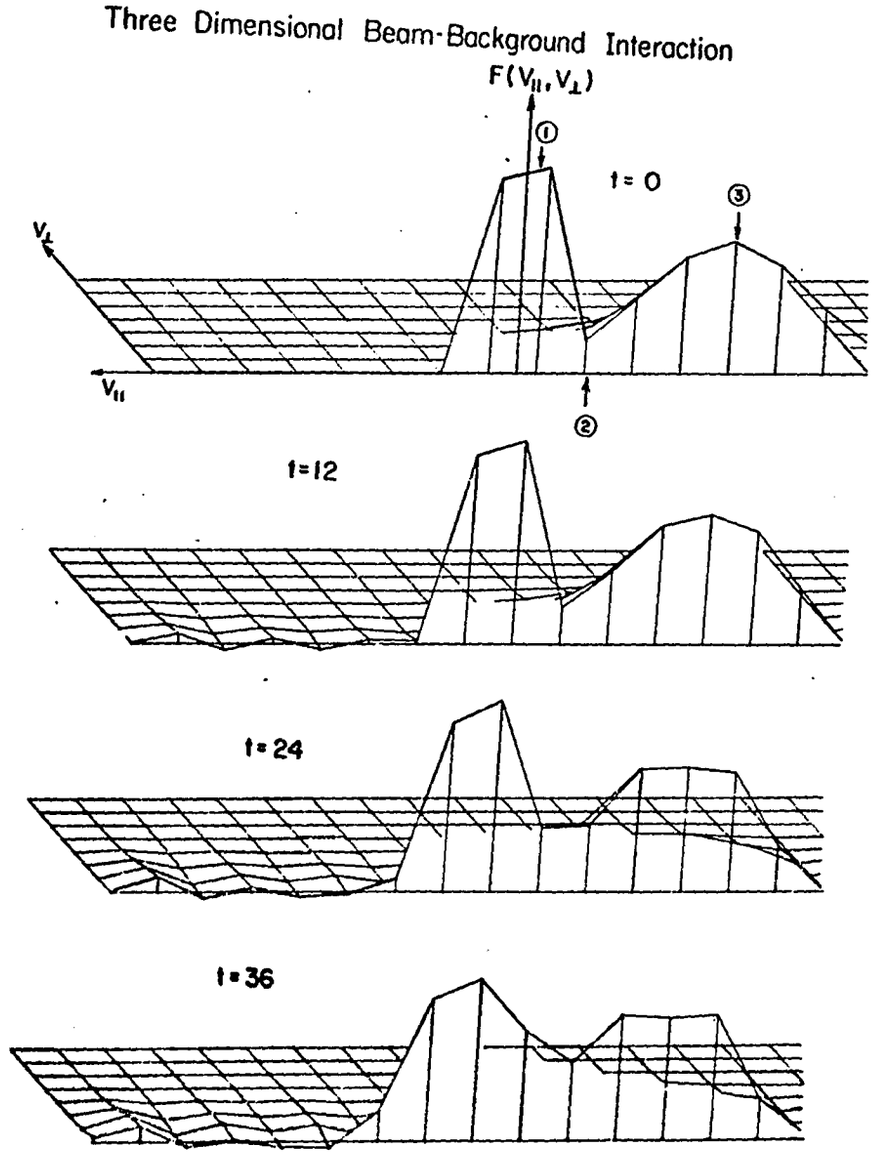
Three Dimensional Beam-Background Interaction
F(V∥, V⊥)
①
t = 0
③
V⊥
V∥
②
t=12
t=24
t=36

Figure 24

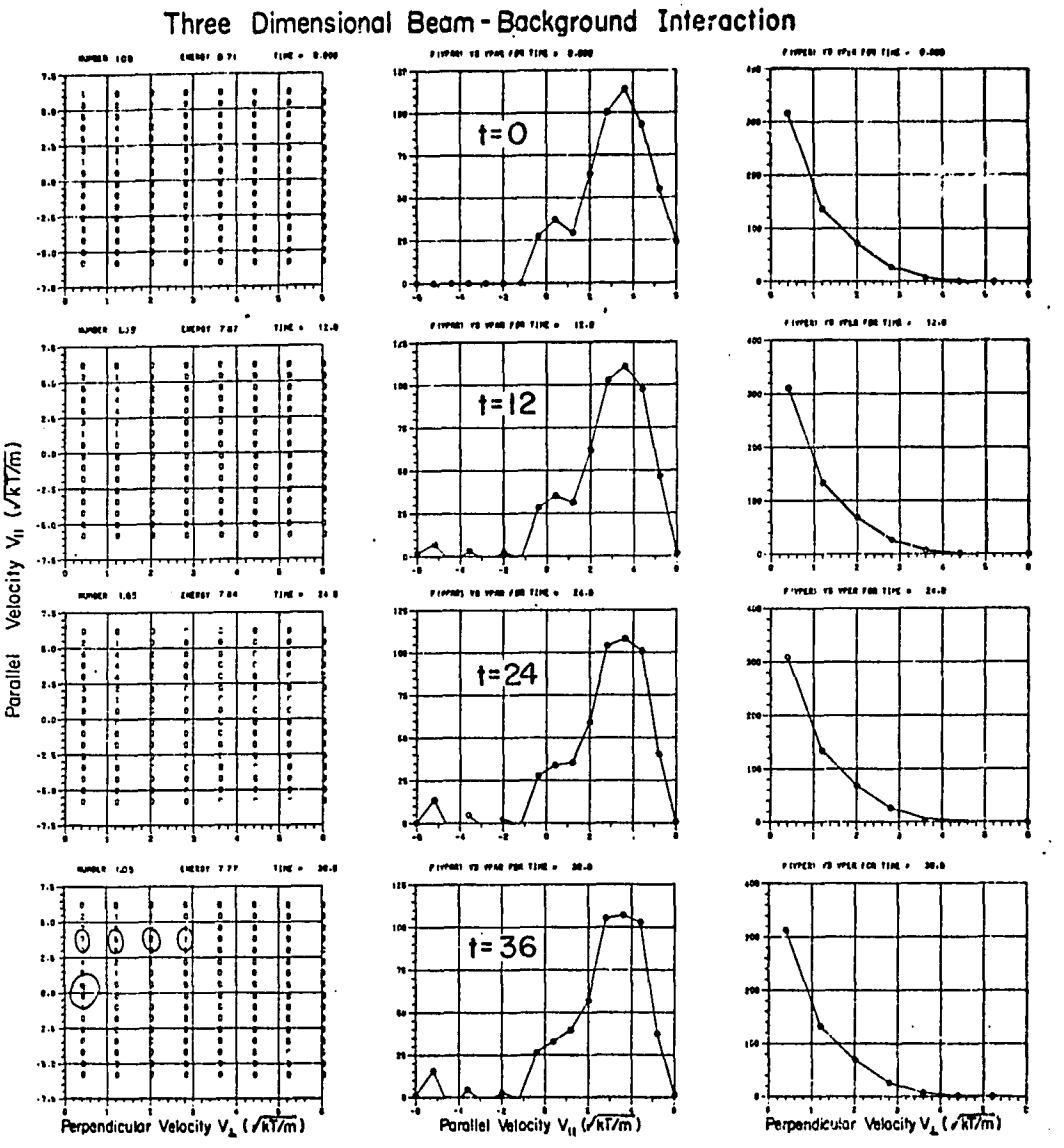
Three Dimensional Beam - Background Interaction
t=0
t=12
t=24
t=36
Parallel Velocity $V_{||}$ ($\sqrt{kT/m}$)
Perpendicular Velocity $V_\perp$ ($\sqrt{kT/m}$)
Parallel Velocity $V_{||}$ ($\sqrt{kT/m}$)
Perpendicular Velocity $V_\perp$ ($\sqrt{kT/m}$)

Figure 25

CHAPTER V

CONCLUSION

5.1 Plasma Waves

The nature of the propagation of electrostatic waves ($\vec{E} \parallel \vec{k}$) in a plasma is well understood[60 46]. Much work has been done in determining dispersion relations[75 76] relating wavelength and frequency for various plasmas. Electrostatic electric fields are formed by charge "bunching" to form a periodic spatial variation in charge density. The electric field can be calculated from Poisson's equation relating the electric field and charge density. Electrostatic waves propagate as traveling charge density waves, so that the electric field is in the direction of propagation.

An exchange of energy between the kinetic energy of charge motion and the electric field energy associated with charge "bunching" can take place in a collisionless Vlasov plasma. In the case of a plasma distribution that is unstable to Vlasov instabilities, the electrostatic electric field grows at the expense of particle kinetic energy in such a way as to remove the unstable feature in the plasma velocity distribution function (see the two-stream instability in figure 14 of chapter 3). In other cases an electrostatic field imposed on the plasma may be damped giving up energy to increase the kinetic energy of the plasma particles (see Landau damping in figure 12 of chapter 3).

The propagation of an electrostatic wave in a Maxwellian plasma and its subsequent Landau damping is depicted in figures 12 and 13 of chapter 3. The initial Maxwellian distribution is given a spatial dependence corresponding to a cosine electron density variation and an electrostatic electric field with a wavelength determined by the wave number of the cosine dependent factor (see equation 3.21). The electrostatic wave propagates with a frequency determined by the dimensionless (see Appendix B) warm plasma dispersion relation

$$\omega^2 = 1 + \frac{3}{2} k^2 \quad , \qquad (5.1)$$

where $k=2\pi/(L/\lambda_D)$ is the wave number of the plasma wave determined by the cosine dependence imposed initially. The rapid, high frequency electric field oscillations shown in figure 13 occur with twice the frequency calculated from equation 5.1 because figure 13 is a graph of the magnitude of the electric field components. Electric field amplitudes corresponding to smaller wavelength, higher wave number oscillations than the initial oscillation E_1 show higher oscillation frequencies as expected from equation 5.1.

The initial plasma oscillations shown in figure 13 are damped in time as the electrostatic electric field gives up energy to increase the electron kinetic energy. The electrons that form the plateau structure shown in the distribution function in figure 12 have been accelerated by the electrostatic electric field to higher velocities in the extended plateau region. Electrons with velocities just below the phase velocity of the electric field are accelerated to higher velocities while those with velocities above the phase velocity of the initial electric field give up energy to the wave and are decelerated[57]. There are more electrons with velocities just below the phase velocity of the wave than above, so that the net result is the formation of the Landau damping plateau structure.

The two-stream instability distribution function time evolution shown in figure 14 of chapter 3 is well known from the linear Vlasov equation theory.[71] Kinetic energy

from two colliding electron beams streaming in opposite directions is converted into the energy of a growing electrostatic electric field. The electrostatic field created by charge "bunching" occurs in the oppositely streaming beams giving an electron density that varies periodically in space. This spatial variation of the electron density gives rise to an electrostatic electric field that may be calculated from Poisson's equation relating the electric field to the electron charge density. Figure 14 shows the growth of the first four Fourier transform components of the electric field defined by equation 3.13 as the instability grows in time. The Fourier components are the amplitudes of the electrostatic waves with wavelengths equal to a fraction of the repetition length L chosen for the finite Fourier series representation of the electric field and charge density. The Fourier transform components shown in Figure 14 are the amplitudes of electrostatic waves with wavelengths ranging from the repetition length L to 1/4 of the repetition length.

The two stream instability shown in figure 14 shows that the electric field amplitude grows from a very small value of .05 in the dimensionless system of units described in Appendix B to .5 over the 60 plasma oscillation time period shown. This corresponds to a growth in electric field energy from .015 kT to 1.5 kT or a factor of 100. Thus, the driving force of two colliding electron beams creates an electrostatic field with an energy comparable to

the average electron energy at the expense of the electron kinetic energy. The decrease in total electron kinetic energy can be observed in the increase in the number of low velocity electrons near zero velocity in figure 14.

Electrostatic plasma wave growth is also seen in the beam-background interaction models shown in figures 15 and 16 of chapter 3. Figures 16a and 16b show that the first Fourier component electric field amplitudes grow by two orders of magnitude over the 60 plasma periods shown for the high beam to background electron density ratios shown (.2825 and .02825). Linear Vlasov theory predicts that instability electric field growth will be seen over 2,000 plasma periods (table 4) for a beam to background density ratio of 10^{-5}. Table 5 shows that in all cases a 2 keV strongly anisotropic electron beam does not travel more than 100 km through a Maxwellian electron background before causing electrostatic electric field growth to its maximum amplitude. Figure 15 shows that the result of the growth in electric field energy in the low beam to background density cases is a decrease in energy of the beam electrons. The final one-dimensional distribution function form for the 0.2825 density ratio case in row "a" of figure 15 shows that the beam electrons have been assimilated into the background increasing its temperature and increasing the electric field energy. A similar result is obtained for the .02825 density ratio case in row "b" of figure 15. In this case the one dimensional beam is completely assimilated into the background after 120

plasma oscillations (not shown). The numerical simulation results of Papadopoulos[63] show that the electrostatic electric field energy grows by two orders of magnitude to its maximum value after 5,000 plasma periods for a beam-background density ratio of 3×10^{-2}. If the electrostatic electric field growth has the same effect on the electron distribution function for the low beam to background density ratio cases ($.2825 \times 10^{-2}$ and 0.2825×10^{-5}) as for the high density ratio cases (.2825 and .02825), then the low density one-dimensional electron beams are assimilated into the Maxwellian background increasing its temperature and giving up energy to the electric field (see figure 15). The assimilation process takes place within at most 100 km of travel for a 2 keV beam (see table 5).

The generation and growth of electrostatic plasma waves by electron beam collision with a Maxwellian background shown in figures 14 through 19 of chapter 3 depends on the strongly anisotropic nature of the beam-background electron distribution function. An isotropic distribution function is stable to Vlasov instabilities[43] and will not give electrostatic electric field growth. Only those one-dimensional electron distribution function vs velocity curves that show a beam peak along the magnetic field direction after integrating over all other space and velocity coordinates give parallel electrostatic plasma wave growth according to the one-dimensional Vlasov theory.[44] Three dimensional isotropic electron distributions that have

an isotropic beam peak in velocity space (similar to figure 8) do not give rise to growing parallel Langmuir waves (electrostatic plasma waves) because the one-dimensional distribution function obtained by integrating over nonparallel velocity and space coordinates is monotone decreasing in the remaining parallel velocity coordinate, and therefore, stable to Vlasov instabilities. The typical auroral electron distribution at rocket altitudes (200 km) shown in figure 8 of chapter 2 has a quasi-isotropic beam peak in the downward hemisphere that is stable to Vlasov instabilities that produce parallel Langmuir waves[44]. However, short duration (<1 sec) strongly anisotropic electron "bursts" with fluxes along the magnetic field equal to ten times that in nonparallel directions have been measured at rocket altitudes[52 53 16]. These strongly field aligned rocket altitude electron beams can be expected to give rise to parallel plasma wave growth and exhibit the behavior shown in the one-dimensional beam-background interactions of figures 14 through 19.

In addition to electron "bursts" measured at low altitude (200 km) high altitude (7,000 to 8,000 km) measurements of strongly field aligned high energy electrons (~16 keV) have been reported from the S3-3 satellite by R.Sharp et. al.[77] and Mizera and Fennell[78]. These satellite altitude strongly field aligned, high energy electrons can be expected to give rise to parallel Langmuir wave growth in a background of low energy electrons . The

one-dimensional representation of the beam electrons is expected to show assimilation of the one-dimensional distribution function peak into the background. This implies a dissipation of the three-dimensional high energy electron beam peak unless the electrons are pitch angle scattered to a more stable isotropic distribution. The observation of pitch angle scattering requires a two or three dimensional theory in which nonparallel plasma waves and Bernstein electrostatic waves[75] derived from the electron cyclotron motion in the earth's magnetic field can propagate.

Chapter 4 describes a 2 1/2 dimensional solution to the Vlasov equation with two space and three velocity dimensions. Figures 21 and 22 of chapter 4 show the damping of a parallel initial electrostatic electric field equivalent to the one-dimensional calculation shown in figures 12 and 13 of chapter 3. The perspective drawing of the distribution function in velocity space shows the expected plateau structure due to the acceleration of electrons with velocities just below the phase velocity of the electric field. No pitch angle scattering is found in the contour plots to the left of figure 21 because the initial electrostatic electric field propagates parallel to the magnetic field and electron acceleration takes place in the parallel direction. Figure 23 shows the damping of an initial electric field propagating at an angle of 45° to the magnetic field. It can be seen from the contour and

one-dimensional plots in figure 23 that extensive pitch angle scattering occurs and a plateau structure is formed in both the parallel and perpendicular velocity directions (ellipses drawn on contour plots). The formation of a plateau in the distribution function perpendicular velocity curve is caused by acceleration of electrons by the perpendicular component of the electrostatic electric field. The result is the pitch angle scattering and acceleration of low energy electrons into the perpendicular plateau region shown in figure 23. The plateaus formed in the parallel velocity direction also show some pitch angle scattering in the broad plateaus extending in the perpendicular velocity direction indicated by the ellipses in the contour plot of figure 23.

The introduction of a second space dimension perpendicular to the magnetic field direction in the 2 1/2 dimensional model of chapter 4 allows a cyclotron motion of the electrons about the magnetic field axis. This additional orbital motion is caused by the -e/c vxB Lorentz force on the electrons and gives rise to additional modes of oscillation in the electrostatic electric field. All nonaxial electrostatic electric field oscillations are described by the dispersion relation for Bernstein waves[75]. Unlike parallel plasma waves that occur at a single frequency for a given wave number determined from the dispersion relation of equation 5.1, electrostatic density waves propagate at an angle to the magnetic field and have

an infinite number of frequency modes of propagation with frequencies approximately equal to integer multiples of the electron cyclotron frequency [75].

The 45° Landau damping case of figures 23 and 22 may be analyzed by considering the parallel and perpendicular components of the electrostatic electric field separately. The parallel component gives rise to parallel Langmuir waves that propagate with frequencies determined from equation 5.1 and leads to the formation of a plateau structure in the parallel velocity direction (see figure 23). In general, the perpendicular electric field component should be described by the dispersion relation for Bernstein waves[75] since the analysis should include the cyclotron motion of the electrons. However, in the 45 Landau damping case actually shown in figure 23, the magnetic field was taken to be zero and the electrons did not undergo cyclotron motion. The perpendicular electrostatic electric field is purely a Langmuir plasma wave propagating with a frequency given by the dispersion relation for plasma waves (equation 5.1). The magnetic field was chosen to be nonzero with a cyclotron frequency of $\omega_c = .1\omega_p$ in the beam-background interaction of figure 24 in chapter 4, so that in this case the propagation of electrostatic waves must be described by the dispersion relation for Bernstein waves[75].

5.2 Low energy Electrons (10-1,000 eV)

High above the auroral ionosphere at 7,000 to 8,000 km satellite S3-3[77 78] has measured magnetic field aligned fluxes of high energy (~16 keV) electrons traveling through an approximately equal density background of 70 to 1,100 eV electrons. According to the 2 1/2 dimensional results depicted in the perspective plot in figure 24 and the distribution function plots in figure 25 of chapter 4, a strongly field aligned, high energy electron beam streaming parallel to the magnetic field through a low energy electron background gives rise to parallel Langmuir waves and the filling in of the velocity range between the beam peak and background (marked by arrow "2" in figure 24) . The increase in low energy electron population in the "valley" region between beam and background peaks is accomplished by the acceleration of low energy background electrons (note diminishment of background peak in figure 24) and a deceleration of high energy beam electrons as they give up energy to the electrostatic field.

The increase in low energy electron population in the "valley" region of the 2 1/2 dimensional model due to the deceleration of beam electrons is similar to the increase in electron population observed in the one dimensional calculations made for the symmetric two stream instability shown in figure 14 of chapter 3. The colliding electron beams generate growing electrostatic waves with

phase velocities just below the beam peaks that gain energy from beam electrons decelerating them to lower velocity and increasing the low energy electron population. Figure 15a shows the one dimensional interaction between a Maxwellian electron beam of 1/3 the background density. The deceleration of beam electrons due to the electric field growth shown in figure 16a ultimately results in the complete dissipation of the one-dimensional beam and an increase in electron population in the "valley" region. Electrostatic field components with phase velocities just below the beam peak (E_1 and E_2 in figure 16a) gain energy from beam electrons. Smaller wavelength electric field components with phase velocities in the electron background velocity range (E_5 and E_7 in figure 16a) grow by parametric coupling with the initial high phase velocity wave[63 65] or some other wave-particle interaction and accelerate low energy electron background electrons to higher velocities. The net result is the increase in electron population in the intermediate velocity "valley" regions shown in figures 14, 15 and 24.

The increase in low energy electron population in the "valley" region over the number expected[8 5 63 65] from secondary electrons produced by the ionization of nitrogen and oxygen in the ionosphere may be due to the production of Langmuir waves through a beam-background interaction that decelerates beam electrons and increases the energy of low energy background electrons. The production of parallel

Langmuir waves and the increase in "valley" electron population at high altitudes (7,000-8,000), where strongly anisotropic beam electron distributions and equal density backgrounds have been measured[77 78] follows from the application of the one or 2 1/2 dimensional Vlasov theory (figures 14, 15 and 24). However, at lower rocket altitudes (200 km) typical electron distributions measured over several second time intervals such as the one shown in figure 8 are isotropic and stable to parallel Langmuir waves[44]. Short "bursts" of less than one second duration of anisotropic strongly field aligned high energy electrons have occasionally been measured at rocket altitude[52 53 16] and, these can be expected to lead to the growth of parallel electrostatic waves and a filling in of the intermediate "valley" region in parallel velocity space. The increase in electron population in the "valley" region in parallel velocity space is then presumably spread to other nonparallel velocities to give an isotropic low energy background by some mechanism leading to pitch angle scattering such as ionospheric collisions or magnetic field mirroring.

Figure 18 of chapter 3 shows the simulation of the interaction between an anisotropic electron beam "burst" in the form of an accelerated Maxwellian traveling along the magnetic field line with a background ionosphere of 10 eV at rocket altitudes. Because of the long growth time in plasma periods expected for parallel plasma waves ($\sim 5{,}000\omega_p^{-1}$) for

the beam to background density ratio of 10 chosen in figure 18, a high initial electric field energy of .125 kT with a phase velocity equal to the beam peak velocity of $20\sqrt{kT/m}$ is used to start the distribution function time evolution at t=0. The one-dimensional distribution function is expected to evolve to a stable monotone decreasing form in which the high energy beam is dissipated by absorption into the background (see figure 15a) over a period of several thousand plasma periods (see table 5). The t=150 curve of figure 18 shows the one-dimensional distribution function after 150 plasma periods of evolution. The increase in electron population in the "valley" region can be seen in the spiked structure in the negative parallel velocity range. A greater number of spatial grid points and electric field components may lead to the smooth curve (shown in the positive velocity region of the t=150 curve of figure 18) drawn by connecting the peaks (open circles) in the "valley" velocity range. It can be seen that a definite "valley" region population region increase has occured by comparison of the solid Vlasov equation evolved curve with the dashed curve showing the initial distribution function.

An electron distribution function calculated from the rocket flux data shown in figure 2 assuming an iostropic distribution is shown by the alternately dashed and dotted curve in figure 18, t=150. The value $v^2 f(v,x)$ for the measured distribution function is plotted because for the spherical velocity coordinates used, the area under this

curve is equal to the electron density. Therefore, the electron density over a velocity range in figure 18 is given by the integral of $v^2f(v,x)$ in v for the measured distribution function and the integral of F(v)/L for the evolved distribution function (normalized to one electron per cube of side equal to one Debye length - see Appendix B). The measured distribution function in the t=150 curve of figure 18 shows a smaller slope magnitude in the "valley" region than the initial (dashed line) or t=150 (solid line) distribution functions. However, the t=150 evolved distribution function shows a sharp reduction in slope magnitude in the 10 to 180 eV range compared with the initial distribution function. The increase in "valley" electron population may lead to even smaller slope magnitudes as the distribution function continues to evolve.

An increase in "valley" electron population has been demonstrated for strongly anisotropic electron beams incident on a Maxwellian low energy background in figures 14, 15, 18, 24 and 25. Anisotropic beams typical of high altitude (7,000-8,000 km) measurements[77 78] and occasional rocket altitude (200 km) electron beam "bursts"[52 53 16] have been reported. However, an increase in electron population in the "valley" velocity range for the typical isotropic electron distribution function measured at low altitude (see figure 8) by the collisionless Vlasov instability mechanism used here requires a strongly anisotropic beam that gives a two peaked structure in the

one-dimensional distribution function $F(v_{||})$. It is possible that strongly anisotropic electron beam peaks in the parallel velocity direction do occur on a time scale short by comparison with the time period of several seconds required to collect the data needed for the construction of a two-dimensional distribution function such as the one shown in figure 8. Short lived anisotropic peaks may give rise to growing electrostatic waves and an increase in low energy "valley" electron population accompanied by a diminishment of the peak to form a plateau structure shuch as the one shown in figures 8 and 24. Table 5 shows that electric field instability growth at rocket altitudes where the beam to background density ratio is about 10^{-5} requires a time period on the order of .1 msec to grow to maximum amplitude. Therefore, peaks in the one-dimensional distribution function dissipate themselves and strong anisotropies in the two-dimensional distribution function are removed by giving up energy to an electrostatic plasma wave (see figure 15a) well within the time required for data collection (several seconds). The periodic appearance and disappearance of strongly anisotropic electron beam peaks along the magnetic field line requires a continuous acceleration process active throughout the auroral ionosphere. Such acceleration mechanisms are currently the subject of active speculation and research.(13 16 64 17)

5.3 Acceleration Mechanism

Figures 14, 15, 24 and 25 show that for beam to background density ratios on the order of one the unstable double peak structure of the anisotropic beam-background interaction is removed within 30 plasma periods (ω_p^{-1}) of evolution. This corresponds to a time period of ~.1msec for a beam density of 1 cm^{-3} (table 5) and a distance of ~10 km for a 2 keV beam. Lower density ratio interactions require several thousand plasma periods for the removal of unstable features. However, for 1 cm^{-3} beam electron densities, the time required for the growth of parallel Langmuir waves is still less than 1 msec because the plasma period (ω_p^{-1}) decreases with increasing background density (see table 5). Therefore, it can be concluded that anisotropic beam peaks in the one dimensional electron distribution function along the magnetic field line are dissipated by giving up electron kinetic energy to the growth of parallel electrostatic plasma waves within milliseconds of formation. The distance travelled by a 2 keV anisotropic beam through a background before removal of the double peaked structure in the one dimensional distribution function ranges from 3.2 to 97 km depending on the beam to background electron density ratio (see table 5).

The two-dimensional distribution function $f(v_{//}, v_{\perp})$ may retain some peaked structure along the field line (figure 24) even after the evolution to a monotone

decreasing one-dimensional integrated distribution function $F(v_{\parallel})$ (figure 25). This is because the integral of $v_{\perp} f(v_{\parallel}, v_{\perp})$ over $v_{\perp}$ may remove a peaked structure in the two-dimensional distribution function $f(v_{\parallel}, v_{\perp})$. This is the case in the 2 1/2 dimensional evolution shown in figures 24 and 25 and in the measured distribution shown in figure 8[44]. According to Mizera and Fennell[78] and Sharp et. al.[77], the electron distribution functions measured at 7,000-8,000 km by satellite S3-3 show a strong peaking in the parallel direction indicative of a field aligned acceleration region. If this peaking is strong enough to give a two peaked structure in the one dimensional distribution function, then the growth of parallel electrostatic waves can be expected. If the acclereation region were of limited extent, confined to an altitude range of a few kilometers, then strong peaking in the parallel velocity direction would be removed within milliseconds through the Vlasov instability mechanism. A 2 keV beam travelling through an equal density background would dissipate its unstable one-dimensional two peak feature derived from a strongly anisotropic, two-dimensional distribution function within 15 km of travel. However, a strongly anisotropic parallel peaking in the electron distribution function is reported[77 78] in the S3-3 data over a 1,000 km range. Therefore, it is suggested that the auroral electron acceleration process is a continuous process and extends over at least 1,000 km.

The higher than expected electron population in the "valley" region between beam peak and ionosphere background at rocket altitudes (200 km) and the small slope magnitude when compared with atmospheric scattering calculations[7] (see figure 3) indicates that collisionless processes may be important. The calculations shown in figures 15, 18 and 24 indicate that parallel plasma wave production on a millisecond time scale may account for an increase in "valley" electron population at rocket altitudes. However, this requires a continuous acceleration region extending from satellite to rocket altitudes in order to maintain the growth of parallel plasma waves, since the unstable two peaked structure in the one-dimensional distribution function can be expected to dissipate within 3 to 100 km of travel for a typical 2 keV auroral electron beam.

REFERENCES

(1) R. E. Haines, Friends, 35, 15 (1978)

(2) S. Akasofu and S. Chapman, Solar-Terrestrial Physics, (Oxford University Press, London, 1972) p. 678.

(3) M. H. Rees, "Processes and Emissions Associated with Electron Precipitation," in Atmosphere of the Earth and the Planets, ed. B. McCormac, (D. Reidel, Hingham, MA, 1975) p. 328.

(4) M. Rees, et al., J. Geo. Res. 82, 2250 (1977)

(5) R. Arnoldy and P. Lewis, J. Geo. Res. 82 2755 (1975)

(6) R. Arnoldy, et al., Rev. Sci. Instr. 44, 172 (1973).

(7) P. Banks, et al., J. Geo. Res. 79, 1459 (1974).

(8) D. Strickland, et al., J. Geo. Res. 81, 2755 (1976).

(9) R. Jones and M. Rees, Planet. Space Sci. 21, 537 (1973).

(10) D. Reasoner and C. Chappel, J. Geo. Res. 78, 2176-2186 (1973).

(11) P. Feldman and J. Doering, J. Geo. Res. 80, 2808 (1975).

(12) W. Sharp and P. Hays, J. Geo. Res. 77, 6828 (1974).

(13) K. Papadopoulos, Rev. Geo. Space Phy. 15, 1977.

(14) M. Montgomery, J. Geo. Res. 75, 1217 (1970).

(15) S. Akasofu and L. Lanzerotti, Physics Today, Dec. 1975.

(16) K. Papadopoulos and T. Coffey, J. Geo. Res. 79, 674 (1974).

(17) A. Hasegawa, J. Geo. Res. 12, 273 (1974).

(18) L. Frank, Rev. Geo. Space Phy. 13, 974 (1975).

(19) Earth's Particles and Fields, ed. B.McCormac (Reinhold, 1967), p. 69.

(20) L. Frank, J. Geo. Res. 76, 5202 (1971).

(21) S. Akasofu, J. Geo. Res. 78, 7257 (1973).

(22) H. Rosenbauer, et al., J. Geo. Res. 80, 2723 (1975).

(23) R. Arnoldy, J. Geo. Res. 79, 4203 (1974).

(24) E. Hones, J. Geo. Res. 76, 63 (1971).

(25) C. Chappell, Rev. Geo. Space Phy. 10, 951 (1972).

(26) J. Winninghand, W. Heikkila, J. Geo. Res. 79 949 (1974).

(27) L. Frank, J. Geo. Res. 77, 4116 (1972).

(28) L. Frank, Rev. Geo. Space Phy. 13, 974 (1975).

(29) R. Boyd, Space Physics (Clarendon, Oxford, 1974).

(30) G. Rostoker and R. Bostrom, J. Geo. Res. 81, 235 (1976).

(31) A. Zmuda and J. Armstrong, J. Geo. Res. 79, 4611 (1974).

(32) P. Cloutier et al., J. Geo. Res. 78, 640 (1973).

(33) E. Hones et al., J. Geo. Res. 77, 5503 (1972).

(34) E. Hones et al., J. Geo. Res. 79, 1385 (1974).

(35) E. Hones et al., J. Geo. Res. 76, 63 (1971).

(36) N. Rees and K. Maeda, J. Geo. Res. 78 (1973).

(37) N. Krall and A. Trivelpiece, Principles of Plasma Physics, (McGraw-Hill, 1973) p. 79.

(39) D. ter Haar, Elements of Statistical Mechanics (Rinehart, NY, 1955) p. 103.

(40) A. Vlasov, J. Phys. (USSR), 9, 25 (1945).

(41) S. Brown, Basic Data of Plasma Physics, (M.I.T. Press, Cambridge, MA, 1959) p. 12.

(42) F. Chen, Introduction to Plasma Physics, (Plennum Press, NY, 1974) p. 322.

(43) Reference 38, p. 447.

(44) R. Kaufmann, et al., Stability of the Auroral Plasma: Parallel and Perpendicular Propagation of Electrostatic Waves, submitted to J. Geo. Res., December 1977.

(45) C. Cheng, J. Comp. Phys. 24, 348-360 (1977).

(46) C. Cheng and G. Knorr, J. Comp. Phys. 22, 330 (1976).

(47) F. Hildebrand, Introduction to Numerical Analysis, (McGraw-Hill, Inc., NY, 1974) p. 453.

(48) J. Ahlberg, et al., The Theory of Splines and Their Applications, (Academic Press, NY, 1967).

(49) Reference 47, p. 481.

(50) Reference Manual (International Mathematical and Statistical Libraries, Inc.), IMSL, Houston, TX, 1975) p. I-1.

(51) Plot 10 Advanced Graphing II, (Tektronix, Inc., Beaverton, Oregon, 1973).

(52) B. O'Brien and R. Reasoner, J. Geo. Res. 76, 8258 (1971).

(53) R. Arnoldy, et al., J. Geo. Res. 79, 4208 (1974).

(54) E. Brigham, The Fast Fourier Transform (Prentice-Hall, Inc., Englewood Cliffs, Nj, 1974) p. 99.

(55) Methods in Computational Physics, Vol. 9, Ed. B. Alder et al., (Academic Press, NY, 1970) p. 39.

(56) Reference 39, p. 520.

(57) F. Chen, Introduction to Plasma Physics, (Plenum Press, NY, 1974) p. 219.

(58) R. Kaufmann, et al., J. Geo. Res. 83, 586 (1978).

(59) A. Mikhailovskii, Theory of Plasma Instabilities, v. 1 (Consultants Bureau, NY, 1974) p. 27.

(60) Reference 38, p. 369.

(61) Reference 59, p. 11.

(62) Reference 59, p. 58.

(63) K. Papadopoulos, Rev. Geo. Space Phys. 15, 113 (1977).

(64) R. Kaufmann, D. Walker and R. Arnoldy, J. Geo. Res. 81, 1673 (1976).

(65) K. Papadopoulos and H. Rowland, Collisionless Effects on the Spectrum of Secondary Electrons at Low Altitudes, submitted to J. Geo. Res. 1977.

(66) Reference 66, p. 136.

(67) R. Hockney, J. Assoc. Comp. Mach., 12, 95 (1965).

(68) J. Gazdag, J. Comp. Physics 13, 100 (1973).

(69) J. Gazdag, J. Comp. Physics 19, 77 (1975).

(70) Reference 38, p. 529.

(71) Reference 38, p. 533.

(72) C. Kennel and F. Engelmann, Phys. Fluids 9, 2377 (1966).

(73) Atmosphere of the Earth and Planets, ed. B. McCormac (D. Reidel Pub. Co., Boston, MA, 1974), p. 103.

(74) Ref. 2, p. 243.

(75) I. Bernstein, Phys. Rev. 109, 10 (1958).

(76) Physics of Hot Plasmas, ed. B. Rye and J. Taylor (Plenum Press, NY, 1968), p. 158.

(77) R. Sharp et al., Energetic Particle Measurements from within Ionospheric Structures Responsible for Auroral Acceleration Processes, preprint, March 1978.

(78) P. Mizera, J. Fennell, Geo. Res. Letters, 4, 311 (1977).

APPENDIX A

PARTICLE DENSITY AND DISTRIBUTION

DISTRIBUTION FROM FLUX

Figure A-1 shows a particle detector aperature of area dA and a source of particles in volume dV. The source volume is a distance r from the aperature and subtends a solid angle $d\Omega$ at the detector. The particle flux through the detector aperature $4\pi r^2$ is given by

$$\frac{dJ}{dE}\ (\text{electrons/cm}^2\text{-sec-sr-ev}) = \frac{dN'\ dV}{(dA\ \cos\theta)dt\ dE\ d\Omega} \qquad \text{(A-1)}$$

where dN' dV is the number of particles in volume dV that enter the detector and dA cos(θ) is the area of the detector normal to the particle flux from dV. Particles entering the detector during a time interval dt with a velocity v directed toward the detector and passing through the source volume of solid angle $d\Omega$ must have come from a

volume

$$dV = vr^2 d\Omega\, dt \quad . \tag{A-2}$$

Therefore, the flux is

$$\frac{dJ}{dE} = \frac{dN'\, r^2 v}{(dA \cos\theta)\, dE} \quad . \tag{A-3}$$

The number of particles per unit volume that contribute to the flux through the detector from dV is

$$dN' = \frac{(dA \cos\theta)}{r^2} \frac{dJ}{dE} \frac{dE}{\sqrt{2E/m}} \quad , \tag{A-4}$$

where $v = \sqrt{2E/m}$ has been used, and the quantity $dA \cos(\theta)/r^2$ is the solid angle subtended by the detector ($d\Omega'$) at the source volume. If the detector covered an entire sphere enclosing volume dV at a distance r, then all the particles leaving dV would be detected. Therefore, the total number of particles per unit volume in the energy range dE emanating from dV is

$$dN = \sqrt{m/2} \int_{\text{sphere}} 1/\sqrt{E} \ \frac{dJ}{dE} \ dE \ d\Omega' = 4\pi\sqrt{m/2E} \ \frac{dJ}{dE} \ dE \ , \qquad \text{(A-5)}$$

where an isotropic flux has been assumed. The number of particles per unit volume over all energies is

$$N(cm^{-3}) = 4\pi\sqrt{m/2} \int_0^{\infty} 1/\sqrt{E} \ \frac{dJ}{dE} \ dE$$

$$= 2.119 \times 10^{-7} \int_0^{\infty} \frac{dE(ev)}{\sqrt{E(ev)}} \ \frac{dJ}{dE} \ (\#/cm^2\text{-sec-sr-ev}). \qquad \text{(A-6)}$$

The electron distribution function in spherical coordinates $f(v,\theta,\phi)$ can be related to the flux by writing the number of electrons in the source volume dN' per unit volume that pass through the detector aperature during a time interval dt as

$$dN' = (f(v,\theta,\phi)v^2 d\Omega_v)(dA \cos\theta/4\pi r^2)(v\ dt\ r^2\ d\Omega) \quad , \qquad \text{(A-7)}$$

electron density	fraction emitted from source volume that enter aperature	source volume

where $d\Omega_v = \sin(\theta)\ d\theta\, d\phi$ is the solid angle in velocity space. The flux is

$$\frac{dJ}{dE} = \frac{(fv^2 dv\ d\Omega_v)(dA \cos\theta/4\pi r^2)(v\ dt\ r^2\ d\Omega)}{(dA \cos\theta)\ dt\ dE\ d\Omega}$$

$$= \frac{v\ f(v,\theta,\phi)\ dv\ d\Omega_v}{4\pi\ dE} \qquad \text{(A-8)}$$

from equations A-1 and A-7. For an isotropic flux

$$f(v) = \int_{\text{sphere}} f(v,\theta,\phi)\ d\Omega_v = 4\pi\ f(v) \quad , \qquad \text{(A-9)}$$

and using $v=\sqrt{2E/m}$, the isotropic flux integrated over all solid angles in velocity space is

$$\frac{dJ}{dE} = (v\,\frac{2E}{m})\,\frac{4\pi f(v)}{4\pi}\,\frac{(dE/mv)}{dE}$$

$$\frac{dJ}{dE} = \frac{2E}{m^2}\,f(v) \quad . \qquad \text{(A-10)}$$

The relation between the distribution function in cylindrical coordinates $f(v_{//}, v_{\perp}, \phi)$ and the detector electron is obtained by writing the electron density in equation A-7 as

$$dN = f(v_{\shortparallel}, v_{\perp}, \phi)\; v_{\perp}\; d\phi\; dv_{\shortparallel}\; dv \qquad \text{(A-11)}$$

so that the flux becomes

$$dJ(v_{\shortparallel}, v_{\perp}, \phi) = \frac{\sqrt{v_{\shortparallel}^2 + v_{\perp}^2}\; f(v_{\shortparallel}, v_{\perp}, \phi)}{4\pi}\; v_{\perp}\; d\phi\; dv_{\shortparallel}\; dv \quad , \qquad \text{(A-12)}$$

where equations A-7, A-1 and $v=\sqrt{v_{//}^{\,2}+v_{\perp}^{\,2}}$ have been used.

Note that the units of differential flux dJ are electrons/cm²-sr-sec in cgs units since no division by the energy range dE has been made. If the magnetic field direction with respect to analyzer acceptance angle is measured by onboard magnetometers, the differential flux as a function of pitch angle can be determined and the distribution function calculated from

$$f(v_{\parallel} = v \cos \alpha,\ v_{\perp} = v \sin \alpha) dv_{\parallel}\, dv_{\perp} = \frac{m}{E \sin \alpha}\, dJ(E,\alpha) \quad , \qquad \text{(A-13)}$$

where α is the pitch angle (angle between electron velocity and magnetic field), E is determined from the electrostatic analyzer energy value at the time the magnetometer data indicates a pitch angle of α for electrons entering the analyzer detector and isotropy about the field line ($\ln \phi$) has been assumed.

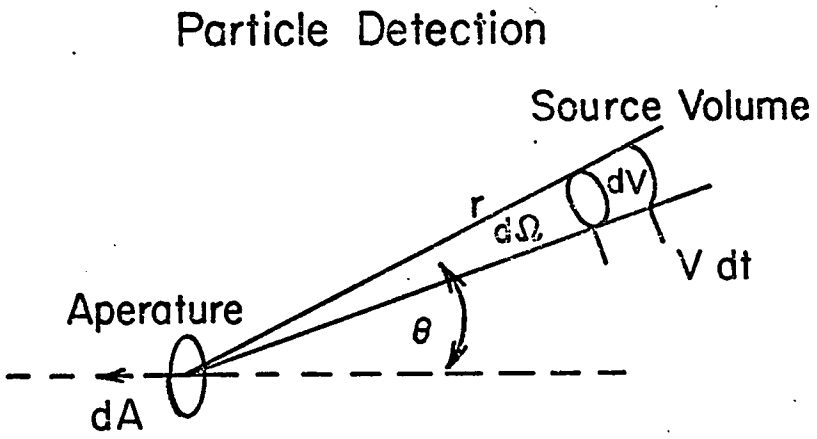

Figure A-1

APPENDIX B

THE DIMENSIONLESS VLASOV EQUATION

IN 2 1/2 DIMENSIONS

B.1 Dimensionless form

Poisson's equation

$$\frac{\partial E_x}{\partial x} + \frac{\partial E_y}{\partial y} = 4\pi ne\left(1 - \int_{-\infty}^{\infty} f \, d^3\vec{v}\right) \qquad \text{(B-1)}$$

can be converted into a dimensionless form by first multiplying both sides by e/m to get

$$\frac{e}{m}\left(\frac{\partial E_x}{\partial x} + \frac{\partial E_y}{\partial y}\right) = \omega_p^2 \left(1 - \int f \, d^3\vec{v}\right) \quad , \qquad \text{(B-2)}$$

where ω_p is the electron plasma frequency. The length variables (x and y) must be written in units of the Debye length so that equation B-2 becomes

$$\frac{e}{m}\frac{1}{\omega_p^2}\left(\frac{1}{\lambda_D}\frac{\partial E_x}{\partial x'}+\frac{1}{\lambda_D}\frac{\partial E_y}{\partial y'}\right) = 1 - \int f\, d^3\vec{v}$$

$$\omega_p^2 = 4\pi ne^2/m$$

$$\lambda_D = kT/4\pi ne^2$$

$$x' = x/\lambda_D$$

$$y' = y/\lambda_D \quad , \qquad \text{(B-3)}$$

where x' and y' are the new dimensionless space varibles. The substitution of

$$E' = \frac{e}{m\,\lambda_D\omega_D^2}E \qquad \text{(B-4)}$$

into B-3 gives the dimensionless format Poisson's equation

$$\frac{\partial E'_x}{\partial x'}+\frac{\partial E'_y}{\partial y'} = 1 - \int f\, d^3\vec{v} \quad . \qquad \text{(B-5)}$$

The Vlasov equation is transformed to dimensionless form by writing the time and space variable in units of ω_p^{-1} and λ_D respectively. Writing the new variables with

a prime superscript, and noting that the new dimensionless velocity is equal to the velocity divided by the thermal velocity $v_{th} = \lambda_D \omega_p$, gives

$$\frac{1}{\omega_p^{-1}} \frac{\partial f}{\partial t'} + \frac{\lambda_D \omega_p}{\lambda_D} \vec{v}' \cdot \vec{\nabla}' f - \frac{e}{m} \vec{E} \cdot \left(\frac{1}{\lambda_D \omega_p} \vec{\nabla}_{v'} f\right) +$$

$$- (\vec{v}' \times \vec{\omega}_c) \cdot \vec{\nabla}_{v'} f = 0 \quad , \qquad \text{(B-6)}$$

where $\vec{\omega}_c = e\vec{B}/mc$ is the electron cyclotron frequency. Rearranging terms gives

$$\frac{\partial f}{\partial t} + \vec{v}' \cdot \vec{\nabla}' f - (\vec{E}' + \vec{v}' \times \vec{\omega}_c') \cdot \vec{\nabla}_{v'} f = 0 \quad , \qquad \text{(B-7)}$$

where ω_c' is in units of ω_p and equation B-4 has been used. Dropping the primes in equation B-7 and B-5 gives the final form of the dimensionless Vlasov and Poisson equation system

$$\frac{\partial f}{\partial t} + \vec{v} \cdot \vec{\nabla} f - (\vec{E} + \vec{v} \times \vec{\omega}_c) \cdot \vec{\nabla}_v f = 0$$

$$\frac{\partial E_x}{\partial x} + \frac{\partial E_y}{\partial y} = 1 - \int f \, d^3 \vec{v} \qquad \text{(B-8)}$$

B.2 Identities

The following identities were determined using the coordinate system shown in Figure B-1. They assume a spatial dependence on x and y only.

$$\vec{\nabla} f = \hat{i}\,\frac{\partial f}{\partial x} + \hat{j}\,\frac{\partial f}{\partial y}$$

$$\vec{\nabla}_v f = \hat{e}_\perp\,\frac{\partial f}{\partial v_\perp} + \hat{e}_\parallel\,\frac{\partial f}{\partial v_\parallel} + \hat{e}_\phi\,\frac{1}{v_\perp}\,\frac{\partial f}{\partial \phi}$$

$$= \hat{e}_\parallel\,\frac{\partial f}{\partial v_\parallel} + \hat{i}\,\frac{\partial f}{\partial v_x} + \hat{e}_{y_\perp}\,\frac{\partial f}{\partial y_\perp}$$

$$\vec{E} = E_x\hat{i} + E_y\hat{j}$$

$$\vec{v} = \vec{v}_\parallel + \vec{v}_x + \vec{v}_{y_\perp} = \vec{v}_\parallel + \vec{v}_\perp \qquad \text{(B-9)}$$

The partial derivative relations

$$\frac{\partial v_\perp}{\partial v_x} = \cos\phi$$

$$\frac{\partial v_\perp}{\partial v_y} = \sin\phi \qquad \text{(B-10)}$$

can be established from the definitions

$$v_x = v_\perp \cos\phi \qquad v_y = v_\perp \sin\phi \qquad v_\perp^2 = v_x^2 + v_{y_\perp}^2 \qquad \text{(B-11)}$$

by implicity differentiation of the expression for $v_\perp^2$

$$2\, v_{\perp}\, dv_{\perp} = 2\, v_x\, dv_x + 2\, v_{y_{\perp}}\, dv_{y_{\perp}}$$

$$dv_{\perp} = \frac{v_x}{v_{\perp}}\, dv_x + \frac{v_{y_{\perp}}}{v_{\perp}}\, dv_{y_{\perp}}$$

$$dv_{\perp} = \cos\phi\, dv_x + \sin\phi\, dv_{y_{\perp}} \qquad \text{(B-12)}$$

and the expression for the total derivative of $v_{\perp}(v_x, v_{y_{\perp}})$

$$dv_{\perp} = \frac{\partial v_{\perp}}{\partial v_x}\, dv_x + \frac{\partial v_{\perp}}{\partial v_{y_{\perp}}}\, dv_{y_{\perp}} \qquad \text{(B-13)}$$

Equating the final form of equation B-12 to equation B-13 yields the partial derivative relations in equation B-10. By a similar, but more difficult sequence of manipulations, the definition

$$\tan\phi = v_{y_{\perp}} / v_x \qquad \text{(B-14)}$$

can be implicitly differentiated and equated to an expression for the total derivative of ϕ in terms of $\partial\phi/\partial v_{y_{\perp}}$ and $\partial\phi/\partial v_x$ to give

$$\frac{\partial\phi}{\partial v_{y_{\perp}}} = \frac{\cos\phi}{v_{\perp}}$$

$$\frac{\partial\phi}{\partial v_x} = -\frac{\sin\phi}{v_{\perp}} \qquad \text{(B-15)}$$

B.3 Final Form

The identities of section 3.2 are used to evaluate the terms in the dimensionless Vlasov equation below.

$(\vec{v} \times \vec{B}) \cdot \vec{\nabla}_v f$:

$$(\vec{v} \times \vec{B}) \cdot \vec{\nabla}_v f = [(\vec{v}_\parallel + \vec{v}_\perp) \times \vec{B}] \cdot \vec{\nabla}_v f$$

$$= v_\perp B\, (\hat{e}_\perp \times \hat{e}_\parallel) \cdot \left(\frac{\partial f}{\partial v_\perp} \hat{e}_\perp + \frac{\partial f}{\partial v_\parallel} \hat{e}_\parallel + \frac{1}{v_\perp} \frac{\partial f}{\partial \phi} \hat{e}_\phi\right)$$

$$= v_\perp B\, (-\hat{e}_\phi) \cdot \left(\frac{\partial f}{\partial v_\perp} \hat{e}_\perp + \frac{\partial f}{\partial v_\parallel} \hat{e}_\parallel + \frac{1}{v_\perp} \frac{\partial f}{\partial \phi} \hat{e}_\phi\right)$$

$$(\vec{v} \times \vec{B}) \cdot \vec{\nabla}_v f = -B \frac{\partial f}{\partial \phi} \qquad \text{(B-16)}$$

$\vec{E} \cdot \vec{\nabla}_v f$:

$$\vec{E} \cdot \vec{\nabla}_v f = (E_x \hat{i} + E_y \hat{j}) \cdot \left(\frac{\partial f}{\partial v_x} \hat{i} + \frac{\partial f}{\partial v_{y_\perp}} \hat{e}_{y_\perp} + \frac{\partial f}{\partial v_\parallel} \hat{e}_\parallel\right)$$

$$= E_x \frac{\partial f}{\partial v_x} + E_y \left(\frac{\partial f}{\partial y_\perp} \cos\theta + \frac{\partial f}{\partial v_\parallel} \sin\theta\right)$$

$$\vec{E} \cdot \vec{\nabla}_v f = E_x \left[\frac{\partial f}{\partial v_\perp} \cos\phi + \frac{\partial f}{\partial \phi} \left(-\frac{\sin\phi}{v_\perp}\right)\right] +$$

$$E_y \left[\frac{\partial f}{\partial v_\perp} \sin\phi + \frac{\partial f}{\partial \phi} \frac{\cos\phi}{v_\perp}\right] \cos\theta + E_y \frac{\partial f}{\partial v_\parallel} \sin\theta \qquad \text{(B-17)}$$

$\vec{v} \cdot \vec{\nabla} f$:

$$\vec{v} \cdot \vec{\nabla} f = (v_\parallel \hat{e}_\parallel + v_x \hat{i} + v_y \hat{e}_y) \cdot \left(\hat{i} \frac{\partial f}{\partial x} + \hat{j} \frac{\partial f}{\partial y}\right)$$

$$= v_x \frac{\partial f}{\partial x} + v_\parallel \sin\theta \frac{\partial f}{\partial y} + v_{y_\perp} \cos\theta \frac{\partial f}{\partial y}$$

$$\vec{v} \cdot \vec{\nabla} f = v_\perp \cos\phi \frac{\partial f}{\partial x} + v_\parallel \sin\theta \frac{\partial f}{\partial y} + v_\perp \sin\phi \cos\theta \frac{\partial f}{\partial y} \qquad \text{(B-18)}$$

The dimensionless form of the Vlasov equation is obtained by substituting equations B-16 through B-18 into equation B-8 to get

$$\frac{\partial f}{\partial t} + [v_\perp \cos\phi \frac{\partial f}{\partial x} + v_\parallel \sin\theta \frac{\partial f}{\partial y} + v_\perp \sin\phi \cos\theta \frac{\partial f}{\partial y}] +$$

$$- \frac{\partial f}{\partial v_\perp} [E_x \cos\phi + E_y \sin\phi \cos\theta] - E_y \sin\theta \frac{\partial f}{\partial v_\parallel} +$$

$$\frac{\partial f}{\partial \phi} [\frac{E_x \sin\phi - E_y \cos\phi \cos\theta}{v_\perp} + \omega_c] = 0 , \qquad \text{(B-19)}$$

where $f = f(v_\parallel, v_\perp, \phi, x, y)$. for $\theta = \pi/2$ the Vlasov equation becomes

$$\frac{\partial f}{\partial t} + [v_\perp \cos\phi \frac{\partial f}{\partial x} + v_\parallel \frac{\partial f}{\partial y}] +$$

$$- \frac{\partial f}{\partial v_\perp} E_x \cos\phi - E_y \frac{\partial f}{\partial v_\parallel} + \frac{\partial f}{\partial \phi} [\frac{E_x \sin\phi}{v_\perp} + \omega_c] = 0 \quad \text{(B-20)}$$

and the dimensionless equation is

$$\frac{\partial f}{\partial t} + v_{\parallel} \frac{\partial f}{\partial y} - E_y \frac{\partial f}{\partial v_{\parallel}} = 0 \quad , \tag{B-21}$$

where f is allowed to vary in spatial and velocity coordinates along the field direction only.

Coordinate System

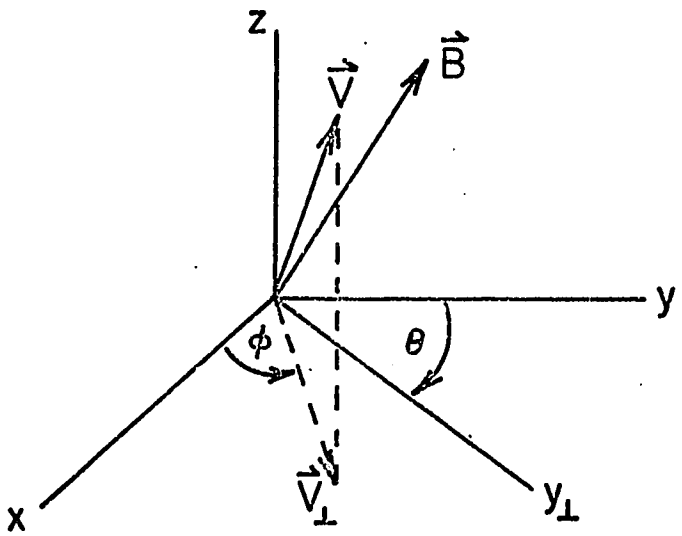

Figure B-1

APPENDIX C

VLAS1D and SUPPORTING PROGRAMS

C.1 Description of VLAS1D, FUNCT, PLOT2, and PLOT1

Program VLAS1D is a FORTRAN IV program written for use on the Digital Equipment Corp. PDP-10 computer at the University of New Hampshire. The program has a core size requirement of 9.2K 36 bit words and a typical run time of 10 minutes of CPU time. VLAS1D and its supporting programs make use of IMSL[50] subroutines stored on disk files at the University of New Hampshire facility. VLAS1D makes use of IMSL subroutine ICSICU to calculate a matrix of constant coefficients to be used in the spline interpolation and DCSQDU to integrate the distribution function in velocity using the ICSICU spline fit to the distribution function.

VLAS1D requires an initial distribution function from disk file FUNCT.DAT as input. The disk file is created by program FUNCT in free, list directed format. VLAS1D asks the interactive user for the following input:

DELT: Time step size in units of ω_p^{-1}

NTIME: No. times through time loop before storage of distrbution function for plotting.

NMAX: No. distribution function plots to be made (total number times through loop is NTIME*NMAX)

The last distribution function file is also stored in file FUNCT.SAV in the same format as that created by FUNCT so that FUNCT.SAV can be used as input to VLAS1D to continue the evolution of the distribution function.

Program FUNCT is designed to create a disk file for input of the initial electron distribution function into VLAS1D. The general form of the function calculated is

$$F(IX,IV) = (F1 * e^{-\alpha,v^2} + F2 * e^{-\alpha_2(v^2-v_o^2)} + \frac{second}{v^4}) * (1 + FA * \cos(FK * X)) \quad , \qquad (C\text{-}1)$$

where F2= ϕ for V<V0 and SECOND=0 for $|V|$<VZMIN. In addition to the parameters defined by equation C-1, FUNCT asks for the following input:

FLZ: Distribution periodic in length FLZ in spacial coordinate. (units of Debye lengths)

NZ: Number of Spacial grid points (y=FLZ/NZ)

VZMAX: Maximum velocity value in units of thermal velocity(kT/m)

NVZ: Number of velocity grid points.

Program PLOT2 uses the Tektronix PLOT10 software available at the University of New Hampshire facility to plot the distribution function stored on disk file FUNCT.DAT by VLAS1D throughout the calculation. The input parameters required are :

IFILE: Number of distribution function plots to be made.

IANS: To be typed in answer to question "Calcomp Plots ?" IANS=Y creates a disk file for a subsequent Calcomp plot IANS=N displays plots on CRT

FFZMIN,FFZMAX: Minimum and maximum distribution values to be plotted.

IXTYPE,IYTYPE: 1 for linear plot, 2 for log plot on x and y axes.

Program PLOT1 plots the electric field Fourier component amplitudes calculated and stored on disk file EMAX.DAT by VLAS1D as a function of time. The first plot is E(0) which is the total energy (sum of squares of component amplitudes) in the field. The input parameters are similar to PLOT2.

```
C
C PROGRAM VLAS1D CALCULATES THE ELECTRON DISTRIBUTION
FUNCTION AS A
C FUNCTION OF TIME, POSITION AND VELOCITY IN A TWO
DIMENSIONAL
C PHASE SPACE(ONE VELOCITY AND ONE SPACE DIMENSION). THE
DISTRIBUTION
C FUNCTION IS CALCULATED FROM THE ONE DIMENSIONAL VLASOV
EQUATION:
C
C     DF/DT + VZ*DF/DZ + E*DF/DVZ = 0
C
C TOGETHER WITH POISSONS EQUATION. THE SOLUTIONS CAN BE USED
TO DETERMINE
C THE TIME EVOLUTION OF THE DISTRIBUTION FUNCTION CAUSED BY
ELECTROSTATIC
C LANGMUIR OSCILLATIONS. THE CALCULATIONS ARE MADE FOR
DISTRIBUTION
C FUNCTIONS ISOTROPIC IN VELOCITY SPACE AND SYMMETRIC UPPER
AND LOWER
C HEMISPHERES IN THE SPACIAL COORDINATES.
C INPUT DATA:
C THE PROGRAM REQUIRES AN INITIAL DISTRIBUTION FUNCTION ON
DISK FILE
C FUNCT.DAT CREATED BY PROGRAM FUNCT.FOR
C
C NTIME,DELT - NUMBER OF TIME STEPS OF LENGTH DELT IN UNITS
OF THE PLASMA
C OSCILLATION PERIOD. DISTRIBUTION FUNCTION STORED FOR
PLOTTING
C  AFTER NTIME-1 TIME STEPS.
C
C
C NMAX - NUMBER OF COMPLETE DISTRIBUTION FUNCTION FILES TO
BE
C  STORED ON DISK FOR INTERMEDIATE TIMES TAKEN THROUGHOUT
RUN.
C
C THE FOURIER COMPONENTS OF THE ELECTRIC FIELD ARE PRINTED
OUT ON DISK
C FILE EMAX.DAT IN THE FORMAT (EMAX(K),K=1,NZ),TIME WHERE
EMAX(NZ) IS
C EQUAL TO THE AMPLITUDE OF THE TOTAL ELECTRIC FIELD
C
C
C THE PLASMA PERIOD IS (M/4*PI*N*Q**2)**.5 AND
C THE DEBYE LENGTH IS (KT/4*PI*N*Q**2)**.5
C
C
      DIMENSION
F(50,150),VZ(150),Z(50),A(50),B(50),RRHO(50),FVZ(150),
     1
BPAR(4),C(150,3),E(50),CC(50,150,3),COSNKZ(50,50),SINNKZ(50,5
0),
     1  FFVZ(50,150),EMAX(50)
```

```
C
      COMPLEX CE,CEE(50),COMPI,CDENOM
C
      DATA COMPI/(0.,1.)/
      DATA PI/3.14159/
      DATA
IDISK/1/,ICARD/2/,IPRINT/7/,ITTY/5/,IDISK2/6/,IDISK3/10/
      DATA IDISK4/40/
      DATA BPAR/0.,0.,0.,0./
C
      OPEN(UNIT=IDISK,DEVICE='DSK',ACCESS='SEQIN',
     1  FILE='FUNCT.DAT')
      OPEN(UNIT=IDISK2,DEVICE='DSK',ACCESS='SEQOUT',DISPOSE='
SAVE',
     1  FILE='EMAX.DAT')
      OPEN(UNIT=ITTY,DEVICE='TTY',ACCESS='SEQINOUT',DISPOSE='
DELETE')
C
      READ(IDISK,*) FA,FK,ALPHA1,ALPHA2,FN1,FN2,V0,TIME
      READ(IDISK,*)
FLZ,NZ,VZMAX,NVZ,DELZ,DELVZ,NZP1,NVZP1,NZTWO,NZTOP1
      READ(IDISK,*) ((F(I,J),J=1,NVZP1),I=1,NZP1)
      READ(IDISK,*) (Z(I),I=1,NZP1)
      READ(IDISK,*) (VZ(J),J=1,NVZP1)
      WRITE(ITTY,12)
12    FORMAT(' DELT,NTIME,NMAX?')
      READ(ITTY,*) DELT,NTIME,NMAX
      NTM1 = (NTIME-1)*NMAX
      WRITE(IDISK2,*) NTM1,DELT,NZ
      CLOSE(UNIT=IDISK,DISPOSE='SAVE')
      OPEN(UNIT=IDISK3,FILE='FUNCT.DAT',DEVICE='DSK',ACCESS='
APPEND',
     1DISPOSE='SAVE')
C
C TIME STEP DO LOOP
C
      ICOUNT = 0
      HDELT = .5*DELT
      TOPIL = 2.*PI/FLZ
C
C CALCULATE TRIGONOMETRIC FUNCTIONS  STORE
C
      DO 23 I=1,NZ
      DO 23 N=1,NZP1
      COSNKZ(I,N) = COS((N-1)*TOPIL*Z(I))
      SINNKZ(I,N) = SIN((N-1)*TOPIL*Z(I))
C     WRITE(IPRINT,*) I,N,COSNKZ(I,N),SINNKZ(I,N)
23    CONTINUE
C
25    CONTINUE
      DO 100 L=1,NTIME
      DT = DELT
      IF((L-1)*(L-NTIME).EQ.0) DT = DT-HDELT
      IF(L.NE.1) TIME = TIME + DELT
C
```

```
C LOOP OVER VELOCITY
C
      DO 50 J=1,NVZP1
C
C FOURIER INTERPOLATION
C
      DO 35 JJ=1,NZTOP1
      A(JJ) = 0.
      B(JJ) = 0.
      DO 35 IP=1,NZ
      A(JJ) = A(JJ) + F(IP,J)*COSNKZ(IP,JJ)
      B(JJ) = B(JJ) + F(IP,J)*SINNKZ(IP,JJ)
C     WRITE(IPRINT,*)
L,J,JJ,A(JJ),B(JJ),IP,F(IP,J),COSNKZ(IP,JJ)
35    CONTINUE
C
C LOOP OVER SPACE
C
      DO 50 I=1,NZ
      XZ= (Z(I)-VZ(J)*DT)*TOPIL
C
      SUMZ = 0.
      DO 40 K=2,NZTWO
      KK = K - 1
40    SUMZ = SUMZ + A(K)*COS(XZ*KK) + B(K)*SIN(XZ*KK)
C
      F(I,J) = ((A(1) + A(NZTOP1)*COS(XZ*NZTWO))*.5 +
SUMZ)/NZTWO
C
C     WRITE(IPRINT,*) L,I,J,F(I,J),SUMZ,NZTWO
50    CONTINUE
C
      IF(L.GE.NTIME)  GO TO 110
C
C CUBIC SPLINE INTERPOLATION
C
      DO 70 I=1,NZ
      DO 60 K=1,NVZP1
60    FVZ(K) = F(I,K)
C
      CALL ICSICU(VZ,FVZ,NVZP1,BPAR,C,150,IER1)
C
C SPLINE VELOCITY INTEGRATION
C
      CALL
DCSQDU(VZ,FVZ,NVZP1,C,150,VZ(1),VZ(NVZP1),RHO,IER2)
      RRHO(I) = RHO
C
      DO 65 IK = 1,NVZP1
      FFVZ(I,IK) = FVZ(IK)
      DO 65 JK = 1,3
      CC(I,IK,JK) = C(IK,JK)
65    CONTINUE
C
70    CONTINUE
```

```
C
C ELECTRIC FIELD CALCULATION
C
C
C CALCULATE FOURIER TRANSFORM OF RHO(I)
C
      DO 71 JJ=1,NZ
      CEE(JJ) = 0.
      DO 71 IP=1,NZ
      CEE(JJ) = CEE(JJ) +
RRHO(IP)*(COSNKZ(IP,JJ)+COMPI*SINNKZ(IP,JJ))
71    CONTINUE
C
      DO 73 K=2,NZTOP1
73    EMAX(K) = 0.
      DO 75 I=1,NZ
      EMAX(1) = 0.
      E(I) = 0.
C
C SUM OVER FOURIER COMPONENTS
C
      DO 75 NN = 2,NZTOP1
      NNM1 = NN - 1
      CDENOM = CMPLX(TOPIL*(NNM1)*NZ,0.)
      CE = COMPI*CONJG(CEE(NN))/CDENOM
      EMAX(NN) = AMAX1(CABS(CE),EMAX(NN))
      E(I) =
2.*(COSNKZ(I,NN)*REAL(CE)-SINNKZ(I,NN)*AIMAG(CE)) + E(I)
      IF(NN.EQ.NZTOP1) E(I)=E(I) + ISIGN(-1**I,1)*REAL(CE)
75    CONTINUE
      DO 77 N=2,NZTOP1
      EMAX(1) = EMAX(N)**2 + EMAX(1)
77    CONTINUE
      WRITE(IDISK2,*) (EMAX(K),K=1,NZTOP1),TIME
C
C FULL TIME STEP FOR VELOCITY SHIFT
C
      DO 100 I=1,NZ
      DO 100 J=1,NVZP1
      TZ = VZ(J) + E(I)*DELT
      DO 80 K=1,NVZ
      IF(TZ.LT.VZ(K+1)) GO TO 90
80    CONTINUE
90    CONTINUE
      D = TZ - VZ(K)
      F(I,J) = ((CC(I,K,3)*D+CC(I,K,2)) * D + CC(I,K,1)) * D
+ FFVZ(I,K)
      IF(TZ.GE.VZ(NVZP1)) F(I,J) = 0.
      IF(TZ.LE.VZ(1)) F(I,J) = 0.
C
100   CONTINUE
C
110   CONTINUE
C
      WRITE(IDISK3,*) FA,FK,ALPHA1,ALPHA2,FN1,FN2,V0,TIME
```

```
      WRITE(IDISK3,*)
FLZ,NZ,VZMAX,NVZ,DELZ,DELVZ,NZP1,NVZP1,NZTWO,
     1 NZTOP1
      WRITE(IDISK3,*) ((F(I,J),J=1,NVZP1),I=1,NZP1)
      WRITE(IDISK3,*) (Z(I),I=1,NZP1)
      WRITE(IDISK3,*) (VZ(J),J=1,NVZP1)
      ICOUNT = ICOUNT + 1
      IF(ICOUNT.LT.NMAX) GO TO 25
C
      OPEN(UNIT=IDISK4,DEVICE='DSK',ACCESS='SEQOUT',DISPOSE='
SAVE')
      WRITE(IDISK4,*) FA,FK,ALPHA1,ALPHA2,FN1,FN2,V0,TIME
      WRITE(IDISK4,*)
FLZ,NZ,VZMAX,NVZ,DELZ,DELVZ,NZP1,NVZP1,NZTWO,
      1NZTOP1
      WRITE(IDISK4,*) ((F(I,J),J=1,NVZP1),I=1,NZP1)
      WRITE(IDISK4,*) (Z(I),I=1,NZP1)
      WRITE(IDISK4,*) (VZ(J),J=1,NVZP1)
      CLOSE(UNIT=IDISK4,DISPOSE='SAVE',FILE='FUNCT.SAV')
      CLOSE(UNIT=IDISK3,DISPOSE='SAVE',FILE='FUNCT.DAT')
      CLOSE(UNIT=ITTY)
      CLOSE(UNIT=IDISK2,DISPOSE='SAVE',FILE='EMAX.DAT')
C
      STOP
      END
```

```
C
C PROGRAM PLOT2 PLOTS THE INTEGRAL OF THE TWO DIMENSIONAL
FUNCTION F(I,J)
C VS THE REMAINING UNINTEGRATED DIMENSION.
C INPUT PARAMETERS:
C REQUIRES FUNCT.DAT DISK FILE WITH FORMAT SAME AS THAT
CREATED BY
C PROGRAM FUNCT.FOR
C IFILE: NMAX(VLAS1D PROGRAM) COMPLETE FILES ARE WRITTEN TO
DISK
C  AT EQUAL TIME INTERVALS THROUGHOUT THE RUN OF VLAS1D.
C  IFILE GIVES THE FILE NUMBER TO BE PLOTTED DURING THE
CURRENT
C  RUN OF PLOT2.
C FFZMIN,FFZMAX: MAXIMUM  MINIMUM DISTRIBUTION FUNCTION
VALUES
C IXTYPE,IYTYPE : 1 FOR LINEAR PLOT, 2 FOR LOG PLOT
C
      DIMENSION
IARRAY(20),JARRAY(100),CONPRT(250),CONENG(250)
      DIMENSION F(50,250),VZ(250),Z(50),VVZ(251),FFZ(251),
     1  IVEL(9),IDIST(22),FZ(50),C(250,3),BPAR(4)
      DATA BPAR/0.,0.,0.,0./
      DATA IBAUD/240/,IYES/1HY/
      DATA IDISK/1/,ICARD/2/,IPRINT/3/,ITTY/5/
      DATA IVEL/8,86,69,76,79,67,73,84,89/
      DATA IDIST/21,68,73,83,84,82,73,66,85,84,73,79,78,32,
     1  70,85,78,67,84,73,79,78/
C
      OPEN(UNIT=IDISK,DEVICE='DSK',ACCESS='SEQIN',DISPOSE='SA
VE',
     1  FILE='FUNCT.DAT')
      OPEN(UNIT=ITTY,DEVICE='TTY',ACCESS='SEQINOUT',DISPOSE='
DELETE')
      OPEN(UNIT=20,ACCESS='APPEND',FILE='PLOTF.DAT',DISPOSE='
SAVE')
C
      WRITE(ITTY,2)
2     FORMAT(' IFILE?')
      READ(ITTY,*) IFILE
      WRITE(ITTY,150)
150   FORMAT(' CALCOMP PLOT?')
      READ(ITTY,160) IANS
160   FORMAT(A1)
      WRITE(ITTY,10)
10    FORMAT(' FFZMIN,FFZMAX = ?')
      READ(ITTY,*) FFZMIN,FFZMAX
      WRITE(ITTY,15)
15    FORMAT(' IXTYPE,IYTYPE = ?')
      READ(ITTY,*) IXTYPE,IYTYPE
      DO 5 ICOUNT=1,IFILE
      READ(IDISK,*) FA,FK,ALPHA1,ALPHA2,FN1,FN2,V0,TIME
      READ(IDISK,*)
FLZ,NZ,VZMAX,NVZ,DELZ,DELVZ,NZP1,NVZP1,NZTWO,NZTOP1
      READ(IDISK,*) ((F(I,J),J=1,NVZP1),I=1,NZP1)
```

```
      READ(IDISK,*)  (Z(I),I=1,NZP1)
      READ(IDISK,*)  (VZ(J),J=1,NVZP1)
C
C
C
C INTEGRATE USING SPLINE INTERPOLATION TO OBTAIN THE
DISTRIBUTION
C FUNCTION AS A FUNCTION OF VELOCITY ONLY.
      VVZ(1) = NVZP1
      FFZ(1) = NVZP1
C
      DO 310 J=1,NVZP1
      DO 300 K=1,NZ
300   FZ(K) = F(K,J)
      FZ(NZP1) = FZ(1)
      CALL ICSICU(Z,FZ,NZP1,BPAR,C,250,IER1)
      CALL DCSQDU(Z,FZ,NZP1,C,250,0.,Z(NZP1),Q,IER2)
      Q = Q/FLZ
      FFZ(J+1) = Q
      VVZ(J+1) = VZ(J)
      CONPRT(J) = Q
      CONENG(J) = Q*(VZ(J)**2)
310   CONTINUE
C
C CHECK CONSERVATION OF ENERGY AND NUMBER OF PARTICLES
C
      CALL ICSICU(VZ,CONPRT,NVZP1,BPAR,C,250,IER3)
      CALL
DCSQDU(VZ,CONPRT,NVZP1,C,250,VZ(1),VZ(NVZP1),PARTCL,IER3)
      CALL ICSICU(VZ,CONENG,NVZP1,BPAR,C,250,IER4)
      CALL
DCSQDU(VZ,CONENG,NVZP1,C,250,VZ(1),VZ(NVZP1),ENERG,IER4)
      ENCODE(60,99,IARRAY) PARTCL,ENERG,TIME
99    FORMAT(3X,'NUMBER',1PG10.3,5X,'ENERGY',G10.3,3X,
     1 'TIME = ',G10.3)
      DECODE(60,100,IARRAY) (JARRAY(J),J=2,61)
100   FORMAT(60R1)
      JARRAY(1) = 60
C
C PLOT F(VZ)
C
      CALL INITT(IBAUD)
      IF(IANS.EQ.IYES) CALL OUTMOD('FILE',20)
      CALL BINITT
      CALL DLIMX(VVZ(2),VVZ(NVZP1+1))
      CALL DLIMY(FFZMIN,FFZMAX)
      CALL XTYPE(IXTYPE)
      CALL YTYPE(IYTYPE)
      CALL CHECK(VVZ,FFZ)
      CALL DSPLAY(VVZ,FFZ)
      CALL MOVABS(150,740)
      CALL HSTRIN(JARRAY)
      CALL MOVABS(520,40)
      CALL HSTRIN(IVEL)
      CALL MOVABS(0,700)
```

```
      CALL VSTRIN(IDIST)
5     CONTINUE
C
      CLOSE(UNIT=ITTY,DISPOSE='DELETE')
      CLOSE(UNIT=IDISK,DISPOSE='SAVE',FILE='FUNCT.DAT')
      CLOSE(UNIT=20,FILE='PLOTF.DAT',DISPOSE='SAVE')
      STOP
      END
```

```
C
C PROGRAM PLOT1 PLOTS A FUNCTION F OF ONE VARIABLE T. THE
PROGRAM REQUIRES
C INPUT FORM DISK FILE EMAX.DAT IN THE FORMAT F,T. THE FIRST
NUMBER IN THE
C FILE IS THE NUMBER OF DATA POINTS NT AND THE SECOND NUMBER
IS
C THE ORDINATE INTERVAL DELT.
C TTY INPUT DATA FORMAT:
C IXTYPE,IYTYPE : 1 FOR LINEAR PLOT, 2 FOR LOG PLOT
C FMIN,FMAX : MAXIMUM  MINIMUM EMAX VALUES
C
      DIMENSION IARRAY(20),JARRAY(100)
      DIMENSION T(600),FF(601),E(50,600),TT(601)
      DATA IBAUD/240/
      DATA IDISK/1/,ITTY/5/
      DATA IYES/1HY/
C
      OPEN(UNIT=IDISK,DEVICE='DSK',ACCESS='SEQIN',FILE='EMAX.
DAT',
     1  DISPOSE='SAVE')
      OPEN(UNIT=ITTY,DEVICE='TTY',ACCESS='SEQINOUT',DISPOSE='
DELETE')
      OPEN(UNIT=20,FILE='PLOTE.DAT',ACCESS='APPEND',DISPOSE='
SAVE')
C
      WRITE(ITTY,150)
150   FORMAT(' CALCOMP PLOT?')
      READ(ITTY,160) IANS
160   FORMAT(A1)
      WRITE(ITTY,20)
20    FORMAT(' FMIN,FMAX,IXTYPE,IYTYPE = ?')
      READ(ITTY,*) FMIN,FMAX,IXTYPE,IYTYPE
      READ(IDISK,*) NT,DELT,NZ
C
      NZP1 = NZ + 1
      NZTOP1 = NZ/2 + 1
      DO 10 I=1,NT
      READ(IDISK,*,END=10) (E(K,I),K=1,NZTOP1),T(I)
      TT(I+1) = T(I)
10    CONTINUE
C
C
      FF(1) = NT
      TT(1) = NT
      DO 140 NECOMP=1,NZTOP1
      IF(NECOMP.LT.5) GO TO 200
      IF(MOD(NECOMP,2).EQ.0) GO TO 140
200   CONTINUE
      DO 250 J=1,NT
250   FF(J+1) = E(NECOMP,J)
C
C TITLE ARRAY CREATED IN UNPACKED ASCI11 RIGHT JUSTIFIED
FORMAT
C
```

```
      NECM1 = NECOMP - 1
      ENCODE(26,99,IARRAY) NECM1
99    FORMAT(10X,'EAMP(',I2,') VS TIME')
      DECODE(26,260,IARRAY) (JARRAY(J),J=2,27)
260   FORMAT(26R1)
      JARRAY(1) = 26
C
      CALL INITT(IBAUD)
      IF(IANS.EQ.IYES) CALL OUTMOD('FILE',20)
      CALL BINITT
      CALL DLIMX(TT(2),TT(NT))
      CALL DLIMY(FMIN,FMAX)
      CALL XTYPE(IXTYPE)
      CALL YTYPE(IYTYPE)
      CALL CHECK(TT,FF)
      CALL DSPLAY(TT,FF)
      CALL MOVABS(150,740)
      CALL HSTRIN(JARRAY)
140   CONTINUE
C
      CLOSE(UNIT=20,FILE='PLOTE.DAT',DISPOSE='SAVE')
      CLOSE(UNIT=IDISK,DISPOSE='SAVE',FILE='EMAX.DAT')
      CLOSE(UNIT=ITTY)
C
      STOP
      END
```

```
C
C PROGRAM FUNCT CREATES A DISK FILE CONTAINING THE ELECTRON
DISTRIBUTION
C FUNCTION CALCULATED FROM THE FUNCTIONAL FORM INCORPORATED
INTO THIS PROGRAM
C THE DISK FILE IS WRITTEN IN FREE FORMAT WITH THE ORDER
IMPLIED BY
C ((F(I,J),J=1,NVZP1),I=1,NZP1), (Z(I),I=1,NZP1),
(VZ(J),J=1,NVZP1)
C THE INPUT PARAMETERS ARE:
C FA,FK,ALPHA1,ALPHA2,FN1,FNFN2,V0
C F(I,J) =
[FN1*EXP(-ALPHA1*VZ*VZ)+FN2*EXP(-ALPHA2*(VZ**2-V0**2))](1+FA*
COS(FK*Z))
C FLZ,NZ : DELZ = FLZ/NZ
C VZMAX,NVZ : DELVZ = 2*VZMAX/NVZ
C
      DIMENSION F(50,250),VZ(250),Z(50)
C
      DATA IDISK/1/,ITTY/5/
      OPEN(UNIT=ITTY,DEVICE='TTY',ACCESS='SEQINOUT',DISPOSE='
DELETE')
      OPEN(UNIT=IDISK,DEVICE='DSK',ACCESS='SEQOUT',DISPOSE='S
AVE',
     1  FILE='FUNCT.DAT')
C
C READ IN FUNCTION PARAMETERS
C
      WRITE(ITTY,10)
10    FORMAT(' FA,FK,ALPHA1,ALPHA2,FN1,FN2,V0 = ?')
      READ(ITTY,*) FA,FK,ALPHA1,ALPHA2,FN1,FN2,V0
      WRITE(ITTY,20)
20    FORMAT(' FLZ,NZ,VZMAX,NVZ = ?')
      READ(ITTY,*) FLZ,NZ,VZMAX,NVZ
      WRITE(ITTY,30)
30    FORMAT(' VZMIN,SECOND = ?')
      READ(ITTY,*) VZMIN,SECOND
C
      DELZ = FLZ/NZ
      DELVZ = 2.*VZMAX/NVZ
      NZP1 = NZ + 1
      NVZP1 = NVZ + 1
      NZTWO = NZ/2
      NZTOP1 = NZTWO + 1
C
      VZ(1) = -1.*VZMAX
      DO 40 K=2,NVZP1
      VZ(K) = VZ(K-1) + DELVZ
40    CONTINUE
      ZOLD = -1.*DELZ
      DO 50 I=1,NZP1
      Z(I) = ZOLD + DELZ
      ZOLD = Z(I)
      DO 50 J=1,NVZP1
      F(I,J) =FN1*EXP(-1.*ALPHA1*VZ(J)*VZ(J))
```

```
      FFN2 = FN2
      FACTOR = VZ(J)*VZ(J) - V0*V0
      IF(ABS(VZ(J)).GE.V0)F(I,J) = F(I,J) +
FFN2*EXP(-1.*ALPHA2*FACTOR)
      IF(VZ(J).GE.VZMIN) F(I,J) = F(I,J) + SECOND/VZ(J)**4
      F(I,J) = F(I,J)*(1.+FA*COS(FK*Z(I)))
50    CONTINUE
C
C WRITE FUNCTION AND PARAMETERS ON DISK FILE
C
      TIME = 0.
      WRITE(IDISK,*) FA,FK,ALPHA1,ALPHA2,FN1,FN2,V0,TIME
      WRITE(IDISK,*)
FLZ,NZ,VZMAX,NVZ,DELZ,DELVZ,NZP1,NVZP1,NZTWO,NZTOP1
      WRITE(IDISK,*) ((F(I,J),J=1,NVZP1),I=1,NZP1)
      WRITE(IDISK,*) (Z(I),I=1,NZP1)
      WRITE(IDISK,*) (VZ(J),J=1,NVZP1)
C
      CLOSE(UNIT=IDISK,DEVICE='DSK',DISPOSE='SAVE',FILE='FUNC
T.DAT')
      CLOSE(UNIT=ITTY,DEVICE='TTY',DISPOSE='DELETE')
C
      STOP
      END
```

c.2 VLAS1D Computer Runs

The plasma parameters used to determine the initial electron distribution functions for the VLAS1D computer run results that appear in the figures of this thesis are shown in table C-1. The corresponding input parameters for the FUNCT computer code used to create the initial distribution disk file are shown in table C-2. The FUNCT program input parameters are defined by equation C1.

Table C-1: Plasma Parameters

Run	Beam to Background Density Ratio n_b/n_m	Plasma Frequency ω_p(rad/sec) for n_b=1cm^{-3}	Debye Length λ_d(cm) for n_b=1cm^{-3}	Thermal Velocity v_{th}(cm/s)
T2	0 (no beam)	$\left(\frac{4\pi n_m e^2}{m}\right)^{1/2}$	$\left(\frac{kT_1}{4\pi n_m e^2}\right)^{1/2}$	$\left(\frac{kT_1}{m}\right)^{1/2}$
T4	"	The results obtained for runs T,2, T4 and TS1 are independent of background temperature T_1 and density n_m.		
TS1	"			
AM2	.2825	$.11\times10^{6}$	6.9×10^{3}	7.57×10^{8}
AM3	.02825	.34	1.0×10^{3}	3.47
AM20	.002825	1.1	1.5×10^{2}	1.69
AM4	$.2825\times10^{-5}$	33.6	4.0	1.327
AM25	10^{-5}	17.9	7.4	1.327
AM27	10^{-5}	17.9	7.4	1.327

The beam temperature T_2 is 640 eV and the background temperature kT_2 is 10 eV for all runs with the prefix AM. The number density of the power law secondaries included in runs AM25 and AM27 is equal to the beam density.

Table C-2: FUNCT AND VLAS1D INPUT PARAMETERS*

Run	Δt	FA	FK	α_1	α_2	FN1	FN2	v0	FLZ	NZ	VZMAX	NVZ	VZMIN	SECONI
T2	.2	.5	.5	.5	1.0	.4	0	0	12.6	20	5.0	99	0	0
T4	1.									12				
TS1**	1.	.05	.5	.5	1.0	.4	0	0	12.6	16	5.0	99	0	0
AM2	1.	.002	.2	16.25	.254	1.14	.284	3.5	30.5	30	5.0	99	0	0
AM3		.001	.1	3.41	.053	.95	.024	7.66	62.4	46	10.0			
AM20		4×10^{-4}	.04	.812	.0127	.50	1.26×10^{-3}	15.7	156.7	24	25.0			
AM4		3.3×10^{-6}	3.3×10^{-2}	.5	7.8×10^{-3}	.4	10^{-6}	20.0	188.3	46	30.0			
AM25							3.5×10^{-6}			30			1.414	$8.5\times10^{-}$
AM27		2.5×10^{-2}	5×10^{-2}											

*A blank space indicates the same value as shown immediately above.

**Maxwellian background term modified to the form $v^2e^{-\alpha v^2}$

APPENDIX D

VLAS3D AND SUPPORTING PROGRAMS

D.1 Description of VLAS3D, FUN3D, PLTF3D, PLOTE, TRANS and PLOTFX

Program VLAS3D is a FORTRAN IV program written for use on the Digital Equipment Corporation PDP-10 computer at the University of New Hampshire. The program has a core size requirement of 12.3K 36 bit words and a typical run time of 30 minutes of CPU time. The program integrates the 2-1/2 dimensional electron distribution function (two space and three velocity dimensions) in time according to the Vlasov equation. The initial distribution function matrix is read from disk file FUN3D.DAT created by program FUN3D. The final distribution function matrix is stored in file FUN3D.SAV and distribution files to be plotted are appended

to the initial distribution function file FUN3D.DAT.

The input parameters required by VLAS3D are:

DELT: Time step size in units of plasma periods (ω_p^{-1})

NTIME: Number of integration steps through time loop before storage of distribution function for plotting

NFILE: Number of distribution function matrices to be plotted not counting the initial distribution function matrix. The total amount of time integrated over is NFILE*(NTIME-1).

OMEGAC: The electron cyclotron frequency in units of the electron plasma frequency (ω_p).

Program FUN3D creates the initial distribution function matrix according to

$$F(IVPAR,IVPER,IPHI,IX,IY) = \{A * e^{-\alpha v^2} + B * e^{-\beta v'^2}\} * \{1 + C\,(\cos CKX * X + \sin CKY * Y)\} \qquad (D\text{-}1)$$

where

$$v^2 = v_\perp^2 + v_\parallel^2$$

$$v'^2 = (v_\perp - v_{\perp 0})^2 + (v_\parallel - v_{\parallel 0})^2 \quad , \qquad \text{(D-2)}$$

and B is set equal to zero if $v_\parallel < 0$. In addition to the input parameters defined by equations D-1 and D-2, FUN3D requires the following input parameters:

VPARMX: Magnitude of the maximum parallel velocity in units of thermal velocity.

VPERMX: Maximum perpendicular velocity.

XMAX, YMAX: Repetition lengths in the x and y directions in units of Debye lengths.

NVPAR: Number of parallel velocity grid points. The parallel velocity step size is give by DVPAR=2.0*VPARMX/(NVPAR-1).

NVPER: Number of perpendicular velocity grid points (DVPER=2.0*VPERMX/(2*NVPER-1)).

NPHI: Number of velocity phi coordinate grid points (DPHI=2 /NPHI).

NX, NY: Number of spatial grid points (DX=XMAX/NX).

The plotting routine PLTF3D plots the distribution function matrices stored in file FUN3D.DAT. PLOTE plots the total electric field energy as a function of time stored in file ESQ.DAT by program VLAS3D. The electric field energy plotted is equal to the sum of the squares of the Fourier component amplitudes integrated over the spatial area included in a rectangle with sides equal to the repetition lengths XMAX and YMAX. If a Calcomp plot is desired, program P102PL must be run after program PLTF3D or PLOTE. The input data file names asked for by P102PL are PLTF3D.DAT for program PLTF3D output and PLOTE.DAT for program PLOTE.

Program TRANS creates the Fourier transform of the electric field energy in time. Program PLOTE plots the result $E(\omega)$ vs ω and P102PL must be run for a Calcomp plot.

Program PLTFX gives a three dimensional appearance perspective plot of the distribution function in a velocity coordinate system made up of the parallel and a perpendicular velocity components. This program calls program PLT3D available at the University of New Hampshire computing facility.

```
C
C PROGRAM FUN3D.FOR DETERMINES AN INITIAL ELECTRON
DISTRIBUTION
C FUNCTION F(VPAR,VPER,PHI,X,Y). THE DISTRIBUTION FUNCTION
IS STORRED
C ON DISK FILE FUN3D.DAT IN THE FORMAT RESULTING FROM THE
BINARY
C WRITE STATEMENT
C
C     WRITE(IDISK) VPAR,VPER,PHI,X,Y,F
C
C THE PARAMETERS ARE:
C  NVPAR,NVPER,NPHI:  POINTS IN PARALLEL(TO MAGNETIC FIELD)
C   PERPENDICULAR VELOCITY GRIDS  PHI GRID.(NVPAR ALWAYS
EVEN)
C  NX,NY:   POINTS IN XY DIRECTIONS INCLUDING ORIGIN
C  VPARMX,VPERMX: MAXIMUM PARALLEL  PERPENDICULAR VELOCITIES
C  XMAX,YMAX: MAXIMUM X  Y VALUES
C
C  A,ALPHA: BACKGROUND PARAMETERS
C  B,BETA: BEAM PARAMETERS
C  C,CKX,CKY: INITIAL OSCILLATION PARAMETERS
C
C CALCULATED PARAMETERS:
C  DVPAR = 2*VPARMX/(NVPAR-1)
C  DVPER = 2.*VPERMX/(2*NVPER-1)
C  DPHI = 2*PI/NPHI
C  DX = XMAX/NX
C  DY = YMAX/NY
C
      DIMENSION
VPAR(16),VPER(8),PHI(8),X(4),Y(4),F(16,8,8,4,4)
      DATA IDISK/1/,PI/3.14159265/,ITTY/5/
      OPEN(UNIT=IDISK,DEVICE='DSK',ACCESS='SEQOUT',DISPOSE='S
AVE',
      1FILE='FUN3D.DAT')
C
      TYPE 10
10    FORMAT('$NVPAR,NVPER,NPHI,NX,NY = ?')
      READ(ITTY,*) NVPAR,NVPER,NPHI,NX,NY
20    FORMAT(5I2)
      TYPE 30
30    FORMAT('$VPARMX,VPERMX,XMAX,YMAX = ?')
      READ(ITTY,*)VPARMX,VPERMX,XMAX,YMAX
40    FORMAT(4E15.5)
      TYPE 50
50    FORMAT('$A,ALPHA,B,BETA = ?')
      READ(ITTY,*)A,ALPHA,B,BETA
      TYPE 60
60    FORMAT('$C,CKX,CKY = ?')
      READ(ITTY,*)C,CKX,CKY
      TYPE 70
70    FORMAT('$VPAR0,VPER0 = ?')
      READ(ITTY,*) VPAR0,VPER0
C
```

```
      DVPAR = 1.
      IF(NVPAR.NE.1) DVPAR = 2.*VPARMX/(NVPAR-1)
      DVPER = 2.*VPERMX/(2*NVPER-1)
      DVPER2 = DVPER*.5
      DPHI = 2.*PI/NPHI
      DX = XMAX/NX
      DY = YMAX/NY
      TIME = 0.
C
      WRITE(IDISK,20) NVPAR,NVPER,NPHI,NX,NY
      WRITE(IDISK,40) VPARMX,VPERMX,XMAX,YMAX
      WRITE(IDISK,40) A,ALPHA,B,BETA
      WRITE(IDISK,40) C,CKX,CKY,DVPAR
      WRITE(IDISK,40) DVPER,DPHI,DX,DY
      WRITE(IDISK,40) TIME
C
      DO 100 IX=1,NX
      X(IX) = (IX-1)*DX
      xfact = cos(ckx*x(ix))
      DO 100 IY=1,NY
      Y(IY) = (IY-1)*DY
      space = 1. + c*(xfact + cos(cky*y(iy)))
      DO 100 IPHI = 1,NPHI
      PHI(IPHI) = (IPHI-1)*DPHI
      DO 100 IVPER=1,NVPER
      VPER(IVPER) = (IVPER-1)*DVPER + DVPER2
      VPERSQ = VPER(IVPER)**2
      VPERSB = (VPER(IVPER)-VPER0)**2
      DO 100 IVPAR=1,NVPAR
      VPAR(IVPAR) = (IVPAR-1)*DVPAR-VPARMX
      VSQ = VPERSQ + VPAR(IVPAR)**2
      VSQB = VPERSB + (VPAR(IVPAR)-VPAR0)**2
      bb = b
      if(vpar(ivpar).lt.0.) bb=0.
      FVEL = A*EXP(-1.*ALPHA*VSQ) + bb*EXP(-1.*BETA*VSQB)
      F(IVPAR,IVPER,IPHI,IX,IY) = FVEL*SPACE
100   CONTINUE
C
      WRITE(IDISK,*) VPAR,VPER,PHI,X,Y,F
C
      STOP
      END
```

```
 C
C  PROGRAM VLAS3D INTEGRATES THE VLASOV EQUATION FOR AN
C ELECTRON DISTRIBUTION FUNCTION OF THE FORM:
C
C     F(VPAR,VPER,PHI,X,Y)
C
C THE MAGNETIC FIELD IS TAKEN TO LIE ALONG THE Y-AXIS.
C THE EQUATIONS SOLVED AND METHODS OF SOLUTION ARE DISCUSSED
C IN:
C
C     C.CHENG,THE INTEGRATION OF THE VLASOV EQUATION FOR A
MAGNETIZED
C     PLASMA, J.COMP.PHYS.24,1977(348-360)
C
C  THE PROGRAM READS AN INITIAL DISTRIBUTION FUNCTION FROM
C DISK FILE 'FUN3D.DAT' IN BINARY FORMAT USING THE
STATEMENT:
C
C     READ(IDISK,*) VPAR,VPER,PHI,X,Y,F
C
C  SPACIAL INTERPOLATION IN XY IS PERFORMED BY SUBROUTINE
SPACE AND
C POISSON'S EQUATION IS SOLVED FOR THE ELECTRIC FIELD WITH
SUBROUTINE
C EFOUR.
C
C  THE PARAMETERS READ IN ARE:
C  DELT: TIME STEP SIZE IN UNITS OF WPE-1
C  NTIME: NO. TIMES THROUGH TIME LOOP BEFORE STORAGE OF F
C         FOR SUBSEQUENT PLOTTING. NTIME MUST BE GT 1
C  NFILE: NO. FILES OF F STORED FOR PLOTTING (NOT COUNTING
INITIAL FILE)
C
C  THE TIME INCREMENT IN LOOPING NTIME TIMES THROUGH THE
TIME LOOP
C IS (NTIME-1)*DELT SINCE THE FIRST AND LAST TIMES THROUGH
THE TIME
C IS INCREMENTED BY DELT/2. THE TOTAL TIME THROUGH WHICH F
IS EVOLVED FOR
C THE TOTAL RUN IS (NTIME-1)*NMAX*DELT.
C
C
      PARAMETER N16=16, N8 = 8, N4=4
      COMMON/CONST/ PI,OMEGAC
      COMMON/FAREA/
F(N16,N8,N8,N4,N4),VPAR(N16),VPER(N8),PHI(N8),
     1X(N4),Y(N4)
      COMMON/NAREA/ NVPAR,NVPER,NPHI,NX,NY
      COMMON/DELTA/ DVPAR,DVPER,DPHI,DX,DY,DELT
      COMMON /MAX/ VPARMX,VPERMX,XMAX,YMAX
C
      DATA
IDISK/1/,ITTY/5/,IDSK10/10/,IDSK11/11/,PI/3.14159265/,
     1IDSK12/12/
C
```

```
      OPEN(UNIT=IDISK,DEVICE='DSK',ACCESS='SEQIN',DISPOSE='SA
VE',
     1FILE='FUN3D.DAT')
      OPEN(UNIT=IDSK10,DEVICE='DSK',ACCESS='SEQOUT',DISPOSE='
SAVE',
     1FILE='ESQ.DAT')
      OPEN(UNIT=IDSK12,DEVICE='DSK',ACCESS='SEQOUT',
     1FILE='FUN3D.SAV')
C
C READ INITIAL DISTRIBUTION FUNCTION F(VPAR,VPER,PHI,X,Y)
C
      READ(IDISK,20) NVPAR,NVPER,NPHI,NX,NY
20    FORMAT(5I2)
      READ(IDISK,40) VPARMX,VPERMX,XMAX,YMAX
40    FORMAT(4E15.5)
      READ(IDISK,40) A,ALPHA,B,BETA
      READ(IDISK,40) C,CKX,CKY,DVPAR
      READ(IDISK,40) DVPER,DPHI,DX,DY
      READ(IDISK,40) TIME
      READ(IDISK,*) VPAR,VPER,PHI,X,Y,F
C
      CLOSE(UNIT=IDISK)
      OPEN(UNIT=IDSK11,DEVICE='DSK',ACCESS='APPEND',DISPOSE='
SAVE',
     1FILE='FUN3D.DAT')
C     WRITE(IDSK11,1000)
VPAR(1),VPER(1),PHI(1),((I,J,VPER(I),X(J),
C     1F(5,I,1,J,1),J=1,4),I=1,5)
C1000 FORMAT(1X,3G12.5/1X,16(1X,2I2,3G12.5/))
C
C READ TIME STEP  NO. TIMES THROUGH TIME LOOP
C
      TYPE 100
100   FORMAT(' DELT,NTIME,NFILE = ?')
      READ(ITTY,*) DELT,NTIME,NFILE
      TYPE 200
200   FORMAT(' OMEGAC = ?')
      READ(ITTY,*) OMEGAC
C
C WRITE PARAMETERS TO DISK FILES
C
      WRITE(IDSK12,20) NVPAR,NVPER,NPHI,NX,NY
      WRITE(IDSK12,40) VPARMX,VPERMX,XMAX,YMAX
      WRITE(IDSK12,40) A,ALPHA,B,BETA
      WRITE(IDSK12,40) C,CKX,CKY,DVPAR
      WRITE(IDSK12,40) DVPER,DPHI,DX,DY
C
C CALCULATE PARAMETERS
C
      NTM1 = (NTIME-1)*NFILE
      NONE = 1
      DTHALF = DELT*.5
C
      WRITE(IDSK10,*) NTM1,DELT,NONE
C
```

```
C INITIALIZE ELECTRIC FIELD CALCULATION IN EFOUR
C
      CALL EFOUR
C
C INITIALIZE ACCELERATION EQUATION SUBROUTINES
C
      CALL ACCEL
      CALL OPERAT
C     GO TO 500
C
C
C
C TIME DO LOOP STARTS HERE
C
      ICOUNT = 0
300   CONTINUE
      ICOUNT = ICOUNT + 1
      DO 2000 I=1,NTIME
      IF(I.NE.1) TIME = TIME+DELT
C
C SPACE SHIFT IN XY BY V*DELT
C
      IF((I-1)*(I-NTIME).EQ.0) CALL SPACEI(DTHALF)
      CALL SPACEC
C     WRITE(IDSK11,1000)
VPAR(1),VPER(1),PHI(1),((I,J,X(I),Y(J),
C     1F(1,1,1,I,J),J=1,4),I=1,4)
      IF(I.EQ.1) CALL SPACEI(DELT)
C500  CONTINUE
      IF(I.GE.NTIME) GO TO 2000
C
C
C
C
C CALCULATE CHANGE IN F DUE TO ACCELERATION
C
      CALL ACCEL1(ENERGY)
C
C WRITE ELECTRIC FIELD ENERGY  TIME ON DISK FILE
C
      TPHALF = TIME + DTHALF
      WRITE(IDSK10,*) ENERGY,TPHALF
C     WRITE(IDSK11,1000)
VPAR(1),VPER(1),PHI(1),((I,J,VPER(I),X(J),
C     1F(5,I,1,J,1),J=1,4),I=1,5)
2000  CONTINUE
C
      WRITE(IDSK11,40) TIME
      WRITE(IDSK11,*) VPAR,VPER,PHI,X,Y,F
C
C
      IF(ICOUNT.LT.NFILE) GO TO 300
      WRITE(IDSK12,40) TIME
      WRITE(IDSK12,*) VPAR,VPER,PHI,X,Y,F
C
```

```
      CLOSE(UNIT=IDSK10)
      CLOSE(UNIT=IDSK11)
      STOP
      END
C
C*************************************
C
      SUBROUTINE EFOUR
C
C SUBROUTINE EFOUR SOLVES THE TWO DIMENSIONAL POISSON
EQUATION
C FOR THE ELECTRIC FIELD WITH PERIODIC BOUNDARY CONDITIONS
C IN BOTH DIRECTIONS. THE CHARGE DENSITY RHO(X,Y) IS
OBTAINED
C BY  INTEGRATING THE ELECTRON DISTRIBUTION FUNCTION
C F(VPAR,VPER,PHI,X,Y) OVER ALL VELOCITIES.
C
      PARAMETER N16=16, N8=8, N4=4
      DIMENSION
RHO(N4,N4),F(N16,N8,N8,N4,N4),EX(N4,N4),EY(N4,N4)
      COMPLEX XFACT,YFACT,COMPI,SUMRO,SUMEX,SUMEY,ARGX,ARGY,
     1AARGX,AARGY,TOPIX,TOPIY,TOPIXM,TOPIYM
      COMMON /CONST/ PI
      COMMON /FAREA/
FF(N16,N8,N8,N4,N4),VPAR(N16),VPER(N8),PHI(N8),
     1X(N4),Y(N4)
      COMMON /NAREA/ NVPAR,NVPER,NPHI,NX,NY
      COMMON/DELTA/ DVPAR,DVPER,DPHI,DX,DY,DELT
      COMMON/MAX/ VPARMX,VPERMX,FLX,FLY
C
      DATA COMPI/(0.,1.)/
C
      TWOPI = 2.*PI
      FLXM2 = 1./FLX**2
      FLYM2 = 1./FLY**2
      FACTOR = DX*DY*FLXM2*FLYM2/TWOPI
      XFACT = FLY*FACTOR*COMPI
      YFACT = FLX*FACTOR*COMPI
      NYTOP1 = NY/2 + 1
      NXTOP1 = NX/2 + 1
      TOPIX = TWOPI*COMPI/NX
      TOPIY = TWOPI*COMPI/NY
      TOPIXM = -1.*TOPIX
      TOPIYM = -1.*TOPIY
      AREA = DX*DY
      DEL = DVPAR*DVPER*DPHI
      RETURN
C
      ENTRY EFOUR1(F,EX,EY,ENERGY)
C
C INTEGRATE OVER VELOCITY USING TRAPEZOIDAL RULE
C
      DO 500 IX=1,NX
      DO 500 IY=1,NY
      SPHI = 0.
```

```
      DO 300 IVPAR=1,NVPAR
      DO 300 IVPER = 1,NVPER
      DO 300 IPHI = 1,NPHI
      SPHI = SPHI + F(IVPAR,IVPER,IPHI,IX,IY)*VPER(IVPER)
300   CONTINUE
      RHO(IX,IY) = SPHI*DEL
500   CONTINUE
C
C DETERMINE ELECTRIC FIELD COMPONENTS FROM DOUBLE FOURIER
C TRANSFORM OF POISSON'S EQUATION
C
      ENERGY = 0.
      DO 2000 IX=1,NX
      IIX = IX-1
      DO 2000 IY=1,NY
      SUMEX = 0.
      SUMEY = 0.
      IIY = IY-1
      DO 1000 N=1,NY
      NN = N - NYTOP1
      AARGY = TOPIY*NN*IIY
      FACTN = FLYM2*NN**2
      DO 1000 M=1,NX
      MM = M-NXTOP1
      SUMRO  = 0.
      IF(MM+NN.EQ.0) GO TO 900
      AARGX = TOPIX*MM*IIX
      FACTM = FLXM2*MM**2 + FACTN
      DO 800 K=1,NY
      KK = K-1
      ARGY = NN*KK*TOPIYM
      DO 800 L=1,NX
      LL = L-1
      ARGX = MM*LL*TOPIXM
      SUMRO = SUMRO + RHO(L,K)*CEXP(ARGX+ARGY)
C     WRITE(3,5000) K,L,RHO(L,K),SUMRO,ARGX,ARGY
800   CONTINUE
      SUMRO = SUMRO*CEXP(AARGX+AARGY)/FACTM
900   SUMEX = MM*SUMRO + SUMEX
      SUMEY = NN*SUMRO + SUMEY
C     WRITE(3,5000) N,M,SUMRO,SUMEX,SUMEY,AARGX,AARGY
1000  CONTINUE
      EX(IX,IY) = REAL(SUMEX*XFACT)
      EY(IX,IY) = REAL(SUMEY*YFACT)
      ENERGY = (EX(IX,IY)**2 + EY(IX,IY)**2)*AREA + ENERGY
C     TYPE 5000,IX,IY,EX(IX,IY),EY(IX,IY),ENERGY
C5000 FORMAT(2I2,10(E12.5,2X))
2000  CONTINUE
C
      RETURN
      END
C
C*************************
C
C
```

```
      SUBROUTINE ACCEL
C
C SUBROUTINE ACCEL ADVANCES THE ELECTRON DISTRIBUTION
FUNCTION
C F(VPAR,VPER,PHI,X,Y) IN TIME ACCORDING TO THE ACCELERATION
C TERM IN THE VLASOV EQUATION. THE CALCULATION USES THE
ACCURATE
C SPACE DERIVATIVE (ASD) METHOD DESCRIBED IN:
C
C     J.GAZDAG,NUMERICAL SOLUTION OF THE VLASOV  EQUATION
WITH
C     THE ACCURATE SPOACE DERIVATIVE
METHOD,J.COMP.PHYS.19,77-89(1975).
C
C SUBROUTINE OPERAT IS CALLED TO PERFORM A DOUBLE FOURIER
EXPANSION
C IN F IN THE VARIABLES VPERPHI AND TO CALCULATE PARTIAL
DERIVATIVES
C IN THESE VARIABLES. SUBROUTINE EFOUR IS CALLED TO
CALCULATE THE
C ELECTRIC FIELD AND ITS TIME DERIVATIVES.
C
      PARAMETER N16=16,N8=8,N4=4
      DIMENSION
SAVE1(N16,N8,N8,N4,N4),SAVE2(N16,N8,N8,N4,N4),
      1DFDT(N16,N8,N8,N4,N4),DFDT2(N16,N8,N8,N4,N4),
      2 EX(N4,N4),EY(N4,N4),DEXDT(N4,N4),DEYDT(N4,N4),
      3DEXDT2(N4,N4),DEYDT2(N4,N4)
      COMMON /FAREA/
F(N16,N8,N8,N4,N4),VPAR(N16),VPER(N8),PHI(N8),
      1X(N4),Y(N4)
      COMMON /OPER/ IPAR,IPER,IPHI,IX,IY,RSUM1,RSUM2
      COMMON /NAREA/ NVPAR,NVPER,NPHI,NX,NY
      COMMON /DELTA/ DVPAR,DVPER,DPHI,DX,DY,DELT
      COMMON /CONST/ PI,OMEGAC
      COMMON /MAX/ VPARMX,VPERMX,XMAX,YMAX
      FACT1 = DVPAR/VPARMX
      TOPIL = PI/VPARMX
      NPARM1 = NVPAR - 1
      NPAR2 = NVPAR/2
      DELTSQ = DELT*DELT*.5
      DELT3 = DELT**3/6.
      RETURN
C
      ENTRY ACCEL1(ENERGY)
C
C DETERMINE EX FROM F
C
C40   CONTINUE
      CALL EFOUR1(F,EX,EY,ENERGY)
C50   CONTINUE
C
C DETERMINE DF/DT FROM EX  F
C
      DO 100 IX=1,NX
```

```
      DO 100 IY=1,NY
      DO 100 IPHI = 1,NPHI
      DO 100 IPER = 1,NVPER
      DO 100 IPAR = 1,NVPAR
C60   CONTINUE
      CALL OPER1(F)
C70   CONTINUE
      SAVE1(IPAR,IPER,IPHI,IX,IY) = RSUM1
      DFDT(IPAR,IPER,IPHI,IX,IY) = EX(IX,IY)*RSUM1 + RSUM2
100   CONTINUE
C
C CALCULATE DEXDT
C
      CALL EFOUR1(DFDT,DEXDT,DEYDT,ENRG)
C
C CALCULATE DFDT2 FROM DEXDT  DF/DT
C
      DO 200 IX=1,NX
      DO 200 IY=1,NY
      DO 200 IPHI = 1,NPHI
      DO 200 IPER = 1,NVPER
      DO 200 IPAR = 1,NVPAR
      CALL OPER1(DFDT)
      SAVE2(IPAR,IPER,IPHI,IX,IY) = RSUM1
      DFDT2(IPAR,IPER,IPHI,IX,IY) = RSUM1*EX(IX,IY) + RSUM2
+
      1 DEXDT(IX,IY)*SAVE1(IPAR,IPER,IPHI,IX,IY)
200   CONTINUE
C
C CALCULATE DEX/DT2 FROM DF/DT2
C
      CALL EFOUR1(DFDT2,DEXDT2,DEYDT2,ENRG)
C
C CALCULATE DFDT3  NEW F FROM DF/DT2 DEX/DT2
C
      DO 300 IX=1,NX
      DO 300 IY=1,NY
      DO 300 IPHI = 1,NPHI
      DO 300 IPER = 1,NVPER
      DO 300 IPAR = 1,NVPAR
      CALL OPER1(DFDT2)
      DFDT3 = EX(IX,IY)*RSUM1 + RSUM2 +
      1DEXDT2(IX,IY)*SAVE1(IPAR,IPER,IPHI,IX,IY) +
      2 2.*DEXDT(IX,IY)*SAVE2(IPAR,IPER,IPHI,IX,IY)
      F(IPAR,IPER,IPHI,IX,IY) = F(IPAR,IPER,IPHI,IX,IY) +
      1 DELT*DFDT(IPAR,IPER,IPHI,IX,IY) +
      2 DELTSQ*DFDT2(IPAR,IPER,IPHI,IX,IY) +
      3 DELT3*DFDT3
C
      SAVE1(IPAR,IPER,IPHI,IX,IY) = F(IPAR,IPER,IPHI,IX,IY)
300   CONTINUE
C     WRITE(11,1000)
VPAR(1),VPER(1),PHI(1),((I,J,VPER(I),X(J),
C     1F(5,I,1,J,1),J=1,4),I=1,5)
C1000 FORMAT(1X,3G12.5/1X,16(1X,2I2,3G12.5/))
```

```
C
C SHIFT IN VPARALLEL WITH ACCELERATION -EY
C
      DO 400 IX=1,NX
      DO 400 IY=1,NY
      DO 400 IPAR=1,NVPAR
      VEL = VPAR(IPAR) + EY(IX,IY)*DELT
      DO 400 IPER = 1,NVPER
      DO 400 IPHI = 1,NPHI
      SUM = 0.
      DO 350 N=1,NPAR2
      NN = N-1
      FACTOR = 1.
      IF(NN.EQ.0) FACTOR = .5
      DO 350 K=1,NPARM1
      ARG = TOPIL*NN*(VEL-VPAR(K))
      SUM = SUM + SAVE1(K,IPER,IPHI,IX,IY)*COS(ARG)*FACTOR
350   CONTINUE
      F(IPAR,IPER,IPHI,IX,IY)=SUM*FACT1
400   CONTINUE
C
C500  CONTINUE
      RETURN
      END
C
C*******************
C
C
      SUBROUTINE OPERAT
C SUBROUTINE OPERAT CALCULATES THE FOURIER TRANSFORM OF THE
ARGUMENT
C FUNCTION AND THE VALUE OF THE TIME DERIVATIVE FROM SPACE
DERIVATIVES
C USING THE ASD METHOD.
C
      PARAMETER N16=16, N8=8,N4=4
      DIMENSION  CPHI(N8),SPHI(N8)
      DIMENSION
FF(N16,N8,N8,N4,N4),SINPER(N16,N8,N8),SINPHI(N8,N8,N8)
      COMMON /OPER/ IPAR,IPER,IPHI,IX,IY,RSUM1,RSUM2
      COMMON /MAX/ VPARMX,VPERMX,XMAX,YMAX
      COMMON /CONST/ PI,OMEGAC
      COMMON /FAREA/ F(N16,N8,N8,N4,N4),VPAR(N16),VPER(N8),
      1 PHI(N8),X(N4),Y(N4)
      COMMON /NAREA/ NVPAR,NVPER,NPHI,NX,NY
      COMMON /DELTA/ DVPAR,DVPER,DPHI,DX,DY,DELT
C
C CALCULATE PARAMETERS
C
      NPHI2 = NPHI/2
      NVPRM1 = NVPER - 1
      NPER2 = 2*NVPER - 1
      NPERP1 = NVPER + 1
      FLPER = 2.*VPERMX
      TOPI = 2.*PI
```

```
      TPILPR = TOPI/FLPER
      FACPER = -1.*PI*DVPER/VPERMX/VPERMX
      FACPHI = -1.*DPHI/PI
C
C DETERMINE SINE FUNCTIONS FOR SUBSEQUENT USE
C
      DO 100 M=1,NVPRM1
      ARG = M*TPILPR
      DO 100 K=1,NPER2
      VEL = (K-1)*DVPER-VPERMX
      DO 100 IPER=1,NVPER
      SINPER(K,IPER,M) = M*SIN(ARG*(VPER(IPER)-VEL))
100   CONTINUE
C
      DO 200 IPHI = 1,NPHI
      CPHI(IPHI) = COS(PHI(IPHI))
      SPHI(IPHI) = SIN(PHI(IPHI))
      DO 200 N=1,NPHI2
      DO 200 L=1,NPHI
      SINPHI(IPHI,L,N) = N*SIN(N*(PHI(IPHI)-PHI(L)))
200   CONTINUE
      RETURN
C
      ENTRY OPER1(FF)
C2000 CONTINUE
C
C DETERMINE DF/DVPER  FIRST TERM IN RSUM1
C
      RSUM1 = 0.
      NEWPHI = IPHI+NPHI2
      IF(NEWPHI.GT.NPHI) NEWPHI = NEWPHI-NPHI
      DO 500 M=1,NVPRM1
      DO 400 K=1,NVPER
      RSUM1 = RSUM1 +
FF(IPAR,NPERP1-K,NEWPHI,IX,IY)*SINPER(K,IPER,M)
400   CONTINUE
      DO 500 K=NPERP1,NPER2
      RSUM1 = RSUM1 +
FF(IPAR,K-NVPER,IPHI,IX,IY)*SINPER(K,IPER,M)
500   CONTINUE
      RSUM1 = RSUM1*CPHI(IPHI)*FACPER
C3000 CONTINUE
C
C DETERMINE DF/DPHI  RSUM2 TERM
C
      RSUM2 = 0.
      DO 1000 N=1,NPHI2
      DO 1000 L=1,NPHI
      RSUM2 = RSUM2 + FF(IPAR,IPER,L,IX,IY)*SINPHI(IPHI,L,N)
1000  CONTINUE
      RSUM2 = RSUM2*FACPHI
C4000 CONTINUE
C
C RSUM2 IS DF/DPHI AT THIS POINT
C
```

```
      RSUM1 = RSUM1 - SPHI(IPHI)*RSUM2/VPER(IPER)
C
      RSUM2 = -1.*OMEGAC*RSUM2
C
C
C
C5000 CONTINUE
      RETURN
      END
```

```
      SUBROUTINE SPACEI(DELT)
      PARAMETER N16=16,N8=8,N4=4,N7=7
C     CALCULATE GX AND GY WITH 5 PHASE SPACE VARIABLES
C     THETA=90
      DIMENSION       GX(N8,N8,N7),GY(N16,N7)
      DIMENSION       DELX(N8,N8),DELY(N16)
      COMMON /NAREA/ NPAR,NPER,NPHI,NX,NY
      COMMON  /CONST/ PI
      COMMON  /DELTA/ DVPAR,DVPER,DPHI,DX,DY,DDELT
      COMMON  /GAREA/ GX,GY
      TPIPHI=2.*PI/NPHI
      XNX=NX
      XNY=NY
      DVNTX=DVPER*DELT/DX
      DVNTY=DVPER*DELT/DY
      DVBTY=DVPAR*DELT/DY
C     GENERATE DELX
      DO 1000 K=1,NPHI
      DO 1000 J=1,NPER
1000  DELX(J,K)=(2*J-1)*.5*COS((K-1)*TPIPHI)*DVNTX
C     GENERATE GX
      DO 1010 K=1,NPHI
      DO 1010 J=1,NPER
      DO 1020 M2=1,NX
      GMD=PI*(M2-DELX(J,K))
      GMDNX=GMD/XNX
      SGMDNX=SIN(GMDNX)
      GX(J,K,M2)=1.
1020  IF(ABS(SGMDNX).GT.1.E-12)
GX(J,K,M2)=SIN(GMD)*COS(GMDNX)/
     1XNX/SGMDNX
      DO 1010 M2=NX+1,2*NX-1
1010  GX(J,K,M2)=GX(J,K,M2-NX)
C     GENERATE DELY
      DO 1130 I=1,NPAR
1130  DELY(I)=(2*I-NPAR-1)*.5*DVBTY
C     GENERATE GY
      DO 1200 I=1,NPAR
      DO 1210 N2=1,NY
      GMD=PI*((NY-N2)+DELY(I))
      GMDNY=GMD/XNY
      SGMDNY=SIN(GMDNY)
      GY(I,N2)=1.
1210  IF(ABS(SGMDNY).GT.1.E-12)
GY(I,N2)=SIN(GMD)*COS(GMDNY)/
     1XNY/SGMDNY
      DO 1200 N2=NY+1,2*NY-1
1200  GY(I,N2)=GY(I,N2-NY)
      END
      SUBROUTINE SPACEC
      PARAMETER N16=16,N8=8,N4=4,N7=7
C     SHIFT ALONG X AND Y AXES
C     THETA=90
      DIMENSION       F(N16,N8,N8,N4,N4),F1(N16,N8,N8,N4,N4)
      DIMENSION       GX(N8,N8,N7),GY(N16,N7)
```

```
      COMMON /NAREA/ NPAR,NPER,NPHI,NX,NY
      COMMON  /FAREA/ F,VPAR,VPER,PHI,X,Y
      COMMON  /GAREA/ GX,GY
C     X SHIFT
      DO 1300 N=1,NY
      DO 1300 M=1,NX
      DO 1300 K=1,NPHI
      DO 1300 J=1,NPER
      DO 1300 I=1,NPAR
      F1(I,J,K,M,N)=0.
      DO 1300 M1=1,NX
1300  F1(I,J,K,M,N)=F1(I,J,K,M,N)+F(I,J,K,M1,N)*GX(J,K,NX+M-M
1)
C     Y SHIFT
      DO 1400 N=1,NY
      DO 1400 M=1,NX
      DO 1400 K=1,NPHI
      DO 1400 J=1,NPER
      DO 1400 I=1,NPAR
      F(I,J,K,M,N)=0.
      DO 1400 N1=1,NY
1400  F(I,J,K,M,N)=F(I,J,K,M,N)+F1(I,J,K,M,N1)*GY(I,NY+N-N1)
      END
```

```
C PROGRAM PLTF3D.FOR PLOTS F(VPAR,VPER) AS CONTOURS OF
C CONSTANT F IN VPAR,VPER SPACE. THE PROGRAM INTEGRATES F
C OVER PHI,X  Y. AND PLOTS THE REMAINING FUNCTION OF
VPAR,VPER USING
C PLOT10 SOFTWARE. ALL ITERATIONS ARE DONE BY FIRST FITTING
THE FUNCTION
C WITH A CUBIC SPLINE CURVE. THE DATA REQUIRED FOR THE PLOT
IS READ IN
C FROM FILE FUN3D.DAT USING
C
C     READ(IDISK,*) VPAR,VPER,PHI,X,Y,F
C
C THE PLOT10 DATA FOR THE PLOT IS WRITTEN ON DISK FILE
PLTF3D.DAT
C THE PARAMETERS ARE:
C  EPS: FRACTION OF FMAX USED FOR CONTOUR RESOLUTION(SUGGEST
.05)
      DIMENSION
F(16,8,8,4,4),VPAR(16),VPER(8),PHI(8),X(4),Y(4),
     1WK(500),VVPER(500),F2(5,5),F3(20,10,8),
     2IARRAY(20),JARRAY(100),F1(8),BPAR(4),CC(19,3),FF(20,10
),
     3ENERGY(20,10),CONT(10),FPAR(21),FVPER(11),FVPAR(21),VV
PAR(21)
      EQUIVALENCE (VVPER,WK)
      DATA
IDISK/1/,ITTY/5/,IDSK10/10/,BPAR/0.,0.,0.,0./,IBAUD/240/
      DATA IYES/1HY/
      OPEN(UNIT=IDISK,DEVICE='DSK',ACCESS='SEQIN',DISPOSE='SA
VE',
     1FILE='FUN3D.DAT')
      OPEN(UNIT=20,DEVICE='DSK',ACCESS='APPEND',DISPOSE='SAVE
',
     1FILE='PLTF3D.DAT')
      OPEN(UNIT=IDSK10,DEVICE='DSK',ACCESS='SEQOUT',DISPOSE='
SAVE',
     1FILE='PLTFX.DAT')
      READ(IDISK,20) NVPAR,NVPER,NPHI,NX,NY
20    FORMAT(5I2)
      READ(IDISK,40) VPARMX,VPERMX,XMAX,YMAX
40    FORMAT(4E15.5)
      READ(IDISK,40) A,ALPHA,B,BETA
      READ(IDISK,40) C,CKX,CKY,DVPAR
      READ(IDISK,40) DVPER,DPHI,DX,DY
      TYPE 50
50    FORMAT(' NFILE=?')
      READ(ITTY,*) NFILE
      TYPE 60
60    FORMAT('$ CALCOMP PLOTS ?')
      READ(ITTY,70) IANS
70    FORMAT(A1)
      TYPE 80
80    FORMAT(' F(VPER) VS VPER ?')
      READ(ITTY,70) IANS2
      TYPE 90
```

```
90    FORMAT(' F(VPAR) VS VPAR ?')
      READ(ITTY,70) IANS3
      WRITE(IDSK10,*) NFILE,NVPAR,NVPER,DVPAR,DVPER
      DO 6000 ICOUNT = 1,NFILE
      READ(IDISK,40) TIME
      READ(IDISK,*) VPAR,VPER,PHI,X,Y,F
C
C INTEGRATE OUT XY DEPENDENCE
C
      DO 300 IVPAR = 1,NVPAR
      DO 300 IVPER=1,NVPER
      SUM = 0.
      DO 200 IPHI = 1,NPHI
      DO 200 IX=1,NX
      DO 200  IY = 1,NY
      SUM = SUM + F(IVPAR,IVPER,IPHI,IX,IY)
200   CONTINUE
      FF(IVPAR,IVPER) = SUM*DPHI*DX*DY
      ENERGY(IVPAR,IVPER) = (VPAR(IVPAR)**2+VPER(IVPER)**2)*
      1FF(IVPAR,IVPER)
300   CONTINUE
C
C CHECK CONSERVATION OF ENERGY AND PARTICLES
C
      SPER = 0.
      SPERE = 0.
      DO 350 IVPAR=1,NVPAR
      DO 350 IVPER=1,NVPER
      SPER = FF(IVPAR,IVPER)*VPER(IVPER) + SPER
      SPERE = SPERE + ENERGY(IVPAR,IVPER)*VPER(IVPER)
350   CONTINUE
      TOTPAR = SPER*DVPAR*DVPER
      TOTENG = SPERE*DVPAR*DVPER*.5
C
C SAVE RESULTS FOR PLTFX
C
      WRITE(IDSK10,*) TIME,FF
400   FORMAT(F12.5)
C
C PLOT RESULTS
C
      CALL INITT(IBAUD)
      IF(IANS.EQ.IYES) CALL OUTMOD('FILE',20)
      CALL BINITT
      CALL DLIMX(0.,VPER(NVPER))
      CALL DLIMY(VPAR(1),VPAR(NVPAR))
      CALL LINE(0)
      CALL SYMBL(0)
      CALL CHECK(VPER,VPER)
      CALL DSPLAY(VPER,VPER)
      FMAX = 0.
      DO 500 IVPAR=1,NVPAR
      DO 500 IVPER=1,NVPER
      FMAX = AMAX1(FMAX,FF(IVPAR,IVPER))
500   CONTINUE
```

```
C
      CONTOR = .1*FMAX
      DO 600 I=1,10
      FI = I
      CONT(I) = FI*CONTOR
600   CONTINUE
C
      DO 900 IVPAR=1,NVPAR
      DO 900 IVPER=1,NVPER
      DO 650 I=1,10
      J = I + 47
      IF(FF(IVPAR,IVPER).LE.CONT(I)) GO TO 660
650   CONTINUE
660   CONTINUE
      CALL MOVEA(VPER(IVPER),VPAR(IVPAR))
      CALL ANCHO(J)
900   CONTINUE
C
C     TITLE
C
      ENCODE(60,1000,IARRAY) TOTPAR,TOTENG,TIME
1000  FORMAT(3X,'NUMBER',1PG10.3,5X,'ENERGY',G10.3,3X,
     1'TIME = ',G10.3)
      DECODE(60,1010,IARRAY) (JARRAY(J),J=2,61)
1010  FORMAT(60R1)
      JARRAY(1) = 60
      CALL MOVABS(150,740)
      CALL HSTRIN(JARRAY)
      IF(IANS.NE.IYES) CALL TINPUT(IVALUE)
      CALL NEWPAG
      CALL ANMODE
C
      IF(IANS3.NE.IYES) GO TO 5000
C
C PLOT F(VPAR) VS VPAR
C
      FVPRMX = 0.
      FPAR(1) = NVPAR
      VVPAR(1) = NVPAR
      DO 5500 IVPAR=1,NVPAR
      VVPAR(IVPAR+1) = VPAR(IVPAR)
      DO 5400 IVPER=1,NVPER
      FVPER(IVPER) = FF(IVPAR,IVPER)*VPER(IVPER)
5400  CONTINUE
      CALL ICSICU(VPER,FVPER,NVPER,BPAR,CC,19,IER7)
      CALL
DCSQDU(VPER,FVPER,NVPER,CC,19,0.,VPER(NVPER),Q,IER8)
      FPAR(IVPAR+1) = Q
      FVPRMX = AMAX1(Q,FVPRMX)
5500  CONTINUE
C
      CALL INITT(IBAUD)
      IF(IANS.EQ.IYES) CALL OUTMOD('FILE',20)
      CALL BINITT
      CALL DLIMX(VPAR(1),VPAR(NVPAR))
```

```
      CALL DLIMY(0.,FVPRMX)
      CALL SYMBL(1)
      CALL CHECK(VVPAR,FPAR)
      CALL DSPLAY(VVPAR,FPAR)
C
C
      ENCODE(40,5600,IARRAY) TIME
5600  FORMAT(3X,'F(VPAR) VS VPAR FOR TIME = ',G10.3)
      DECODE(40,2600,IARRAY) (JARRAY(J),J=2,41)
      JARRAY(1) = 40
      CALL MOVABS(150,740)
      CALL HSTRIN(JARRAY)
      IF(IANS.NE.IYES) CALL TINPUT(IVALUE)
      CALL NEWPAG
      CALL ANMODE
C
5000  IF(IANS2.NE.IYES) GO TO 6000
C
C PLOT F(VPER) VS VPER
C
      FVPRMX = 0.
      FVPER(1) = NVPER
      VVPER(1) = NVPER
      DO 2000 IVPER=1,NVPER
      VVPER(IVPER+1) = VPER(IVPER)
      DO 1500 IVPAR=1,NVPAR
      FPAR(IVPAR) = FF(IVPAR,IVPER)
1500  CONTINUE
      CALL ICSICU(VPAR,FPAR,NVPAR,BPAR,CC,19,IER5)
      CALL
DCSQDU(VPAR,FPAR,NVPAR,CC,19,VPAR(1),VPAR(NVPAR),Q,IER6)
      FVPER(IVPER+1) = Q
      FVPRMX = AMAX1(Q,FVPRMX)
2000  CONTINUE
C
      CALL INITT(IBAUD)
      IF(IANS.EQ.IYES) CALL OUTMOD('FILE',20)
      CALL BINITT
      CALL DLIMX(0.,VPER(NVPER))
      CALL DLIMY(0.,FVPRMX)
      CALL SYMBL(1)
      CALL CHECK(VVPER,FVPER)
      CALL DSPLAY(VVPER,FVPER)
C
      ENCODE(40,2500,IARRAY) TIME
2500  FORMAT(3X,'F(VPER) VS VPER FOR TIME = ',G10.3)
      DECODE(40,2600,IARRAY) (JARRAY(J),J=2,41)
2600  FORMAT(40R1)
      JARRAY(1) = 40
      CALL MOVABS(150,740)
      CALL HSTRIN(JARRAY)
      IF(IANS.NE.IYES) CALL TINPUT(IVALUE)
      CALL NEWPAG
      CALL ANMODE
6000  CONTINUE
```

```
C
      CALL FINITT(0,700)
      CLOSE(UNIT=20)
      CLOSE(UNIT=IDISK)
      CLOSE(UNIT=IDSK10)
      STOP
      end
```

```
C
C PROGRAM PLOTE PLOTS A FUNCTION F OF ONE VARIABLE T. THE
PROGRAM REQUIRES
C INPUT FORM DISK FILE ESQ.DAT IN THE FORMAT F,T. THE FIRST
NUMBER IN THE
C FILE IS THE NUMBER OF DATA POINTS NT AND THE SECOND NUMBER
IS
C THE ORDINATE INTERVAL DELT.
C TTY INPUT DATA FORMAT:
C IXTYPE,IYTYPE : 1 FOR LINEAR PLOT, 2 FOR LOG PLOT
C FMIN,FMAX : MAXIMUM  MINIMUM EMAX VALUES
C
      DIMENSION IARRAY(20),JARRAY(100)
      DIMENSION T(600),FF(601),E(50,600),TT(601)
      DATA IBAUD/240/
      DATA IDISK/1/,ITTY/5/
      DATA IYES/1HY/
C
      OPEN(UNIT=IDISK,DEVICE='DSK',ACCESS='SEQIN',FILE='ESQ.D
AT',
     1  DISPOSE='SAVE')
      OPEN(UNIT=ITTY,DEVICE='TTY',ACCESS='SEQINOUT',DISPOSE='
DELETE')
      OPEN(UNIT=20,FILE='PLOTE.DAT',ACCESS='APPEND',DISPOSE='
SAVE')
C
      WRITE(ITTY,150)
150   FORMAT(' CALCOMP PLOT?')
      READ(ITTY,160) IANS
160   FORMAT(A1)
      WRITE(ITTY,20)
20    FORMAT(' FMIN,FMAX,IXTYPE,IYTYPE = ?')
      READ(ITTY,*) FMIN,FMAX,IXTYPE,IYTYPE
      READ(IDISK,*) NT,DELT,NZ
C
      NZP1 = NZ + 1
      NZTOP1 = NZ/2 + 1
      DO 10 I=1,NT
      READ(IDISK,*,END=10)  (E(K,I),K=1,NZTOP1),T(I)
      TT(I+1) = T(I)
10    CONTINUE
C
C
      FF(1) = NT
      TT(1) = NT
      DO 140 NECOMP=1,NZTOP1
      IF(NECOMP.LT.5) GO TO 200
      IF(MOD(NECOMP,2).EQ.0) GO TO 140
200   CONTINUE
      DO 250 J=1,NT
250   FF(J+1) = E(NECOMP,J)
C
C TITLE ARRAY CREATED IN UNPACKED ASCI11 RIGHT JUSTIFIED
FORMAT
C
```

```
      NECM1 = NECOMP - 1
      ENCODE(26,99,IARRAY) NECM1
99    FORMAT(10X,'EAMP(',I2,') VS TIME')
      DECODE(26,260,IARRAY) (JARRAY(J),J=2,27)
260   FORMAT(26R1)
      JARRAY(1) = 26
C
      CALL INITT(IBAUD)
      IF(IANS.EQ.IYES) CALL OUTMOD('FILE',20)
      CALL BINITT
      CALL DLIMX(TT(2),TT(NT))
      CALL DLIMY(FMIN,FMAX)
      CALL XTYPE(IXTYPE)
      CALL YTYPE(IYTYPE)
      CALL CHECK(TT,FF)
      CALL DSPLAY(TT,FF)
      CALL MOVABS(150,740)
      CALL HSTRIN(JARRAY)
140   CONTINUE
C
      CALL NEWPAG
      CLOSE(UNIT=20,FILE='PLOTE.DAT',DISPOSE='SAVE')
      CLOSE(UNIT=IDISK,DISPOSE='SAVE',FILE='ESQ.DAT')
      CLOSE(UNIT=ITTY)
C
      STOP
      END
```

D.2 VLAS3D Computer Runs

The plasma parameters used to determine the initial electron distribution functions for the VLAS3D computer run results that appear in the figures of this thesis are shown in table D-1. The corresponding input parameters for the FUN3D computer code used to create the initial distribution disk file are shown in table D-2. The FUN3D program input parameters are defined by equation D-1.

Table D-1: Plasma Parameters

Run	Beam to Background Density Ratio	Plasma Frequency ω_p(rad/sec) for n_b=1cm^{-3}	Debye Length λ_d(cm) for n_b=1cm^{-3}	Thermal Velocity v_{th}(cm/s)
Parallel Landau Damping	No beam	$\left(\frac{4\pi n_m e^2}{m}\right)^{1/2}$	$\left(\frac{kT_m}{4\pi n_m e^2}\right)^{1/2}$	$\left(\frac{kT_m}{m}\right)^{1/2}$
45° Landau Damping	No beam	The results obtained for Landau damping are independent of background density.		
Three Dimensional Beam-Background Interaction	≈5 From Fig. 25	5.65×10^4	.9	2.2×10^9

The beam temperature is 640 eV for the beam background case, and the Maxwellian background temperature is 10 eV for the first two cases and 50 eV for the last case. The beam peak is at a velocity corresponding to a kinetic energy of 2 keV.

Table D-2: FUN3D and VLAS3D INPUT PARAMETERS

RUN	A, α, B, β	NVPAR, NVPER, NHPI, NX, NY	VPARMX, VPERMX, XMAX, YMAX	C, CKX, CKY	VPAR0, VPER0	OMEGA
Parallel Landau Damping	.0635, .5, 0. 0	12, 6, 4, 4, 4	3.0, 3.0, 10.0, 10.0	.5, 0, .6	0, 0	0
45^{o} Landau Damping				.5, .6, .6		
Three Dim. Beam-Background Interaction	.558 4.43 .023, .3461		5, 5, 17.3, 17.3	.0364, .364, .364	3.01, 0	.1